Library and
Archives Canada

Published Heritage
Branch

395 Wellington Street
Ottawa ON K1A 0N4
Canada

Bibliothèque et
Archives Canada

Direction du
Patrimoine de l'édition

395, rue Wellington
Ottawa ON K1A 0N4
Canada

Your file Votre référence
ISBN: 978-0-494-46448-9
Our file Notre référence
ISBN: 978-0-494-46448-9

NOTICE:
The author has granted a non-exclusive license allowing Library and Archives Canada to reproduce, publish, archive, preserve, conserve, communicate to the public by telecommunication or on the Internet, loan, distribute and sell theses worldwide, for commercial or non-commercial purposes, in microform, paper, electronic and/or any other formats.

The author retains copyright ownership and moral rights in this thesis. Neither the thesis nor substantial extracts from it may be printed or otherwise reproduced without the author's permission.

In compliance with the Canadian Privacy Act some supporting forms may have been removed from this thesis.

While these forms may be included in the document page count, their removal does not represent any loss of content from the thesis.

AVIS:
L'auteur a accordé une licence non exclusive permettant à la Bibliothèque et Archives Canada de reproduire, publier, archiver, sauvegarder, conserver, transmettre au public par télécommunication ou par l'Internet, prêter, distribuer et vendre des thèses partout dans le monde, à des fins commerciales ou autres, sur support microforme, papier, électronique et/ou autres formats.

L'auteur conserve la propriété du droit d'auteur et des droits moraux qui protège cette thèse. Ni la thèse ni des extraits substantiels de celle-ci ne doivent être imprimés ou autrement reproduits sans son autorisation.

Conformément à la loi canadienne sur la protection de la vie privée, quelques formulaires secondaires ont été enlevés de cette thèse.

Bien que ces formulaires aient inclus dans la pagination, il n'y aura aucun contenu manquant.

Canada

University of Alberta

Library Release Form

Name of Author: Wencong Wang

Title of Thesis: Power-Electronics-Based Online Signaling Techniques and Their Applications to Power Systems

Degree: Doctor of Philosophy

Year this Degree Granted: 2008

Permission is hereby granted to the University of Alberta Library to reproduce single copies of this thesis and to lend or sell such copies for private, scholarly or scientific research purposes only.

The author reserves all other publication and other rights in association with the copyright in the thesis, and except as herein before provided, neither the thesis nor any substantial portion thereof may be printed or otherwise reproduced in any material form whatsoever without the author's prior written permission.

Wencong Wang

Signature

ABSTRACT

The application of power electronics to power systems to facilitate the transmission or conversion of electric energy has been well known. This thesis reviews a different type of application in which power electronics circuits are deployed in power systems to create small but discernible signals online. These signals are utilized for communication, online monitoring, fault diagnosis and other information-oriented purposes. These power-electronics-based online signaling techniques have many potential applications in power systems. This thesis identifies a thyristor-based circuit named "zero-crossing-distortion" as a representative of these techniques, and applies it to solve the following three challenging problems.

Islanding detection of distributed generators (DGs) is a significant technical barrier for the emerging DG industry. This thesis proposes an innovative solution scheme based on power line communication. The scheme broadcasts a signal from a substation to downstream DGs by using the distribution feeders as the signal paths. A DG is considered as islanded if it cannot sense the signal. The zero-crossing-distortion technique is adopted to generate the signals. The signal generation device can also be located downstream of the substation at, for

example, the upstream of an area with many DG installations to improve the flexibility in implementation. The proposed schemes have been verified through laboratory and field tests.

This thesis then presents an effective and easy-to-implement method for measuring power system harmonic impedances. The zero-crossing-distortion technique is utilized to create controlled short-circuits at the measurement point, producing currents and voltage disturbances for measuring the system impedance. The strength of the disturbance is controlled so that it can support precise measurement without causing power quality problems. The method can be implemented into a portable device for low voltage applications.

This thesis also investigates a method for identifying a line experiencing a single-phase grounded fault in noneffectively grounded systems. Faulted line identification in such systems is very difficult due to the small magnitudes of fault currents. The proposed method temporarily grounds the system and creates a fault current large enough for identifying the faulted line and yet small enough not to cause system problems. Lab experiments verified the effectiveness of the proposed method.

ACKNOWLEDGEMENTS

I would like to express my sincere gratitude to Dr. Wilsun Xu for his inspiration and professional instructions in supervising this research work. It has been my great pleasure to be a student of Dr. Xu. I owe my achievements to the opportunity provided by Dr. Xu and to his tireless help.

I also appreciate help from my colleagues in the power quality group at University of Alberta during the progress of this research work. I would like to thank Dr. Guibin Zhang, Professor Guangzhu Wang, Dr. Chun Li and Yu Cui for their work at the early stage of one of the research projects. I need to thank Dr. Sami Abdulsalam and Dr. Xiaoyu Wang for their field test travels for the research project. Also, I want to thank Albert Terheide for his help during my laboratory tests. Moreover, working with Edwin Enrique Nino, Ke Zhu and Jacek Kliber has been a pleasant and productive experience.

I would like to express my deep gratitude to my husband and my parents for their support that has always been with me.

TABLE OF CONTENTS

Chapter 1. Introduction **1**

1.1 Conventional Power Electronics Applications to Power Systems 1
1.2 Online Signaling-Oriented Power Electronics Applications 3
1.3 Challenges Faced by Power Systems 4
1.4 Research Objectives 5
1.5 Thesis Contributions and Outline 6

Chapter 2. Power-Electronics-Based Online Signaling Techniques **8**

2.1 Power Electronics Applications to Power Line Communication 8
  2.1.1 Zero-Crossing-Shift Technique 8
  2.1.2 Zero-Crossing-Distortion Technique 9
  2.1.3 Ripple Control 10
  2.1.4 Hunt Technologies 11
2.2 Power Electronics Applications to Online Monitoring 13
  2.2.1 Converter-Based Harmonic Impedance Measurement 13
  2.2.2 Grid Impedance Measurement for Islanding Detection 14
  2.2.3 Online Motor Thermal Protection 16
2.3 Power Electronics Applications to Fault Detection 17
  2.3.1 Faulted Line Locating in Ungrounded Systems 18
  2.3.2 Generator Stator Ground Fault Detection 19
  2.3.3 Generator Field Circuit Fault Detection 20
  2.3.4 Ground Fault Detection for HVDC System's Neutral Line 21
2.4 Summary of Online-Signaling-Oriented Applications 22
2.5 Conclusion 24

Chapter 3. Islanding Detection of Distributed Generators **25**

3.1 Introduction to DG Islanding Detection 25
3.2 Review of Existing Islanding Detection Methods 28
  3.2.1 Local Passive Methods 29
  3.2.2 Local Active Methods 31
  3.2.3 Communication-Based Methods 32
  3.2.4 Conclusion 34
3.3 The Idea of Power-Line-Signaling-Based Islanding Detection 34
  3.3.1 Requirements for Signaling Techniques 35

3.3.2 Review of Existing Power-Line-Signaling Techniques 36
3.3.3 Comparison and Analysis of Different Techniques 42
3.3.4 Conclusion and Discussion 44
3.4 The Proposed Power-Line-Signaling-Based Method 45
3.4.1 Signal Generator (SG).. 46
3.4.2 Signal Detector (SD)... 47
3.5 Signal Characteristics Analysis and Signal Generator Design......... 48
3.5.1 Simplified Signal Analysis and Signal Generator Design . 48
3.5.2 Detailed Signal Analysis and Simulations 51
3.5.3 Signal Propagation across Transformers............................ 59
3.6 The Signal Detection Algorithms.. 61
3.6.1 RMS-based Signal Detection Algorithm 61
3.6.2 Spectrum-based Signal Detection Algorithm..................... 62
3.6.3 Template-based Signal Detection Algorithm 64
3.7 Conclusion 67

Chapter 4. Field Tests of Power-Line-Signaling-Based Islanding Detection 68

4.1 Field Tests Setting 68
4.2 Summary of Field Test Results 69
4.2.1 Signal Characteristics... 71
4.2.2 Recorded Events 72
4.3 Evaluation of Three Signal Detection Algorithms.......................... 73
4.3.1 Typical Performance 73
4.3.2 Performance with Nuisance Islanding Events 76
4.3.3 Statistical Performance Analysis.. 77
4.4 Interferences between Islanding Detection and AMR 79
4.4.1 AMR Signal Characteristics 80
4.4.2 AMR and Islanding Detection Signal Interference............ 81
4.5 Complete Signal Detection Algorithms 84
4.6 Conclusion 84

Chapter 5. The Scalable Islanding Detection Scheme 86

5.1 The Idea of Scalable DG Islanding Detection 86
5.2 Detection of SG Connection to the Main Supply 89
5.2.1 Base Case Computer Simulations...................................... 89
5.2.2 Theoretical Analysis and the Detection Criterion.............. 92
5.2.3 Sensitivity Study 95
5.3 Experimental Tests.. 97
5.4 Design of the Signal Generator.. 99
5.5 Conclusion 101

Chapter 6. Harmonic Impedance Measurement Using Thyristor-Controlled Short-Circuits **102**

6.1 Introduction 102
6.2 Review of Existing Methods 102
6.3 The Proposed Measurement Scheme 104
  6.3.1 Transient-Based Harmonic Impedance Measurement 104
  6.3.2 The Proposed Device for Single-Phase Systems 105
  6.3.3 The Proposed Device for Three-phase Systems 108
6.4 Computer Simulations and the Finalized Algorithm 109
  6.4.1 Simulations in a Single-Phase LV System 109
  6.4.2 Simulations in a Three-Phase System 111
6.5 Lab Experiment Results 114
  6.5.1 Experiment Results 115
  6.5.2 Criterion for Reliable Measurements 116
6.6 SG Setting for Practical Applications 118
6.7 Impedance-Measurement-Based DG Islanding Detection 120
6.8 Conclusions 122

Chapter 7. Faulted Line Identification in Noneffectively Grounded Systems. **123**

7.1 Introduction 123
7.2 Review of Existing Identification Methods 125
  7.2.1 Steady-State-Based Methods 125
  7.2.2 Transient-Based Methods 128
  7.2.3 Active Methods 130
  7.2.4 Conclusion 131
7.3 The Proposed Method Based on Thyristor-Controlled Grounding 131
  7.3.1 Controllable Grounding Device 132
  7.3.2 Transient Current Signal Detector 133
7.4 Study of Signal Characteristics 134
  7.4.1 Theoretical Analysis 134
  7.4.2 Computer Simulations 139
  7.4.3 Signal Variations with respect to δ, R_f and Grounding 140
7.5 Criterion for Identifying the Faulted Line 143
  7.5.1 Construction of the Detection Criterion 143
  7.5.2 Sensitivity Study of the Current Criterion 145
7.6 Lab Test Results 147
7.7 Design of the Controllable Grounding Device 148
7.8 Conclusion 150

Chapter 8. Conclusions and Recommendations 151

Bibliography 154

Appendix A. Equations about the Anti-islanding Signal 161

Appendix B. Nuisance Tripping Events in ATCO Field Tests 164

Appendix C. Equations for Calculating Harmonic Impedances 165

LIST OF TABLES

Table 1.1 A Summary of Power Electronics Applications 2
Table 1.2 Signaling-Oriented Power Electronics Applications 3

Table 2.1 Classification of Power-Electronics-Based Signaling Circuits 24

Table 3.1 Comparison of Various Power Line Signaling Methods 43
Table 3.2 Equations for Signal Strength at Point X 51
Table 3.3 Example SG Parameters 51
Table 3.4 Signal Propagation Across a Transformer 60

Table 4.1 A Summary of the Field Test Results 70
Table 4.2 AMR Operation Time Schedule 79

Table 6.1 Candidate Indices for DG Islanding Detection 121

LIST OF FIGURES

Figure 2.1 A zero-crossing-shift by injecting a single-cycle modulation voltage. 9
Figure 2.2 A basic implement circuit for the zero-crossing-shift. 9
Figure 2.3 The zero-crossing-distortion (a) signaling circuit and (b) waveforms. 10
Figure 2.4 The one-phase configuration of ripple control technique. 11
Figure 2.5 The ripple control transmitter current and substation voltage waveforms. 11
Figure 2.6 The low frequency bilateral power line communication system. 12
Figure 2.7 The signal waveforms and trigger signal generation of Hunt technologies..... 12
Figure 2.8 Harmonic impedance measurement based on inverter injection. 14
Figure 2.9 PV inverters injecting harmonics for grid impedance monitoring. 15
Figure 2.10 The thyristor-based circuit for measuring the system impedance. 15
Figure 2.11 The structure of a motor soft-starter. 16
Figure 2.12 Online motor stator resistance monitoring using the soft-starter. 17
Figure 2.13 Online motor stator resistance monitoring using an extra circuit. 17
Figure 2.14 A pulsated ground fault detection device. 19
Figure 2.15 A triac-based circuit for generator stator ground fault protection. 20
Figure 2.16 A signal injection method for detecting generator rotor ground fault. 21
Figure 2.17 A HVDC neutral fault detection system. 22
Figure 2.18 A classification of power-electronics-based online signaling techniques. 22

Figure 3.1 A typical distribution system with distributed generators. 26
Figure 3.2 A classification of anti-islanding schemes for distributed generators. 29
Figure 3.3 A classification of power-line-communication methods. 37
Figure 3.4 The ripple carrier communication system. 38
Figure 3.5 The ripple carrier signal waveforms. 39
Figure 3.6 The modulating voltage and carrier waveforms. 39
Figure 3.7 The proposed islanding detection scheme. 45
Figure 3.8 The signaling method and waveforms. 47
Figure 3.9 A sample voltage waveform containing a signal every two cycles. 47
Figure 3.10 The subtraction method for signal extraction. 48
Figure 3.11 The analysis circuit for phase-ground signaling. 49
Figure 3.12 The anti-islanding signal and the thyristor current waveforms. 49
Figure 3.13 The single line diagram of the simulation system. 52
Figure 3.14 The equivalent circuit for signal propagation analysis. 53
Figure 3.15 The representative signal waveforms. 54
Figure 3.16 The anti-islanding signals corresponding to various shunt capacitances. 55
Figure 3.17 The calculated anti-islanding signals of different resonance frequencies. 56
Figure 3.18 The signal strengths *k* as affected by system parameters. 57
Figure 3.19 The system attenuation as affected by system parameters. 57
Figure 3.20 The signal oscillation frequency as affected by system parameters. 58

Figure 3.21 The measured vs. the calculated signal frequency. 58
Figure 3.22 Signal propagation across a Y_g/Δ transformer (P-P signaling). 59
Figure 3.23 Signal propagation across a Y_g/Δ transformer (P-G signaling). 60
Figure 3.24 The original signal detection algorithm. 61
Figure 3.25 The spectrum-based detection algorithm. 62
Figure 3.26 The simulated signals of various frequencies. 63
Figure 3.27 The detection results of the spectrum-based algorithm. 64
Figure 3.28 The waveforms of signal templates. 65
Figure 3.29 The detection results of the template-based algorithm. 66

Figure 4.1 The field test arrangement. 68
Figure 4.2 The installation of the signal generator at the substation. 69
Figure 4.3 Sample waveforms of the carrier voltage and the anti-islanding signals. 70
Figure 4.4 The signal strength during the field test period. 71
Figure 4.5 The dominant signal frequency during field test period. 71
Figure 4.6 A sample of measured anti-islanding signal (Sep. 26, 00:01:22). 72
Figure 4.7 A sample warning event caused by disturbances (Oct. 19, 17:19:32). 73
Figure 4.8 A normal signaling event (Sep. 25 22:55:10). 73
Figure 4.9 The spectra and RMS_h of typical signaling periods. 74
Figure 4.10 The $\sin(\theta_h)$ plot for polarity determination. 75
Figure 4.11 RMS_i of signaling/non-signaling cycles from 31 records. 75
Figure 4.12 Performance of the *RMS*-based algorithm. 76
Figure 4.13 Performance of the spectrum-based algorithm. 76
Figure 4.14 Performance of the template-based algorithm. 76
Figure 4.15 Statistical performance of the *RMS*-based algorithm. 77
Figure 4.16 Statistical performance of the spectrum-based algorithm. 77
Figure 4.17 Statistical performance of the template-based algorithm. 78
Figure 4.18 The distribution of signal to noise ratios. 78
Figure 4.19 Parallel operation of anti-islanding and AMR schemes. 79
Figure 4.20 SG vs AMR signal strength. 80
Figure 4.21 A sample anti-islanding signal. 81
Figure 4.22 AMR signal strength vs. phase angle. 81
Figure 4.23 A warning event caused by AMR signals (Oct.19 17:12:32). 82
Figure 4.24 A record with both SG and AMR ON. 82
Figure 4.25 A warning event caused by AMR signals (Sep. 27, 08:31:19). 83
Figure 4.26 A sample nuisance starting event (Oct. 21, 18:37:48). 83

Figure 5.1 A sample system using power-line-signaling based islanding detection. 87
Figure 5.2 The architecture of the new signal generator (one phase illustration). 88
Figure 5.3 Transient voltage and current signals with SG connected to the main supply. 88
Figure 5.4 Illustration of possible influence of shunt capacitors. 89
Figure 5.5 The PSCAD simulation system. 89
Figure 5.6 The system responses to SG firing in normal condition. 91
Figure 5.7 The system responses to SG firing in SG isolated condition. 91
Figure 5.8 Spectra of the upstream current signals. 91
Figure 5.9 Analysis of the upstream transient current signal. 92

Figure 5.10 The virtual voltage and current source (a) waveforms and (b) spectrum. 93
Figure 5.11 Spectra of upstream current signals calculated with MATLAB. 94
Figure 5.12 The shunt capacitor's impact of on the DC detection criterion. 95
Figure 5.13 Sensitivity study of the DC detection criterion. 96
Figure 5.14 Upstream current signal spectra under two capacitor grounding patterns. 97
Figure 5.15 The sequential circuit for transient current analysis. 97
Figure 5.16 The upstream current signals in normal and SG isolated conditions. 98
Figure 5.17 The spectra of upstream current signals obtained in laboratory tests. 99
Figure 5.18 The DC criteria in laboratory tests. 99

Figure 6.1 A linear network and its transient responses. 105
Figure 6.2 The proposed harmonic impedance measurement method. 106
Figure 6.3 The subtraction method for signal extraction. 107
Figure 6.4 Examples of SG topology for measuring three-phase systems. 108
Figure 6.5 The 120V single-phase simulation system. 110
Figure 6.6 The 120V system responses during SG firing. 110
Figure 6.7 The measured vs. expected supply system harmonic impedance. 110
Figure 6.8 The measured vs. expected load harmonic impedance. 111
Figure 6.9 The 3-phase 25kV simulation system. 112
Figure 6.10 System responses during SG firing; the spectra of thyristor currents. 112
Figure 6.11 Measurement results using events with a single firing angle of 10°. 113
Figure 6.12 Measurement results using events with a single firing angle of 20°. 113
Figure 6.13 Measurement results using events created with both firing angles. 114
Figure 6.14 The 3-phase 120V experimental system configuration. 115
Figure 6.15 The 3-phase 120V experimental system measurement results. 116
Figure 6.16 The criterion for reliable measurements. 117
Figure 6.17 Transient analysis using the injection of a virtual voltage source. 118
Figure 6.18 The peak voltage transient vs. the peak thyristor current. 120
Figure 6.19 Grid impedance measurement for DG islanding detection. 120

Figure 7.1 The analysis circuit for created transient current signals. 124
Figure 7.2 Faulted line identification based on steady-state zero-sequence currents. 126
Figure 7.3 Faulted line identification based on zero-sequence active power flow. 127
Figure 7.4 Illustration of the proposed scheme. 132
Figure 7.5 The controllable grounding device (a) structure and (b) system responses. 132
Figure 7.6 The controllable grounding device connected at PT secondary side. 133
Figure 7.7 The extraction of transient current signals. 134
Figure 7.8 The analysis circuit for neutral voltage rise caused by ground fault. 135
Figure 7.9 Analysis of transient current signals in an ungrounded system. 137
Figure 7.10 The analysis circuit for created transient current signals. 138
Figure 7.11 The responses of the ungrounded system with R_f=250ohm and δ=150°. 140
Figure 7.12 Responses of the ungrounded system with R_f=1000ohm and δ varies. 141
Figure 7.13 Responses of the ungrounded system with R_f=1000ohm and δ varies. 142
Figure 7.14 Responses of the resonant grounded system with R_f=1000ohm. 143
Figure 7.15 The spectra of the transient current signals. 144
Figure 7.16 Sensitivity study with respect to δ, R_f and Line number. 146

Figure 7.17 The transient current signals for the lab test system. 147
Figure 7.18 The spectra of transient current signals in the lab test. 148
Figure 7.19 The circuit for calculating the voltage disturbance. 148
Figure 7.20 The current criterion vs. the voltage disturbances. 149

Figure B.1 The 3-phase simulation system. 165

LIST OF SYMBOLS

AC	Alternating Current
AMR	Automatic Meter Reading
ASF	Active Shunt Filter
CT	Current Transformer
DC	Direct Current
DFT	Discrete Fourier Transform
DG	Distributed Generators
DVR	Dynamic Voltage Restorer
DSTATCOM	Distribution Static Synchronous Compensator
FACTS	Flexible AC Transmission Systems
HVDC	High Voltage Direct Current (system)
LV	Low Voltage
PEST	Power Electronics Based Signaling Techniques
PT	Potential Transformer
PV	Photovoltaic
RMS	Root Mean Square
ROCOF	Rate of Change of Frequency
SD	Signal Detector
SSSC	Static Synchronous Series Compensator
SG	Signal Generator
STATCOM	Static Synchronous Compensator
TCR	Thyristor-Controlled Reactor
TCSC	Thyristor-Controlled Series Capacitor
TSC	Thyristor-Switched Capacitor
TWACS	Two-Way Automatic Communication Systems
UPFC	Unified Power Flow Controller
UPQC	Unified Power Quality Controller
VSR	Voltage Surge Relay
δ	The electric angle between the thyristor firing instant and the coming thyristor voltage zero-crossing-point, also denoted as the thyristor firing angle
RMS_h	The spectrum-based signal detection index defined in (3.16)
RMS_t	The template-based signal detection index defined in (3.20)

Chapter 1. INTRODUCTION

The power electronics revolution since the 1950s has been driven by the demand for fast controllers in the power industry and the attempts in the semiconductor industry to produce devices with greater power-handling capabilities. Power electronics behave as a bridge between the traditional power industry and electronics technology. A combination of power electronics devices, such as thyristors, configured in different circuits and controlled with appropriate electronic signals, can switch on and off high-power circuits and accomplish a variety of functions. Currently, power electronics are playing an important role in modern technology and are still undergoing fast development.

Power electronics have been applied to a great variety of areas, including heat controls, light controls, motor controls, power supplies, vehicle propulsion systems, high-voltage direct current (HVDC) systems, flexible ac transmission systems (FACTS) and active shunt filters. In these applications, power electronics devices either condition the electric energy to suit the needs of various loads, or manipulate the electric energy to increase the transmission capability or improve the power quality. To summarize, power electronics deal with the conversion and transmission of electric energy in these applications. In recent years, a different type of power electronics applications has emerged, in which power electronics is utilized to create small but discernible signals for communication, online monitoring, diagnosis and other information-related purposes. The research conducted in this thesis is related to this type of applications.

This chapter presents a review of the state-of-the-art power electronics application in power systems that deal with energy transmission and conversion. The new stream of applications is then introduced in which power electronics deal with information. The main objectives and the outline of the thesis are also presented.

1.1 Conventional Power Electronics Applications to Power Systems

The power electronics technology evolving since the 1950's behaves as a bridge between the traditional power industry and electronics technology. "Power" means the static and rotating power equipment for the generation, transmission, distribution and conversion of electric power. "Electronics" means the low-power solid-state devices and circuits designed for the desired control objectives. "Power electronics" can be defined as a combination of power semiconductor devices, such as thyristors, configured in many different ways in circuits with appropriate electronic control signals, to switch on and off high-power circuits and accomplish AC to DC or DC to AC conversion, frequency conversion, switching, reactive power generation and many other potential applications.

Power electronics have been widely applied to power systems and motor drive and have resulted in innovative changes in these areas. Table 1.3 summarizes the existing power electronics applications in these two areas [1].

TABLE 1.1 A SUMMARY OF POWER ELECTRONICS APPLICATIONS

Application Area	**Application Category**	**Application Examples**
Power systems	HVDC	* AC to DC converters and DC to AC inverters
	FACTS and Custom Power	* Thyristors as static switches in TCR, TSC, SVC and TCSC * Voltage Source Inverters in STATCOM , SSSC, and UPFC * Voltage Source Inverters in DSTATCOM, DVR, and UPQC
	Distributed generation and storages	* Inverters for interconnecting photovoltaic generators to the main grid * Rectifier and converter cascades to convert the variable frequency and voltage outputs of asynchronous wind generators to constant frequency and voltage outputs * DC-DC chopper to adapt rectifier output to the grid interface inverter
	Protection	* Thyristor-protected series capacitors, thyristor-based ferroresonance suppression, etc.
Motor Drive	AC drives	* Cycloconverter and matrix converter for direct AC-AC conversion (induction and synchronous motors) * PWM VSI (voltage source inverter) drive, and CSI (current source inverter) drive * Motor soft starters using thyristors
	DC drives	* Phase-controlled rectifiers for providing variable armature voltages * Diode rectifiers in cascade with dc choppers for providing variable armature voltages

In the above applications, power electronics circuits are adopted in power systems to facilitate the transmission of electric energy by transforming the form of energy or providing regulations to the AC power flow. Power electronics circuits also participate in the generation of electric energy by providing modulated excitation current. In the motor drive area, power electronics is used to alter the electric energy conversion process to meet various drive requirements. These applications are all used to manipulate the transmission and conversion of electric energy in order to improve the efficiency and performance.

1.2 Online Signaling-Oriented Power Electronics Applications

In recent years, a new stream of power electronics applications has emerged, in which power electronics devices are controlled to manipulate electric power circuits and create small but discernible disturbance signals online. These signals are used for communication, online monitoring, fault diagnosis, and other signaling-oriented purposes. Table 1.2 summarizes these applications. A detailed literature review will be performed for these applications in Chapter 2.

TABLE 1.2 SIGNALING-ORIENTED POWER ELECTRONICS APPLICATIONS

Application Area	**Application Examples**
Communication	Distribution automation such as Automatic meter reading (AMR) and load control using TWACS or Hunt Technologies
Online monitoring	* System harmonic impedance monitoring using active shunt filters for filter control. * Grid impedance monitoring using inverters of photovoltaic (PV) systems for islanding detection. * Motor stator resistance monitoring using soft-starter circuits for thermal protection
Fault Detection	Using power-electronics-based active signal injection scheme to realize: * Ground fault detection in the ungrounded DC field circuits. * Ground fault locating in ungrounded industrial systems or distribution systems. * 100% ground fault protection for the stator of large generators.

One type of application is power line communication techniques designed for distribution automation purposes such as automatic meter reading (AMR) and load control. Power electronics devices, such as thyristors, play an important role in some techniques. They create small and controllable disturbance signals that propagate along distribution lines and are used for communication between the utility and customers. A representative of this type of application is the zero-crossing-distortion technique designed for AMR.

Other types of signaling-oriented applications are online system parameter monitoring and fault diagnosis. In these applications, power electronics circuits are utilized to inject special disturbances into the power system. The system parameters can be monitored online according to the measured responses. According to the monitoring results, some fault conditions can be diagnosed. Examples include multiple grid impedance measurement techniques and ground -fault-locating techniques in ungrounded systems.

In the above signaling-oriented applications, power electronics circuits are used to manipulate not electric energy, but signals and information. Therefore, we regard them as a new stream of applications parallel to and equally important as the traditional applications dealing with electric energy. We denote this stream of applications as "power-electronics-based online signaling techniques" (PEST) and believe that these techniques have many potential applications in power systems.

1.3 Challenges Faced by Power Systems

Power systems are currently faced with many challenging problems. One example is the detection of islanded distributed generators (DGs). An island forms when a portion of the distribution system becomes electrically isolated from the remainder of the power system, yet continues to be energized by distributed generators. Islanded DGs may cause severe safety hazards and therefore must be detected and tripped in a timely manner. Detection of islanded DGs, especially synchronous DGs, is a significant technical barrier for the DG industry. The most common devices used for islanding detection function by monitoring the frequency and/or voltage drifts in an island caused by the imbalance between the generation and the load. However, if the generation and load mismatch is small, these devices cannot function properly or quickly enough [31]. Recent research efforts have focused on schemes that require injecting small disturbances, or transmitting special signals into the systems.

Another example of the challenges faced by the power industry is the locating of single-phase-to-ground faults in ungrounded, high-resistance grounded or resonant grounded systems. When a single-phase-to-ground fault occurs, the above systems can continue operating without tripping immediately. Later after the fault is located, it can be cleared at a convenient time, resulting in minimized losses. However, identifying the faulted line in the above systems is very challenging since the systems produce very small ground fault currents. The existing methods utilizing the steady-state fault currents for fault locating have common problems in accuracy. Also, methods relying on the transient fault currents for identification have low reliability since the transient signals are highly random and non-repeatable. In recent years, researchers have started to locate the fault by injecting special disturbances.

The third example is online monitoring of supply system harmonic impedance values. Online system harmonic impedance data are highly useful in applications such as the control of active shunt filters and the setting of DG anti-islanding protection relays. Among the existing impedance measurement methods, some use natural or equipment-switching-caused variations or disturbances in voltages and currents for impedance determination. These methods are dependent on the availability of the disturbance sources and have poor control of the disturbances generated. Therefore, these methods are inconvenient for continuous monitoring. Methods relying on dedicated power -electronics-based disturbance generators are regarded as more promising.

The common features of the above problems are that they cannot be satisfactorily solved by using traditional passive-measurements-based methods. Moreover, the methods that work by injecting special disturbances signals into power systems tend to provide better performance for the above problems. In view of the potential and flexibility of using power electronics circuits to create signals online in power systems, we plan to design effective and economical solutions to the above problems by using power-electronics-based signaling techniques.

1.4 Research Objectives

This research work focuses on utilizing power-electronics-based online signaling techniques (PEST) to develop effective solutions to the challenges in power system monitoring and fault diagnosis. The objectives of this research work are summarized below:

1. Investigate a power-line-signaling-based islanding detection scheme for distributed generators; design a signal generation device by using a carefully selected PEST, and devise corresponding signal detection algorithms; verify the validity of the entire scheme through extensive field tests; develop variations of the above islanding detection scheme to suit different DG interconnection scenarios.
2. Design an online harmonic impedance measurement device by using a selected PEST; test the device's effectiveness through laboratory

experiments.

3. Develop a faulted line identification scheme in noneffectively grounded distribution systems by using a selected PEST, and test the scheme through theoretical analysis and lab experiments.

1.5 Thesis Contributions and Outline

The objectives outlined in the previous section have been successfully achieved. By using one selected power-electronics-based signaling technique, effective solutions have been found for the three problems reviewed in Section 1.3. This thesis presents the research work and is organized as follows.

Chapter 2 presents a detailed literature review of various power-electronics -based online signaling techniques designed to solve problems in communication, online monitoring and the fault diagnosis of power systems.

Chapter 3 introduces the problem of DG islanding detection and proposes the concept of power-line-signaling-based islanding detection. This concept involves broadcasting a signal from a substation to the DG sites by using the distribution feeders as the signal paths. A DG is considered as "islanded" from the upstream system if the signal cannot be detected at the DG site. A PEST named "zero -crossing-distortion" is chosen to generate the signals. This chapter then studies the signal generator design considerations and signal characteristics in distribution networks. Signal detection algorithms are devised according to the signal characteristics. This study was published in [71].

Chapter 4 introduces the field tests results of the power-line-signaling-based islanding detection scheme. The performances of three signal detection algorithms are evaluated, and the algorithms making use of signal frequency features are found to detect signals more reliably than the other algorithm [72].

Chapter 5 studies a scalable variation of the above power-line-signaling -based islanding detection scheme. The new scheme locates the signal generator anywhere between the substation and DG to suit various DG interconnection scenarios and achieve flexibility. The signal generator can detect its connection status to the main grid according to a transient current signal extracted at its upstream side. Laboratory test results are shown about the scalable scheme [73].

Chapter 6 presents a device for online harmonic impedance measurement. This device injects controllable current signals into the system by using the zero

–crossing-distortion technique. The system harmonic impedance is thereby measured according to the system responses. A criterion is established for determining the range of reliable measurements [74].

Chapter 7 introduces a method for identifying the line experiencing a single-phase ground fault in noneffectively grounded systems. This method overcomes the difficulty of very small fault currents by temporarily creating a controlled grounding of the system neutral. The result is a controllable ground fault current that is large enough for identifying the faulted line and yet small enough not to cause system problems. This method is verified through analysis, simulations, and lab tests [75].

Chapter 8 presents the thesis' conclusions and recommendations for future research.

Chapter 2. POWER-ELECTRONICS-BASED ONLINE SIGNALING TECHNIQUES

In recent years, researchers have sporadically used power electronics for communication, measurement, monitoring and other online signaling-oriented purposes. This chapter reviews these applications in categories, and summarizes what these applications have in common. As well, it's proposed that more potential applications exist in these areas. This chapter also identifies a thyristor-based signaling technique as a promising online signaling circuit that may be used to design new applications.

2.1 Power Electronics Applications to Power Line Communication

The need for distribution automation has driven the development of a variety of communication techniques using the power line as the signal carrier. In many of these techniques, power electronics circuits play key roles. These circuits are utilized to create signal patterns that propagate along power lines and are used for communication purposes. This section introduces several representative examples.

2.1.1 Zero-Crossing-Shift Technique

One of the early power line signaling technologies creates a slight shift on the selected zero-crossing points of the carrier voltage waveform [3]. The existence of the shift would represent digital "1" and no shift digital "zero". This technique is intended to generate outbound signals propagating from utility substations to customers connected to distribution feeders. The signaling is achieved by injecting a small modulation voltage, which is about 1% of the feeder voltage and is phase-shifted, to cause a zero-crossover-deviation in the feeder voltage waveform (see Figure 2.1). A modulation transformer energized by alternate phases of the 3-phase power source provides the modulation voltage. For instance, to modulate phase A, one can use phase B to C line voltage. The created zero-crossing-shifts can propagate along the distribution network and be received at customer locations.

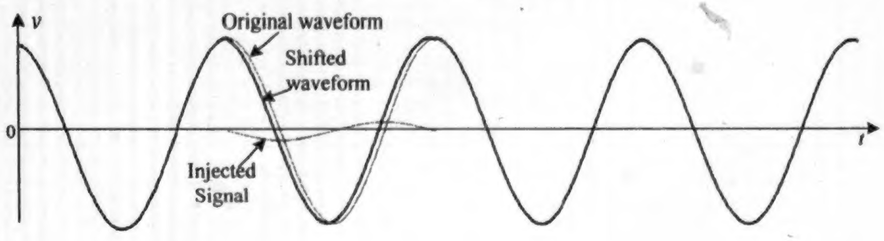

Figure 2.1 A zero-crossing-shift by injecting a single-cycle modulation voltage.

Power electronics switches are adopted to inject the modulation voltage with accurate timing. A basic circuit is shown in Figure 2.2, in which a modulation voltage is injected into phase A voltage. This circuit consists of a shunt arm and a series arm, and each arm comprises a pair of anti-parallel connected thyristors. When no signaling occurs, gates 3 and 4 are continuously triggered to allow passage of the current in phase A while gates 1 and 2 are off. In the signaling condition, gates 3 and 4 are de-energized but 1 and 2 are active to inject a single-cycle voltage into phase A.

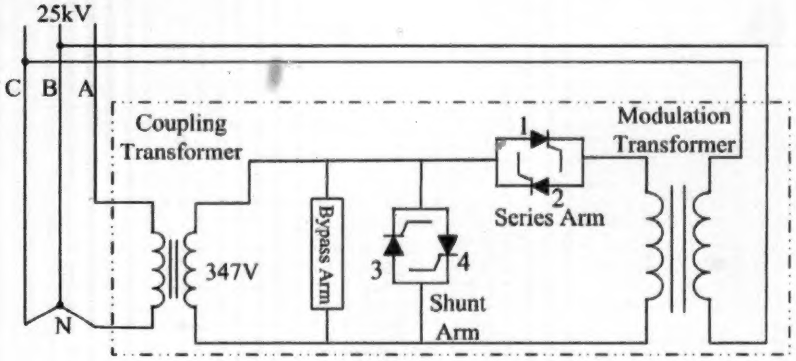

Figure 2.2 A basic implement circuit for the zero-crossing-shift.

2.1.2 Zero-Crossing-Distortion Technique

Another technique named "zero-crossing-distortion" creates a power line communication signal through a controlled short-circuit around the voltage waveform zero-crossing point. This technique patented by TWACS (Two-Way Automatic Communication System) was designed for both outbound (from a substation to the customers) and inbound (from customers to the substation) signaling [4][5]. Figure 2.3(a) shows the configuration for outbound signaling. A thyristor (or a pair of thyristors) are shunt connected to the MV bus of a substation through a stepdown transformer. The thyristor is triggered ahead of its voltage zero crossing point and conducts for a short period. During the conduction, a current pulse is drawn from the supply, and the supply voltage is modulated by a small but detectable distortion signal. This voltage distortion signal can propagate along the distribution lines to remote customers and be used as outbound signals. A disturbance implies a digital "1"; no disturbance implies a digital "0".

For inbound signaling, the device is installed at customer side and works on the same principle. During the thyristor conduction around the voltage zero-crossing point, a pulse current is drawn from the supply system. This pulse current can be detected at the substation as information carrier. In typical applications, the pulse current has a peak of 150A at 120V level and a width about 90°. At the 25kV level, the pulse has a peak of 1.25A. Although this disturbance is extremely small in comparison with the normal feeder current of 100A to 200A, modern signal processing technology has no problem to extract it.

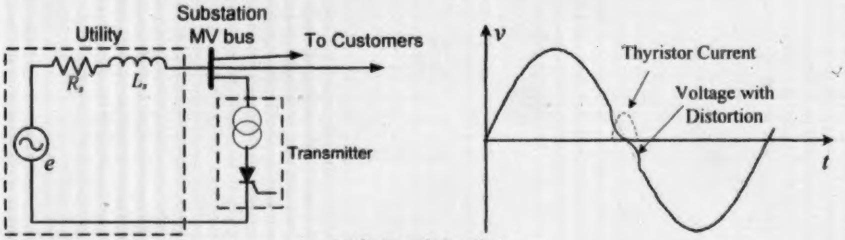
Substation
MV bus
Utility
To Customers
R_s
L_s
e
Transmitter
v
Thyristor Current
Voltage with Distortion
t

(a) Outbound signaling;

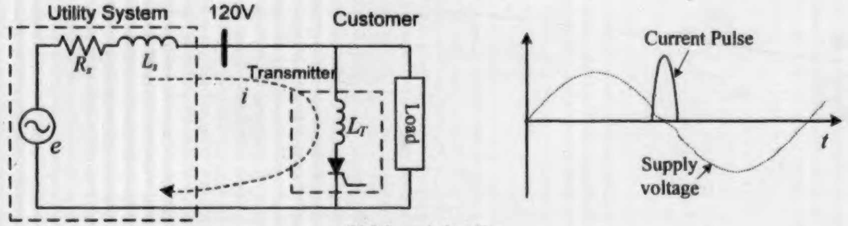
Utility System
120V
Customer
R_s
L_s
Transmitter
i
L_T
Load
e
Current Pulse
Supply voltage
t

(b) Inbound signaling.

Figure 2.3 The zero-crossing-distortion (a) signaling circuit and (b) waveforms.

2.1.3 Ripple Control

Ripple control is also a power line communication technique developed for load control in distribution networks [7]. Figure 2.4 shows the transmitter configuration of this technique.

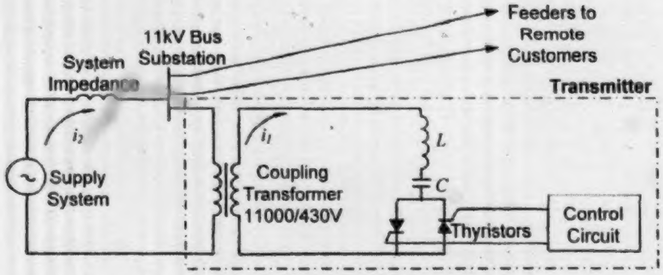

Figure 2.4 The one-phase configuration of ripple control technique.

Inside the transmitter, an inductor in series with a capacitor is controlled by a pair of anti-parallel connected thyristors and fed via a distribution transformer. The thyristors are alternately fired at the desired signal frequency (for example, 819200 Hz). Once a thyristor is fired, a current pulse is drawn from the supply, which goes to zero before the other thyristor is fired, because the L-C resonance frequency is tuned to be 15% to 25% higher than the signal frequency. The thyristor-off period between thyristor conductions enables the L-C circuit to receive energy from the supply and maintain oscillations. The transmitter oscillatory current (see Figure 2.5) produces a voltage distortion on the substation secondary bus (11kV). This voltage signals propagate along the distribution feeders and can be detected as a load control signal.

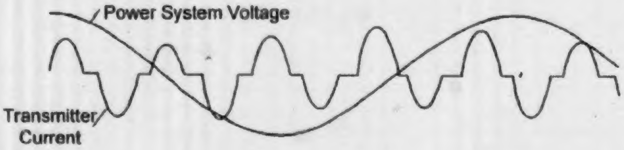

Figure 2.5 The ripple control transmitter current and substation voltage waveforms.

2.1.4 Hunt Technologies

Hunt technologies provide full-duplex communications between an electric power distribution station and a power consumer via the power distribution line at frequencies below the power frequency [8]. This technology is used in the USA for AMR and load control, etc. The principle of the transmitter is to couple a frequency-modulated voltage control signal to the 60Hz distribution system. The first frequency of the voltage control signal (say, 20Hz) represents a binary "1" and a second frequency (say, 15Hz) represents a binary "0". In one embodiment, a voltage control signal is injected between the distribution transformer neutral and the ground. This low-frequency voltage control signal is derived from a 60Hz phase-to-ground voltage waveform by using the circuit in Figure 2.6.

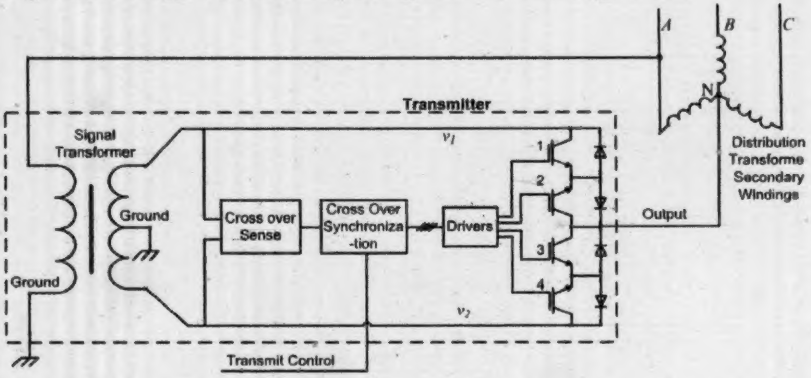
A
B
C
N
Transmitter
Signal Transformer
Ground
Ground
Cross over Sense
Cross Over Synchroniza-tion
Drivers
v_1
v_2
1
2
3
4
Output
Distribution Transforme Secondary Windings
Transmit Control

Figure 2.6 The low frequency bilateral power line communication system.

The transmitter is supplied by a signal transformer connected to the substation secondary side, say, between phase A and the ground. This signal transformer has two secondary low voltage windings that output two voltages of opposite phases, i.e., $v_1 = -v_2$. Four power transistors (1, 2, 3 and 4) are controlled to conduct alternatively, forcing the output voltage to be equal to v_1 or v_2. A low-frequency output voltage signal of 20Hz or 15Hz is therefore derived (see Figure 2.7(a)) and injected between the neutral and the ground. The power transistor trigger signals are generated by a crossover synchronization block (see Figure 2.7(b)) according to a transmit control signal as well as a voltage crossover sense result (see Figure 2.7(a)). For example, when the transmit control is 0 ("L") and the crossover synchronization result is 1 ("H"), transistor 3 is triggered to make the output equal to v_2.

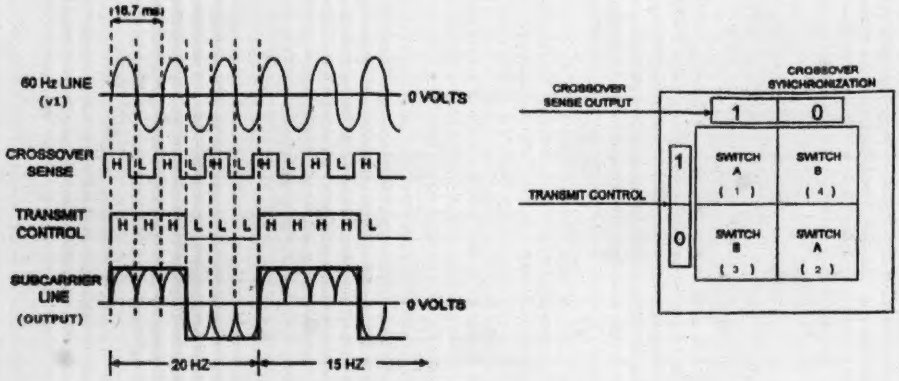
16.7 ms
60 Hz LINE (v1)
0 VOLTS
CROSSOVER SENSE
H L H L H L H L H L H
TRANSMIT CONTROL
H H H L L L H H H H L
SUBCARRIER LINE (OUTPUT)
0 VOLTS
20 HZ
15 HZ
CROSSOVER SENSE OUTPUT
CROSSOVER SYNCHRONIZATION
1
0
TRANSMIT CONTROL
1
0
SWITCH A (1)
SWITCH B (4)
SWITCH B (3)
SWITCH A (2)

(a) (b)

Figure 2.7 The signal waveforms and trigger signal generation of Hunt technologies.

Power-Electronics-Based Online Signaling Techniques

Four power line signaling techniques have been reviewed in which power electronics devices play an important role. Thyristors or power transistors are utilized to create signal patterns and couple them to a distribution system. These signals can propagate along distribution lines and be used for communications between a utility substation and customers.

The above circuits have been applied to

- Distribution automation including AMR, load control.
- DG islanding detection (Hunt technology).

Two types of methods have been used to create communication signals. The series type directly inserts a voltage disturbance signal to the main circuit, such as the zero-crossing-shift and the Hunt technology. The shunt type draws disturbance current signals from the power supply and therefore causes voltage distortions of the supply. Examples include the zero-crossing-distortion, and the ripple control technique. In the second type of method, either the current signals or the voltage distortions can be adopted for communications.

2.2 Power Electronics Applications to Online Monitoring

Power electronics circuits have been used to create signals for the online monitoring of power system or motor parameters. Power system or motor parameters such as the system impedance or the stator resistance represent the system conditions. Their online updated values are highly desired for controller setting or protection purposes. Power electronics circuits are used to inject special disturbance signals into the system. The system parameters can therefore be measured according to responses to the disturbances. This section introduces several power-electronics-based online monitoring techniques.

2.2.1 Converter-Based Harmonic Impedance Measurement

The supply system harmonic impedance values are highly desirable for the normal operation of active shunt filters (ASFs). After an ASF measures the voltage distortions at its point of common coupling (PCC) to the system, it needs the system harmonic impedance values to calculate how many harmonic components should be injected into the system to cancel out the voltage distortion.

Reference [9] proposed a method of using a PWM-converter-based ASF to measure the supply system harmonic impedances online (see Figure 2.8). With this method, the converter is controlled to inject a very short current spike into the point of connection. The width and height of the spike can be fully controlled to minimize the disturbance on the grid. The system harmonic impedance can therefore be calculated as follows according to the injected current spike $i(t)$ and the captured system voltage response $v(t)$:

$$Z(f) = \frac{F(v(t))}{F(i(t))}, \tag{2.1}$$

where "F" denotes the discrete Fourier transform (DFT), and $F(v(t))$ and $F(i(t))$ denotes the DFT results of $v(t)$ and $i(t)$, respectively. The harmonic impedance measurement can be incorporated into the normal operation of an ASF and be performed at intervals.

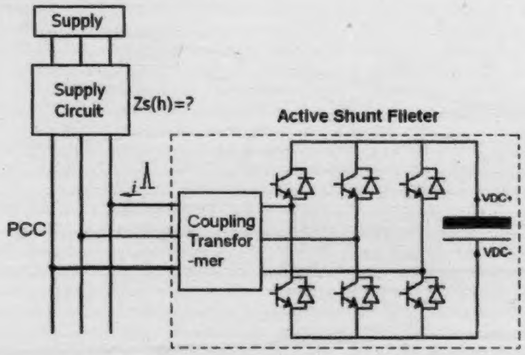

Figure 2.8 Harmonic impedance measurement based on inverter injection.

2.2.2 Grid Impedance Measurement for Islanding Detection

In recent years, researchers have become interested in online monitoring of the system impedance for the purpose of islanding detection of distributed generators (DG). The problem of islanding detection will be explained in detail in Chapter 3. A power island forms when a distributed generator becomes isolated from the utility grid. An increase in the system impedance at the DG site is regarded as an indication of an islanding condition. According to European standard, the supply must be isolated within 5 seconds following an impedance increase of 0.5Ω [10].

Many methods have been developed for various types of DGs to detect islanded conditions. Since photovoltaic (PV) type DGs are interconnected to the distribution network via an inverter interface, they can be easily controlled to inject special current signals into the system for system impedance monitoring. Therefore, several impedance-monitoring-based islanding detection methods have been devised for these generators. Because of the large difference between impedances with and without the supply system, accurate impedance measurement is not necessary.

Reference [11] proposes using the inverter to directly inject a 75Hz noncharacteristics harmonic current into the grid (see Figure 2.9). The system impedance can therefore be measured. Reference [13] proposes injecting a negative sequence current into the system and detecting islanding according to the measured system negative-sequence impedance.

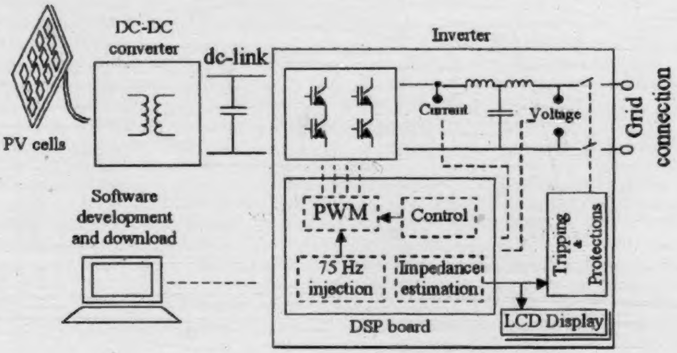
DC-DC converter
dc-link
Inverter
PV cells
Current
Voltage
Grid connection
Software development and download
PWM
Control
75 Hz injection
Impedance estimation
Tripping
Protections
DSP board
LCD Display

Figure 2.9 PV inverters injecting harmonics for grid impedance monitoring.

Reference [14] proposed using a pair of shunt-connected thyristors connected at the DG terminal (see Figure 2.10) for grid impedance measurement. A thyristor creates a short circuit around the voltage zero crossing point. For example, it can be fired 10° ahead of the voltage zero point. The system impedance can be calculated according to the magnitude of the current pulse drawn by the thyristors. This method suits all types of DGs.

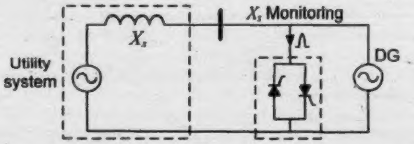
X_s
X_s Monitoring
Utility system
DG

Figure 2.10 The thyristor-based circuit for measuring the system impedance.

2.2.3 Online Motor Thermal Protection

Power electronics circuits have been applied to the online monitoring of motor parameters. Motor stator resistance (*Rs*) varies proportionally to stator winding temperature, and its online estimated value can be used for motor thermal protection.

For soft-started machines, reference [16] proposes a method that utilizes the soft-starter to inject DC components into the motor terminals and measure *Rs*. The basic structure of a soft-starter is shown in Figure 2.11. A soft-starter uses anti-parallel thyristors to control the current flow and, in turn, the terminal voltages of the motor. The soft-starter limits overvoltages, avoids large inrush currents and results in a "soft" motor start.

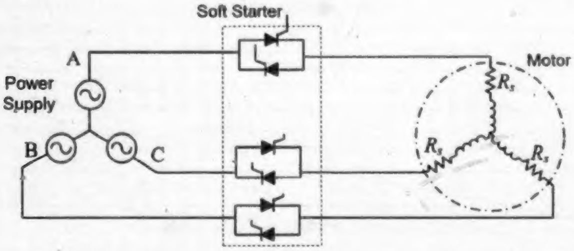

Figure 2.11 The structure of a motor soft-starter.

In order to inject DC components into motor terminals, only one phase (e.g., phase A) of the soft-starter is kept open, while the other two phases are kept in a bypass mode. A short delay is introduced to the gate drive signal of only the backward-conducting thyristor of phase A. Figure 2.12(a) shows the typical waveforms of the motor line voltage (v_{ab}), phase current (i_a) and the gate drive signals of the anti-parallel thyristors (v_{G1} and v_{G2}), while a small delay angle of α is added. According to the equivalent circuit of the induction motor in Figure 2.12(b), the motor stator resistance R_s can be estimated from the terminal voltages and currents by using

$$R_s = \frac{2 \cdot v_{ab}^{dc}}{3 \cdot i_a^{dc}}. \tag{2.2}$$

The motor torque pulsation caused by DC injection can be kept within an acceptable level by using a small enough delay angle α.

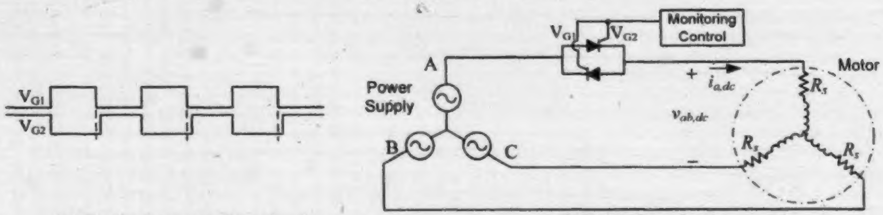

(a) The thyristor gate drive signals; (b) Equivalent circuit.

Figure 2.12 Online motor stator resistance monitoring using the soft-starter.

For machines directly connected to three-phase supplies, reference [15] proposes connecting an external circuit shown in Figure 2.13(a) between the supply and motor terminals of one phase for dc current injection. This external circuit consists of a *n*-channel enhancement-type power MOSFET and an external resistor (R_{ext}) connected in parallel. During the dc injection mode, the MOSFET is turned off when $i_{as} > 0$ and turned on when $i_{as} < 0$. The equivalent circuit for this case is shown in Figure 2.13 (b). The asymmetrical resistance causes the voltage drop across the circuit to be asymmetrical, resulting in the injection of a dc current component into the motor. During the normal operation mode, the MOSFET is always turned on, and there is no dc bias injection.

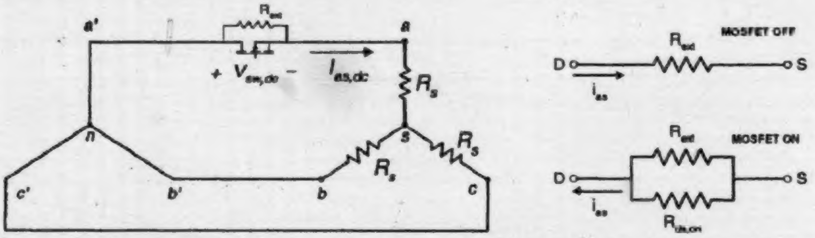

(a) schematic (b) the equivalent circuit in DC injection mode

Figure 2.13 Online motor stator resistance monitoring using an extra circuit.

In this section, power electronics circuits are applied to inject disturbances and monitor system parameters. An important concern for these applications is that the injected disturbance must be controllable and have a negligible impact on the system normal operation. In this way, the measurement can be performed online at intervals. Incorporate the disturbance injecting circuit into existing devices and making the measurement nonintrusive is desirable.

2.3 Power Electronics Applications to Fault Detection

Power electronics circuits also have applications in online fault detection. These circuits are utilized to inject small but discernible signals to the system in operation. If a fault exists in a system, the system response will be different from that of a sound system. The fault can therefore be detected.

This section reviews one type of application to fault detection: the ground fault detection in ungrounded or noneffectively grounded AC or DC circuits. In an ungrounded AC or DC circuit, a ground fault causes little fault current and does not interrupt the operation of the circuit. However, the ground fault must be located and cleared in a timely manner to avoid further insulation deterioration. Detecting a ground fault in an ungrounded circuit is difficult. Many power –electronics-based techniques have been designed to inject special signals into the circuit to facilitate the detection. This section will present several ground fault detection techniques used for four different cases.

2.3.1 Faulted Line Locating in Ungrounded Systems

The power distribution networks in some European and Asian countries, and some industrial power systems in North America are ungrounded, high resistance grounded, or resonant grounded. These systems can continue to operate when a single-phase -to-ground fault occurs. Later when the fault is located, it can be cleared at a convenient time, resulting in minimized losses. However, identifying the faulted feeder among a number of feeders connected to the same bus is difficult since the fault current is very small. This problem will be discussed in detail in Chapter 6. This section reviews several power-electronics-based signaling techniques developed to solve this problem.

A method introduced in [17] works by grounding the distribution system in a pulsating fashion such that a pulsating ground current is produced in the original ground fault path. As shown in Figure 2.14, the pulsed grounding circuit comprises a power transistor, such as a power MOSFET, connected in series with a limiting resistor between the neutral and the ground. A multivibrator circuit alternately turns on and off the MOSFET. A diode rectifier allows an ac fault current to flow through the MOSFET when a ground fault exists in the system. This current can be easily detected by a sensing circuit due to the current's flickering feature. This fault detection circuit is also operable in ungrounded dc circuits, and the rectifier is no longer necessary in this case.

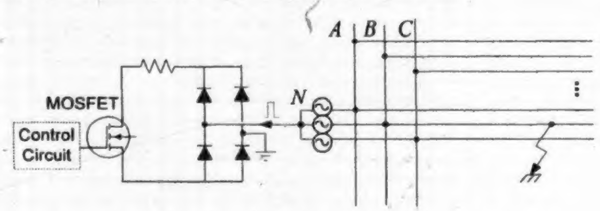

Figure 2.14 A pulsated ground fault detection device.

2.3.2 Generator Stator Ground Fault Detection

By far the most prevalent fault that generators are subjected to is a short circuit to ground. For high-resistance grounded generators, the possibility of fault damage due to overcurrents is greatly reduced. Nevertheless, it is recommended that after a ground fault occurs the generator be immediately tripped off, rather than delaying this action until the generator can be shut down more conveniently. The reason is to avoid a high fault current and major damage to the equipment caused by a second ground fault on either a different phase or the same phase at a different position. A difficulty arises because a traditional overcurrent (or overvoltage) generator ground fault protective scheme cannot detect ground faults near the generator neutral.

It's known in the art a subharmonic signal (10Hz to 20Hz) can be injected for testing a ground fault. However, the generation of such a subharmonic signal requires an expensive amplifier. Reference [18] proposes a power-electronics -based new device that can protect 100% of the generator stator against ground faults. This device works by injecting a modulated test signal into the system. As shown in Figure 2.15, a signaling transformer connected between the system neutral and the ground is used to inject a modulated voltage signal U_v. With two primary windings controlled to conduct alternately by a pair of triacs, this transformer can switch its input between a fundamental voltage v_l and its reverse, i.e., $-v_l$. Each triac is turned on for 45ms, and the 15ms of remaining time serves as a safety redundancy. A large resistor R is connected in series with the signaling transformer secondary winding. When there is no fault, U_v causes no fault current and a zero voltage drop on the resistor R. When a ground fault occurs, a fault current flows through the resistor R, resulting in a voltage drop on R. To detect the fault, the voltage drop across the resistor is multiplied by U_v and then inputted into a filter-performing integration. The integration result will be high when a ground fault occurs and will be used to activate a protection device. Otherwise, the integration value will be zero after a long time.

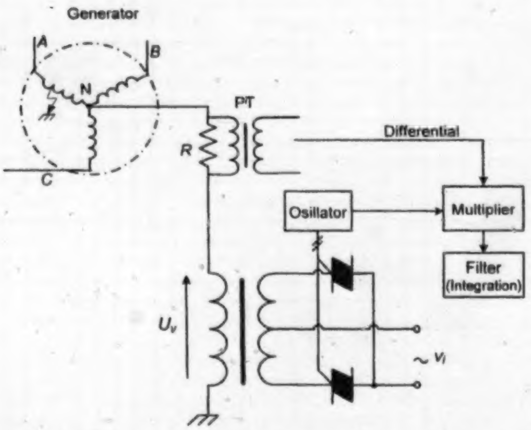

Figure 2.15 A triac-based circuit for generator stator ground fault protection.

The above scheme has several advantages. (1) The fundamental input can be conveniently tapped from the system. (2) The signal generation and the detection method make the scheme immune to random or harmonic noises in the power system. (3) The scheme does not require an expensive amplifier.

2.3.3 Generator Field Circuit Fault Detection

The field circuit of a generator is an ungrounded (typically 600 V) dc system. A single field ground fault generally will not affect the operation of a generator, nor will it produce any immediate damaging effects. However, the probability of a second ground fault occurring is greater after the first ground fault has occurred because the field insulation has deteriorated, and the first ground has established a ground reference. A second ground fault will result in machine vibration and rotor iron heating. Therefore, in the power industry, a ground fault must be detected in a timely manner.

Reference [19] introduces a method that has been widely used in Europe with great success. Similar to the generator stator ground fault detection method in [18], this method injects a ± 15 Volt square wave voltage signal into the field through a coupling network (see Figure 2.16(a)). A signal generator and an amplifier are used to create the square wave signal. The injected frequency setting is adjusted (0.1 to 1.0Hz) to compensate for the field winding capacitance. Since the coupling circuit resistance and the field insulation resistance compose a voltage divider (see Figure 2.16(b)), a relay can calculate the field insulation resistance according to the input and return voltage signals. This method is designed for generators with brushes and uses the slip ring for signal injection into the rotor.

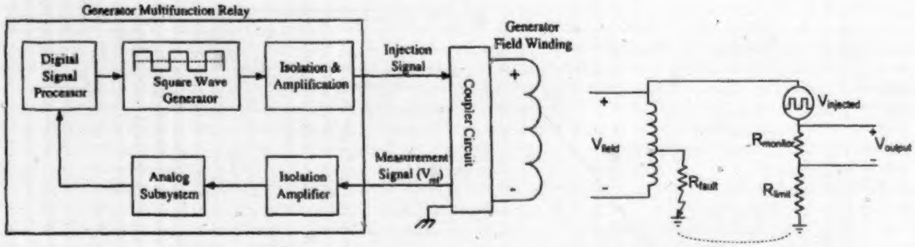
Generator Multifunction Relay
Digital Signal Processor
Square Wave Generator
Isolation & Amplification
Injection Signal
Generator Field Winding
Coupler Circuit
+
-
Measurement Signal (V_{ref})
Analog Subsystem
Isolation Amplifier
V_{field}
$V_{injected}$
$R_{monitor}$
V_{output}
R_{fault}
R_{limit}

(a) (b)

Figure 2.16 A signal injection method for detecting generator rotor ground fault.

2.3.4 Ground Fault Detection for HVDC System's Neutral Line

In a bipolar HVDC transmission system with a neutral line, DC current flows through the converters of both poles, and no current flows through the neutral line during normal operation. In this condition, a grounding fault or breaking of the wire occurring on the neutral line does not affect the operation of the HVDC system. However, if this HVDC system with a neutral line fault is transferred from bipolar to monopolar operation due to, for example, a DC line or converter fault, high level overvoltage might appear and damage equipment in the converter stations. Therefore, a grounding fault or breaking of the neutral line needs to be monitored.

Reference [20] introduces one method that has been successfully used in a Japanese HVDC system. This method injects a small magnitude alternating current (referred to as a "pilot current") into the system through a surge capacitor (see Figure 2.17). This pilot current circulates through the neutral line and the ground in normal condition, and is blocked from flowing into the high voltage line by the smoothing reactor. The pilot current level is monitored at its sending end and at the other terminal. The pilot current at the sending end increases when a grounding fault occurs or decreases when a breaking of the wire occurs. The pilot current at the other terminal decreases when a grounding fault or breaking of the wire along the neutral occurs. By monitoring the change in the pilot current, fault detection can be performed. The pilot current frequency is chosen as 125Hz, in view of the signal attenuation and resonance conditions in the system. A dedicated signal generator is required for the interharmonic injection.

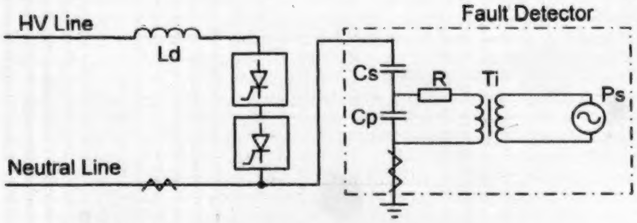
HV Line
Ld
Neutral Line
Fault Detector
Cs
Cp
R
Ti
Ps

Ps: AC power source; Ti: Insulating transformer; Cp: Coupling capacitor; Cs: Surge capacitor; Ld: Smoothing Reactor;

Figure 2.17 A HVDC neutral fault detection system.

2.4 Summary of Online-Signaling-Oriented Applications

The applications reviewed in this chapter are summarized in the flow chart in Figure 2.18.

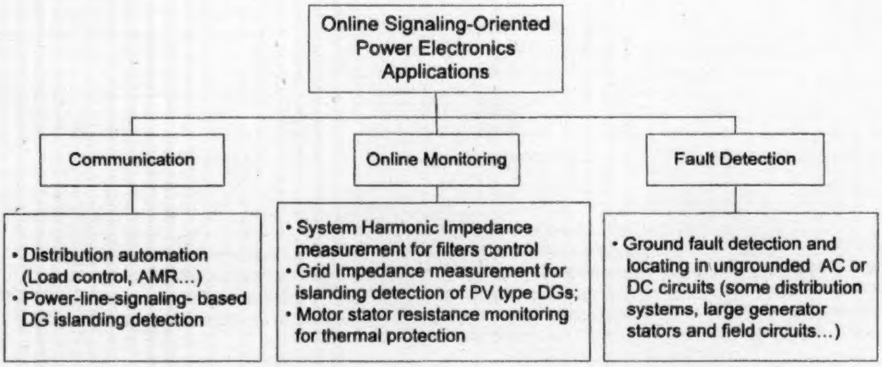
Online Signaling-Oriented Power Electronics Applications
Communication
Online Monitoring
Fault Detection
• Distribution automation (Load control, AMR...)
• Power-line-signaling- based DG islanding detection
• System Harmonic Impedance measurement for filters control
• Grid Impedance measurement for islanding detection of PV type DGs;
• Motor stator resistance monitoring for thermal protection
• Ground fault detection and locating in ungrounded AC or DC circuits (some distribution systems, large generator stators and field circuits...)

Figure 2.18 A classification of power-electronics-based online signaling techniques.

Although the applications reviewed in this chapter have been sporadically developed by different researchers for different purposes, they share commonalties. In these applications, power electronics devices are used to manipulate the voltage and/or current waveforms and to create controllable disturbances in power systems. The disturbances are controlled so that they have not only enough strength to be detected, but also negligible impact on the load normal operations. These disturbances either propagate in power systems and are used to transmit information over distance, or carry system information and are used to monitor system conditions or diagnose faults online. Therefore, unlike other existing applications such as FACTS devices, the applications reviewed in this chapter deploy power electronics devices to manipulate not electric **energy**, but **information**. From this perspective, we regard these devices as a new stream of power electronics applications and describe them as "power-electronics-based online signaling techniques". We believe they have many potential applications in communications, online monitoring and fault detection. We expect that our introduction of the new concept of power-electronics-based online signaling can help to improve the design of new applications in related areas.

To further clarify the new stream of applications, we characterize them as power-electronics-based online signaling. Power electronics circuits have also been used in power system equipment such as static exciters. In this case, power electronic devices manipulate energy, not information. As well, power electronics devices have been used for off-line testing such as generating pulses for cable fault location. We do not consider these two types of applications part of the new area of research. The online signaling oriented power electronics applications are classified into the following three types:

- **Communication-oriented applications**: In this type of application, small but discernible signals propagate in the system to transmit information across distances. The presence of a signal represents a binary 1 (or 0), while the absence of a signal represents 0 (or 1).
- **Online monitoring applications** and **fault detection applications**: In these two types of applications, small disturbances are created in a power system, resulting in response signals from the system. Information about the power system can therefore be derived according to the characteristics of the response signal. According to the use of the information, the applications are classified into two types of monitoring and fault detection.

The power-electronics-based signaling circuits in the reviewed applications are classified in Table 2.1 in order to facilitate the design of new signaling-oriented power electronics applications. Two of the terms in this table are defined as follows.

- **Passive circuits**: signaling circuits comprising only power electronics components, no external power supply, or a supply derived from another phase of the power system.
- **Active circuits**: signaling circuits that introduce external power supplies or power supplies derived from another phase of the system.

TABLE 2.1 CLASSIFICATION OF POWER-ELECTRONICS-BASED SIGNALING CIRCUITS.

	Series connected signaling circuits	Shunt connected signaling circuits
Passive circuits	● Soft-starters (or MOSFET)-based DC injection for motor thermal monitoring	● Zero-crossing-distortion technique ● Ripple control technique ● MOSFET-based pulsating ground fault detector
Active circuits	● Zero-crossing-shift technique ● Subharmonic injection (Hunt technologies) ● Triac-based subharmonic voltage injection for generator stator ground fault detection	● Inverter-based current injection for system parameter monitoring ● Dedicated-signal-generator-based interharmonic current injection for HVDC neutral line fault detection

In the reviewed techniques, the zero-crossing-distortion technique has a simple signaling circuit comprising a shunt-connected thyristor and a current-limiting inductance. The created voltage signal can propagate along power lines and be used for communication. Moreover, the created current signal carries system information and can be used for monitoring and diagnosis. This technique is regarded as a promising implementation of power-electronics-based signaling and may have more potential applications. In the next chapters of this dissertation, this technique is utilized to design solutions for three new problems in power systems.

2.5 Conclusion

This chapter presented a survey of a new class of power electronics applications for signaling-oriented purposes, including communication, online monitoring, and online fault detection. In these applications, power electronics circuits are deployed to manipulate information, instead of energy. The signaling circuits utilized in these applications were classified. A technique named "zero -crossing-distortion" was identified as a representative signaling circuit and was regarded as having more potential applications.

Chapter 3. ISLANDING DETECTION OF DISTRIBUTED GENERATORS

"Distributed generation" (DG) refers to the scheme of generating power by using a large number of small generators (1kW to 20MW) connected at a power distribution system (120V to 44kV). Most distributed generators (DGs) use renewable resources such as wind, solar and small hydro for power generation. DG is an effective solution to help defer the transmission and distribution infrastructure upgrades, reduce the distribution network losses, and mitigate the greenhouse gas emissions.

The traditional electrical distribution networks facilitate the one-way flow of energy from the utility to the customer. The large-scale integration of DGs at the customer is creating new concerns including the need to ensure that the DGs can detect islanding situations and disconnect themselves from the network.

Islanding detection capability is an important requirement for distributed generators. It refers to the capability of a distributed generator to detect in a timely fashion if it is operating in an islanded system. Islanding occurs when a portion of the distribution system becomes electrically isolated from the remainder of the power system, yet continues to be energized by distributed generators. Failure to trip islanded generators can lead to a number of problems for the generator and the connected loads. The current industry practice is to disconnect all distributed generators immediately after the occurrence of islands. This chapter explains the importance of islanding detection, and then provides a literature review of different types of islanding detection techniques. According to the review, the islanding detection of synchronous DGs is a challenging problem. The idea of a power-line-signaling-based islanding detection scheme is proposed as a possible solution for synchronous DGs. A literature review is performed to find a suitable signaling technique.

3.1 Introduction to DG Islanding Detection

A typical power distribution system in North America is shown in Figure 3.1. The substation steps down transmission voltage into distribution voltage and is the sending end of several distribution feeders. One of the feeders is shown in detail. Many customer connection points are present in the feeder. Large DGs are typically connected to the primary feeders (DG1 and DG2). These are typically synchronous and induction generators at present. Small distributed generators such as inverter-based photovoltaic (PV) systems are connected to the low voltage secondary feeders (DG3).

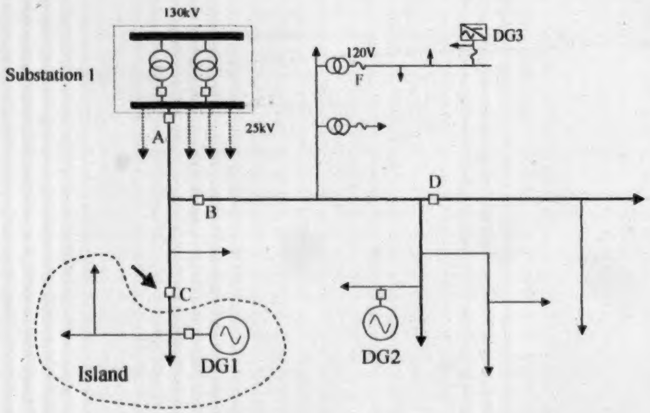

Figure 3.1 A typical distribution system with distributed generators.

An island situation occurs, for example, when recloser C opens. DG1 will feed into the resultant island in this case. The most common cause for a recloser to open is a fault in the downstream of the recloser. A recloser is designed to open and re-close two to three times within a few seconds. The intention is to re-connect the downstream system automatically if the fault clears by itself. In this way, temporary faults will not result in the loss of downstream customers. An island situation could also happen when the fuse at point F melts. In this case, the inverter- based DG will feed the local loads, forming a small islanded power system.

The island is an unregulated power system. Its behavior is unpredictable due to the power mismatch between the load and generation and the lack of voltage and frequency control. The main concerns associated with such islanded systems are

- The voltage and frequency provided to the customers in the islanded system can vary significantly if the distributed generators do not regulate the voltage and frequency and do not have protective relaying to limit voltage and frequency excursions. Since the supply utility is no longer controlling the voltage and frequency, the islanding situation could cause damages to customer equipment. The supply utility has no control over the situation, but may still be found liable for the consequences.
- Islanding may create a hazard for utility line-workers or the public by causing a line that may be assumed to be disconnected from all energy sources to actually, remain energized.
- The distributed generators in the island could be damaged when the

island is reconnected to the supply system because the generators are likely not in synchronism with the system at the instant of reconnection. Such out-of-phase reclosing can inject a large current into the generators and may also result in re-tripping in the supply system.

- Islanding may interfere with the manual or automatic restoration of normal service for the neighbouring customers.

The current industry practice is to disconnect all DGs immediately so that the entire feeder becomes de-energized [21]-[23]. This practice prevents equipment damage and eliminates safety hazards, but calls for a reliable and speedy detection of islanding conditions. The basic requirements for a successful detection are

- The scheme should work for any possible formations of islands. There could be multiple switchers, reclosers and fuses between a distributed generator and the supply substation. The opening of any one of the devices will form an island. Since each island formation can have a different mixture of loads and distributed generators, the behaviour of each island can be quite different. A reliable anti-islanding scheme must work for all possible islanding scenarios.
- The scheme should detect islanding conditions within the required time frame. The main constraint here is to prevent the out-of-phase reclosing of the distributed generators. A recloser is typically programmed to reenergize its downstream system after about a 0.5 to 1 second delay. Ideally, the anti-islanding scheme must trip its DG before the reclosing takes place.

The above goal is achieved by equipping each DG with an anti-islanding protection capability; i.e., each DG must be able to detect if it is islanded and to disconnect itself automatically from the system when islanding occurs.

Many anti-islanding techniques have been proposed, and a number have been implemented in actual DG projects or incorporated into the controls of the inverters used in DG applications. When selecting an islanding detection scheme, the characteristics of the distributed generators must be considered. Almost all distributed generators can be grouped into the following three types:

- Synchronous generator: This type of DG is typically connected to the primary feeder and can be as large as 30MW. Synchronous generators are highly capable of sustaining an island. Due to their large power rating, options for controlling them for the purpose of facilitating islanding detection are limited. As a result, anti-islanding protection for synchronous generators has emerged as the most challenging task faced by the DG industry.

- Induction generator: This type of DG is typically connected to the primary feeder as well. Its size can also be quite large, for example 10 to 20 MW. Due to their need for reactive power support, induction generators are not capable of sustaining an island. As a result, anti-islanding protection is not considered to be an issue for induction generators.
- Inverter-based generator: Due to their relatively small size (typically in the range of a few hundred watts to 1 MW), this type of DG is commonly connected to the secondary feeder. The inverter is actually an interface between the system and the generator, which can be photovoltaic panels, fuel cells, etc. The inverter-based DGs are capable of sustaining an island. However, the inverters can be easily controlled to facilitate the detection of islanding conditions. As a result, many inverter-specific islanding detection techniques have been proposed.

3.2 Review of Existing Islanding Detection Methods

This section will review the major islanding detection techniques published or developed with a focus on synchronous generators. These techniques can be broadly classified into two types according to their working principles: local detection schemes and communication-based schemes (see Figure 3.2) [24][25].

The local detection schemes rely on the voltage and current signals available at the DG site. An islanding condition is detected if the indices derived from the signals exceed certain thresholds. The local detection schemes can be further divided into two sub-types: the passive detection methods, which make decisions based on measured voltage and current signals only, and the active detection methods. The active methods inject disturbances into the supply system and detect islanding conditions based on system responses measured locally. The active methods are highly dependent on the DG units involved. The active methods are widely used by inverter-based DGs due to the methods' ease of implementation in such systems. Although some of the local detection schemes can be applied to both types of DGs, their performances can differ as they are dependent on the operating characteristics of the DGs involved.

The communication-based schemes use telecommunication means to alert and trip DGs when islands are formed. Their performance is independent of the type of distributed generators involved.

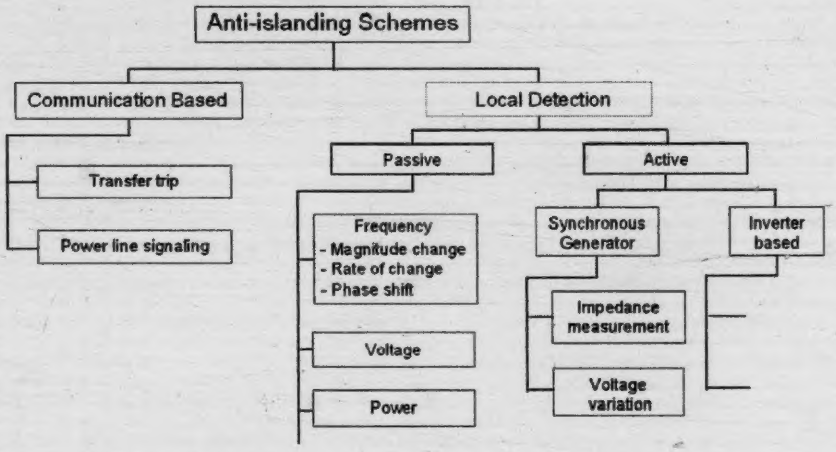
Anti-islanding Schemes
Communication Based
Local Detection
Transfer trip
Power line signaling
Passive
Active
Frequency
- Magnitude change
- Rate of change
- Phase shift
Voltage
Power
Synchronous Generator
Inverter based
Impedance measurement
Voltage variation

Figure 3.2 A classification of anti-islanding schemes for distributed generators.

3.2.1 Local Passive Methods

Power quantities measured at DG sites, such as the frequency or voltage, are used to derive indices for detecting island situations.

A. Frequency-Based Passive Schemes

The frequency-based schemes are the most widely used passive schemes for islanding detection involving synchronous generators. If the generation and load have a large mismatch in a power system, the frequency of the system will change. Since the frequency is constant when the feeder is connected to the transmission system, the islanding condition can be detected by checking the amount and rate of frequency change. Three types of frequency-based relays are commercially available for islanding detection [26][27][28]. The frequency relays trip a DG based on over-frequency or under-frequency criteria. The rate of change of frequency (ROCOF) relay initiates a DG trip when the rate of frequency change exceeds a certain threshold. The vector surge relays (VSR) measure the phase angle shift of the voltage waveform with respect to a reference waveform. This type of relay has a performance characteristic similar to that of the frequency relay [29][30].

The main problem associated with the above relays is that they cannot function properly or fast enough if the generation and load mismatch in an island is below a certain level [31]. This level is denoted as the non-detection zone

(NDZ) for frequency-based relays. The relay can reduce the trip threshold to decrease the non-detection. This approach, however, could make the relays too sensitive and prone to nuisance trips.

B. Voltage-Based Passive Schemes

An under- and over-voltage relay is also used for islanding detection [26]. This relay operates on the principle that a reactive power mismatch in an island will drive up the system voltage or cause voltage decline. By determining the change or rate of change of the voltage at the DG terminal, islanding conditions that cannot be detected by frequency-based relays could be detected. A voltage relay is always available in a DG installation for other purposes such as overvoltage protection. This relay can be utilized to support islanding detection at no extra cost.

The performance of voltage-based relays for islanding detection is not clear at present since no research work has been reported on this subject. What is certain is that a voltage change can occur much faster than a frequency change since no 'inertia' associated with voltage change exists. Thus, a voltage relay can operate with a shorter delay. A power distribution system typically has a small reactive power mismatch due to the need to reduce feeder loss. As a result, the reactive power mismatch and its associated voltage change in an islanded system can be small. On the other hand, other disturbances can cause voltage change. In view of these factors, voltage-based relays can be used only as a complementary device for islanding detection.

C. Other Indices-Based Schemes

Research work has been reported on the use of other indices derived at the DG site for islanding detection. Three examples are:

- Change of active power output [31]: This scheme monitors the change of a DG's active power output. Since frequency change is a direct consequence of active power change, the performance of this method is likely to be similar to that of frequency-based relays. On the other hand, other disturbances could also change the power output level; so establishing a reliable islanding detection criterion for the active-power-change-based method is difficult.

- Change of reactive power output [31]: This scheme monitors the change of

DG's reactive power output and could have a better performance than that of the voltage-based relays because a great deal of reactive power change is required to cause a detectable voltage change. The reactive power change is a more sensitive index. To be effective, this method requires the generator to operate at the voltage control mode. The method also experiences problems similar to those faced by voltage-based relays.

- Power factor (***P/Q***) and (***df/dP***) indices [33][34]: The power factor is affected by both the active and reactive power of the generator. No convincing technical reason suggests that the power factor index will exhibit significantly different behavior before and after islanding. The same conclusion applies to the ***df/dP*** index, so such indices are unlikely to result in improved anti-islanding detection schemes.

3.2.2 Local Active Methods

Active detection schemes inject disturbances into the supply system and detect islanding conditions based on system responses measured locally. Active methods are highly dependent on the DG units involved. Inverter-based DGs can be easily controlled to facilitate islanding detection. As a result, many inverter specific islanding detection techniques have been developed and accepted. The active frequency drift method is a representative example [35]. These techniques are not the focus of this chapter and will not be discussed in detail.

For synchronous generators, the options for injecting disturbances are quite limited since the voltage is high, and the generators are not easy to control. Two active methods have been reported in literature.

A. Grid-Impedance-Measurement-Based Scheme

One of the active methods is to measure the system impedance seen at the DG terminals. If a DG is connected to the main grid, the system impedance seen by the DG will be very small. On the other hand, if it loses connection with the system, the impedance will be large. A possible way to detect an islanding condition, therefore, is to monitor the impedance on a continuous basis.

Reference [36] proposed injecting a high frequency inter-harmonic current into the system for determining the system impedance. Harmonic current cannot be used since the system has harmonic sources that will corrupt the results. Reference [14] proposed using a shunt-connected thyristor connected at the DG terminal to inject a disturbance into the system. Impedance is calculated from the voltage and current responses. Since a large difference exists between impedances with and without the supply system, accurate impedance measurement is not necessary for this scheme.

B. Method of Varying Generator Terminal Voltage

A variation of the impedance measurement scheme is to measure the change of reactive power flow when the terminal voltage of the DG unit is varied [37]. Due to the difference in the system impedances, the change of the DG's reactive power output can be quite different in a normal system and an islanded system. If the system is connected to the grid, the variation will be small. Based on this observation, one can let the Automatic Voltage Regulator of the DG unit make small variations on its voltage setting and monitor the Var output variation of the unit to detect the island condition.

Another reported active method also varies the generator terminal voltage periodically [38]. It was shown in [38] that such a voltage change will accelerate the change of the waveform frequency if the generator is islanded. Thus, the frequency-based relays will be able to detect islanding conditions more easily than without the voltage change, even when the power mismatch is very small. In fact, the technique was proposed to reduce the non-detection zone of the frequency-based anti-islanding schemes.

The significant advantage of active schemes is that the power mismatch level in the island will not affect their performance. The main concern for any active method is, however, about the potential interference if more than one DG is present. When multiple DGs are injecting similar disturbances into the system, measuring the system impedance can become very difficult and even impossible, and the generator responses can be hard to determine. Cost is also a factor since it requires a dedicated disturbance generator at each DG site.

3.2.3 Communication-Based Methods

This section reviews two basic schemes implemented or proposed for anti-islanding applications. Other communication-based schemes are essentally minor variations of these two basic schemes.

A. Transfer Trip Scheme

The basic idea of the transfer trip scheme is to monitor the status of all circuit breakers and reclosers that could island a DG in a distribution system [39][40]. When a switching operation produces a disconnection to the substation, a central algorithm determines the islanded areas. A signal is then sent to trip the DGs in the islanded areas.

The transfer trip scheme can be very simple if a DG is connected to a substation with a fixed topology and through a limited number of reclosers. The status signals can be sent to the DG directly from each recloser, and the central processing algorithm can be avoided. This adaptation is currently the most common use of the scheme for islanding detection [21][41].

The main disadvantages of the transfer trip scheme are the cost and potential complexity. This scheme requires extensive communication support. Radio communication is the most common method used by the transfer trip scheme. For areas where telecommunication coverage is weak or non-existent, the cost of a transfer trip scheme alone could kill a DG project. Moreover, each openable device between the DG and the supply system needs a transmitter, and some of devices need to be reconfigured and equipped with the capability of interfacing with the signal transmitter. Thirdly, if scenarios of feeder reconfiguration exist, the scheme can become very complicated.

B. Power-Line-Signaling-Based Scheme

In recent years, several power-line-signaling-based islanding detection schemes have been developed [42]-[45]. These schemes utilize power lines as the communication carrier. A transmitter is installed at a medium voltage (MV) substation and broadcasts a signal that propagates along the distribution network to all lower levels of the power system. At each DG site, a receiver detects this signal and uses it as a continuity test of the line.

The power-line-signaling-based methods are regarded as promising solutions for the islanding detection of distributed generators, especially synchronous generators. These methods can directly monitor islanding conditions according to the continuity of a locally measured signal. They do not have the non-detection zones of the local passive methods. The switching of any openable devices between the utility and DG can be detected automatically. Therefore, the methods work independent of feeder reconfigurations. One transmitter satisfies the needs of all downstream DGs. There is no interference between DGs.

The power-line-signaling technique needs to be carefully selected. Currently, two techniques have been proposed. Reference [45] proposed using high-frequency (below 1kHz) interharmonic signals that were originally created for AMR by Hunt Technologies. The islanding detection function can possibly be integrated into the AMR communication system as an extra function. Reference [42][43] proposed using even higher frequency (say, 72kHz) power line carrier signals for islanding detection. The disadvantage of using very high frequency power line carrier signals is that they may be excessively attenuated by distribution transformers and capacitor banks.

This thesis will present a novel power-line-signaling-based scheme for DG islanding detection. The scheme has been in development independently of [45] and [42] since 2002 at University of Alberta. The scheme utilizes a signaling technique (TWACS) originally designed for AMR purposes. This scheme will be introduced in detail in this chapter.

3.2.4 Conclusion

Over the past several years, islanding detection for DGs has emerged as one of the most challenging technical barriers for DG interconnection, especially for synchronous generators connected at medium voltages.

Power-line-signaling-based schemes are the most promising solutions for islanding detection of synchronous generators. The key issue in designing such a scheme is to select a suitable signaling technique. The next section will provide a literature review to find such a technique.

3.3 The Idea of Power-Line-Signaling-Based Islanding Detection

This dissertation proposes a novel power-line-signaling-based approach in response to the challenge of synchronous DG islanding detection. The idea of this scheme is to continuously broadcast a signal from the utility substation to the downstream DGs along the power distribution lines. When the detector of the DG does not sense the signal (caused by the opening of any breakers between the substation and the DG) for certain duration such as 200ms, an island condition is determined, and the DG will be tripped immediately.

The above approach uses power lines as the communication medium. Theoretically, the approach can detect any formation of islands without non-detection zones. It is primarily intended for synchronous-machine-based DGs connected to primary distribution systems, although it is applicable to all types of DGs. The key issue in implementing the above idea is to choose an effective signaling technique.

3.3.1 Requirements for Signaling Techniques

The techniques employed for transmitting signals on distribution lines are as diverse as the distribution systems themselves. A technology suitable for one distribution network may not necessarily be transferable to another. For the proposed application of islanding detection, candidate signaling techniques must satisfy the following requirements:

- The signal can be transmitted over distribution networks of vast geographical distances and consisting of overhead wires, and/or underground cables. Methods useful for signal transmission over short distances are inappropriate.
- Signal attenuation is an important concern. If high frequency carrier signals are used, which can be excessively attenuated by distribution transformers or shunt capacitors, boosters or jumpers will be needed to maintain the signal strength or bypass the capacitor. This requirement makes the signaling technique prohibitively expensive for merely the islanding detection purpose. Therefore, the candidate signals are limited to a very low frequency range.
- The communication signal should not be reproduced by any load. If harmonic producing loads exist in the network, appropriate measures must be taken to minimize the harmonic noise. For example, a subharmonic or interharmonic signal, or carefully selected combinations of signals or frequencies should be used.
- One-way, outbound signal transmission is required for islanding detection. Load control is an application that requires similar power line communication techniques.
- The economic consideration is important. Usually, a compromise is made between the reliability and cost of the system.

Before we proceed further, a few terms are defined first to facilitate subsequent discussions:

- *Outbound Signal*: A signal transmitted from the utility side (e.g., from a substation) to a device on the customer side is called an "outbound signal". For example, a control signal sent by an automatic load control device to turn off an air conditioner at a customer's premises is an outbound signal.

- *Inbound Signal*: The signals originating at customers' premises and received on the utility side are inbound signals. The data signal transmitted by an Automated Meter Reading device to a central data-collecting computer is an example of inbound signal.
- *Two-way communication*: A power line communication technique that sends and receives both inbound and outbound signals is a two-way communication system. Some two-way systems transmit inbound and outbound signals simultaneously and are called "full-duplex transmission" systems. In contrast, half-duplex transmission refers to two-way systems that transmit outbound and inbound signals in sequence.

3.3.2 Review of Existing Power-Line-Signaling Techniques

This section reviews various power-line-communication techniques and assesses their applicability to the proposed islanding detection scheme. For islanding detection purposes, the signal transmitter needs to be installed in the upstream of all the interconnected DGs in a distribution network. In past years, the growing interest in remote meter reading and distribution automation has resulted in many research studies. Many power-line-communication techniques have been proposed and implemented around the globe. The existing power-line-signaling techniques can be broadly classified according to their information-carrying principle into two categories: waveform-distortion-based techniques and power-line-carrier-based techniques. Each category can be further divided into several types as shown in Figure 3.3.

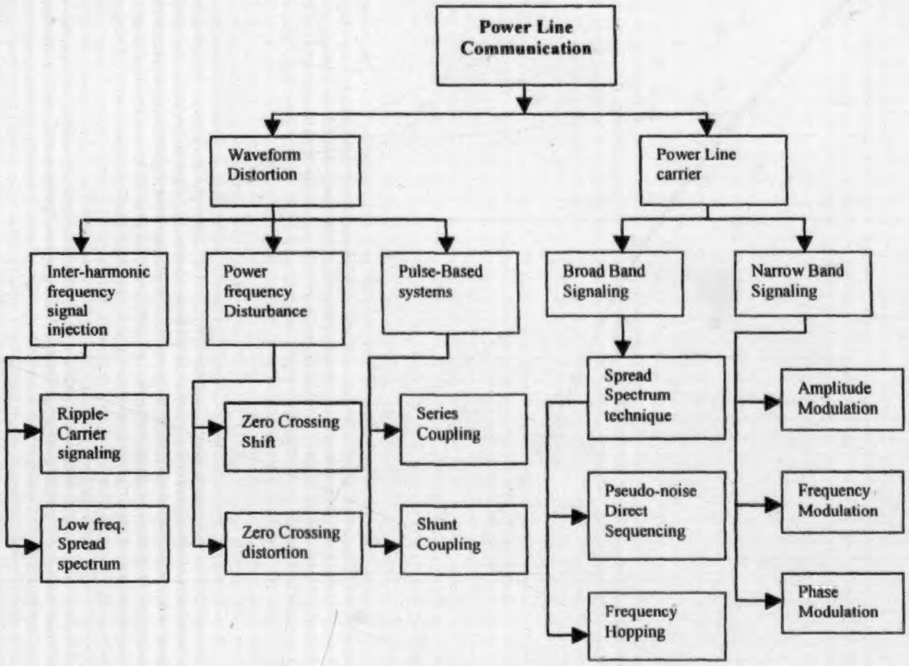
Power Line Communication
Waveform Distortion
Power Line carrier
Inter-harmonic frequency signal injection
Power frequency Disturbance
Pulse-Based systems
Broad Band Signaling
Narrow Band Signaling
Ripple-Carrier signaling
Low freq. Spread spectrum
Zero Crossing Shift
Zero Crossing distortion
Series Coupling
Shunt Coupling
Spread Spectrum technique
Pseudo-noise Direct Sequencing
Frequency Hopping
Amplitude Modulation
Frequency Modulation
Phase Modulation

Figure 3.3 A classification of power-line-communication methods.

For the first category, the waveform distorted can be either the current wave or voltage wave of the power system frequency. Three types of waveform distortion methods can be used for altering the waveform and detecting the alteration.

The second category of power-line-carrier methods uses the power signal as a modulation means to transmit high frequency signals over the distribution line. Amplitude modulation, frequency modulation or phase modulation, etc. are employed. The system can be broadband or narrow band depending upon its intended applications. Special modulation techniques such as spread spectrum are frequently used to increase system reliability.

Since the second category of methods uses very high frequency (say, 70kHz) carrier waves to send information, these methods have a high data transmission rate. Moreover, they require the installation of additional devices such as boosters and trappers along the distribution lines. As a result, the high equipment costs make the use of these methods for islanding detection difficult to justify. Therefore, this thesis does not include a detailed discussion of the power-line-carrier techniques.

A. Interharmonic-Injection-Based Method

The standard name given to this type of techniques is the "ripple carrier signaling" (RCS) technique [52]. It essentially involves the use of interharmonics to transmit signals. The technique impresses an interharmonic signal (150Hz to 2000Hz) directly onto the power lines. The signal, which is pulse-coded to carry information, is transmitted along with and superimposed upon the system voltage. The magnitude of the interharmonic (carrier) frequency and the particular code of pulses enable the signal to provide two levels of selection and identification for signal security. Hence, a wide selection of channels is available through pulse coding, and adjacent coupled power systems are protected from interference due to the diversity of the carrier frequencies used. This system is particularly useful for applications requiring one-way communication over substantial distances, such as load control, although two-way duplex communication is also possible.

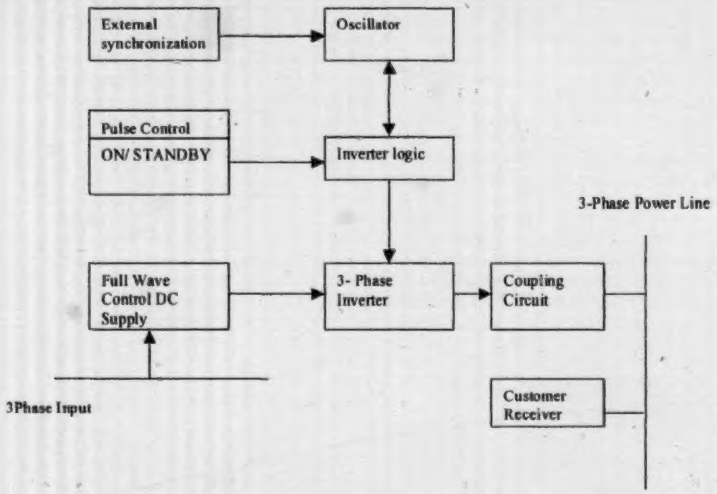

Figure 3.4 The ripple carrier communication system.

Figure 3.4 shows the basic components of a ripple carrier communication system. The oscillator continuously produces pulses and is externally synchronized in accordance with the desired frequency of the signal. The pulse control has two modes: ON and standby. In the ON mode, the utility selects and transmits the desired code to the Inverter Logic. The inverter, which is supplied with DC power, creates interharmonics according to the Inverter Logic. The output is then coupled onto the power line via a coupling circuit. As the conduction of the Inverter is controlled by the Inverter Logic, the Inverter is able to inject a coded high frequency signal. The customer receiver detects the high frequency signal and decodes it to obtain the information contained in the signal.

The carrier waveforms are shown in Figure 3.5. Figure 3.6 shows the composite waveform seen on distribution lines.

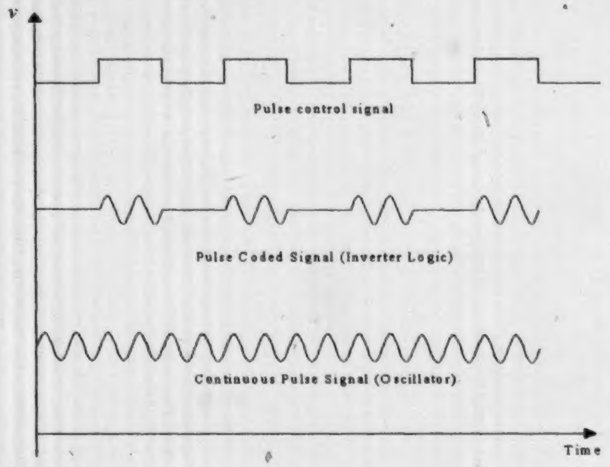
V
Pulse control signal
Pulse Coded Signal (Inverter Logic)
Continuous Pulse Signal (Oscillator)
Time

Figure 3.5 The ripple carrier signal waveforms.

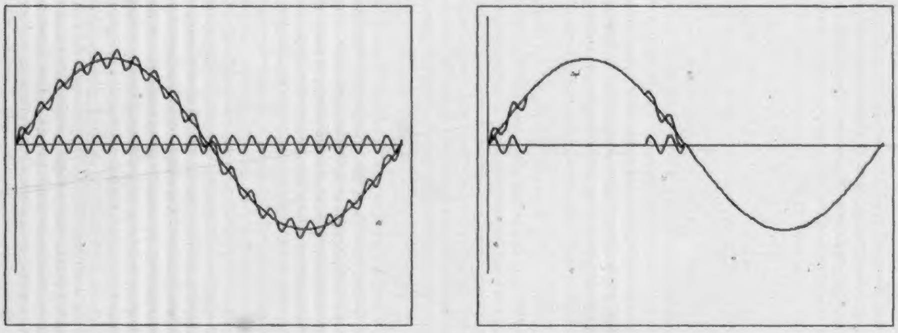

(a) Non-pulse-coded carrier; (b) Pulse-coded carrier.

Figure 3.6 The modulating voltage and carrier waveforms.

In this method of signal transmission, the carrier frequency is deliberately selected to be not too far from the line frequency so as to avoid the problems associated with the transmission of high frequency signals on the power distribution lines. The transmitted signal is small compared to the 60Hz voltage (0.1 to 0.5%), and so it appears as a ripple (Figure 3.6). Typical frequency of the transmitted signal ranges between 150 to 500Hz for distribution systems. Higher frequencies have been used in some cases.

An example application of the ripple carrier technique is a system built by the Swiss firm "*Zellweger Uster*". This company offers a two-way system consisting of two overlaid one-way systems. It has been used for load control. The minimum communication delay time is less than 7 seconds. In North America, two ripple-carrier-based one-way systems have been installed successfully in Vermont, USA for the load control of an 8 kilometer feeder. The main advantages and disadvantages of the ripple control system can be summarized as follows:

Advantages:

- As the frequency of signal is close to the power frequency, no special equipment like boosters, line repeaters or bypass circuits is required for free signal propagation through the power lines. The signals can generally propagate to a large area serviced by the distribution network.
- It can transmit two-way duplex signals.
- The system is simpler and less expensive than the high frequency (power line carrier based) systems.

Disadvantages:

- To achieve sufficient reliability in signal transmission, the transmitter power has to be large. In a typical situation, the transmitter power can range between a few hundred kW to a few megawatts, resulting in higher operating costs.
- Carrier frequencies are kept very low, between 30-1000 Hz, in order to avoid the cost of distribution network changes. However, the use of these frequencies places the signals in the noisiest area of the power line spectrum. For example, the magnitude of power frequency harmonics can be very large below 2.5 kHz and can jam any communication systems that use this frequency range to transmit.
- Data transmission rates are very low. The typical data rate is a few bits per second.

In order to overcome the above disadvantages, spread spectrum techniques have been proposed to improve the basic ripple carrier technique. The spread spectrum techniques spread the coded signal over a large frequency band. Due to constantly changing the carrier frequency of the signal, power line disturbances such as harmonic cannot completely jam the signal. Even if a jamming occurs, only a portion of the transmitted signal corresponding to the jamming frequency will be lost. Since the main jamming signals in this case are the harmonics with known frequencies, communication signals can be spread in between the harmonic frequencies to minimize error. A recent patent (US patent # 6388564 – Power Distribution Grid Communication System) utilizing this technique spreads the signal in a frequency range of 500Hz to 1500Hz about a reference frequency of 990Hz. This system is expected to achieve data rates much higher than those of the ripple carrier system and without its high power requirements as in ripple carrier systems. The spread spectrum technology can make the ripple carrier more reliable and achieve higher data rates with reduced transmitter power. The system, however, is more complex in terms of the signal generator and receiver. The associated cost is higher than that of other systems. It is not clear if the technology has been used or tested in the field.

B. Pulse-Based Communication Technique

The basic idea of this technique is the following: a power switch is used to interrupt the load current or voltage for a short period (1 – 2 ms) near the zero crossing of the current or voltage wave [2]. The pattern of interruptions carries the information to be transmitted. This method has been successfully employed in utilization voltage levels for low power applications. An example is the electronic ballasts that control fluorescent lamps. Their applicability to the distribution voltage level so far is impractical, if not impossible. Pulse-based communication schemes can be further classified as Series schemes and Shunt schemes.

- Series scheme: As the name indicates, a power switch is placed in series with one wire of the AC source, and pulses in the form of zero current are introduced to the load current by momentarily opening the power switch. The interruption takes place near zero crossing. Receivers capable of detecting zero-crossing-distortion are mounted near the appliances to be controlled. The switching pattern of the power switch is determined in accordance with the data to be transmitted.
- Shunt scheme: In this method, the power switch is coupled in parallel with the AC line wires. By momentarily turning on the power switch, the line voltage can be brought to near zero value. The power switch is turned on near zero crossing of the voltage wave, thereby keeping the voltage level at zero for an extended time period (1-2ms). The receivers can detect this change and hence interpret the data being sent.

The main advantages of these techniques are (1) they can avoid the kind of frequency-compatibility problems inherent in the carrier-based systems, and (2) little or no modification is required in the utilization network. The main disadvantages of the techniques are

- Direct implementation of this method in the distribution network is not practical as the power and stress requirements on the power switch can be too high to be economical.

- Due to the limitations of the pulse transmission circuitry, the pulse is usually constrained to occur only at or near the zero crossing of the line voltage. The transmission rate is 2 bits per line cycle at best.

C. Power Frequency Disturbance Techniques

The power frequency disturbance techniques can be considered as a significantly modified version of the pulse-based techniques and are designed for applications at distribution voltage levels. A representative example of these techniques is the TWACS technology used for AMR applications in North America. This technology consists of two waveform alternation techniques, *zero-cross-shift* and *zero-crossing distortion*, one used for outbound signal transmission and the other for both outbound and inbound signal transmission. These two techniques have already been introduced in Chapter 2 already.

The main characteristics of these two techniques can be summarized as follows:

- No appreciable signal attenuation is introduced by shunt capacitors and transformers; therefore, no significant modification of the distribution network is required.
- Relatively inexpensive hardware is employed without impairing the reliability of the communication link.
- They are one-way communication techniques.
- Harmonics have little impact on their performances as harmonics produce consistent distortions or zero-crossing-shifts in the waveform.
- The zero-crossing-shift technique is sensitive to transient noises that can lead to temporary zero-crossing-shifts. The zero-crossing-distortion method seems to be more immune to noises. However, the first method can be more easily implemented in the zero-sequence mode, leading to increased reliability.

3.3.3 Comparison and Analysis of Different Techniques

The literature review results indicate that the waveform-distortion-based techniques are the most promising candidates for the proposed islanding detection application. A comparison of the three types of waveform distortion techniques is shown in Table 3.1. Among the three techniques, the pulse-based methods cannot be adopted without significant research and improvement. As a result, only two types of techniques are left for further assessment: the power frequency distortion techniques and the ripple carrier techniques. Both types of techniques have been successfully used in North America distribution systems for AMR or load control applications.

TABLE 3.1 COMPARISON OF VARIOUS POWER LINE SIGNALING METHODS.

Candidate Techniques / Comparisons	Power frequency disturbance		Ripple carrier signaling	Pulse-based communication
	Zero-crossing shift	Zero-crossing distortion		
Attainability of signal propagation	Good	Good	Medium	Good
Reliability of signal propagation	High	Excellent	Good	Not clear
Infrastructure availability	Yes	Yes	Yes	Yes
Implementation of signal coupling	Easy to medium	Easy	Medium to Complex	Easy
Transmitter power required	Medium	Medium	Large	Medium
Channel noise	High	High	High	Not clear
Data rates	Low	Low	Medium	Low
Territory coverage	Large	Large	Small-medium	Not clear
Cross–talk prevention	Easy	Easy	Not clear	Not clear
System cost	Low	Low	Medium to High	Low
Expanding applications of existing power line system	Easy	Easy	Easy to Medium	Not clear
Adaptability to DG islanding detection	Very Good	Excellent	Good	Not clear
Special problems	One-way communication	One-way communication	Complex design to obtain high reliability	Higher stress on switching devices

Based on existing knowledge, both types of techniques can be used for the islanding detection application. However, we prefer the TWACS technology due to the following considerations.

- Performance predictability: The TWACS uses 60Hz waveforms to transmit signals as opposed to the interharmonics used by the ripple carrier. A 60Hz waveform can travel to all points of a network, whereas the interharmonics might not be able to do so, because harmonic or interharmonic resonance in the system could reduce the ripple to a level undetectable by the receivers.
- Cost of signal generation: The ripple carrier technique requires a more powerful transmitter, and the signal generator is more complicated

(although it could be simplified for our intended application).

- Impact on power quality: The ripple carrier signals introduce interharmonics into the distribution system. The interharmonics may resonant with the system, leading to increased waveform distortions. The signals transmitted by the TWACS system can also be considered as interharmonics, but due to their low frequency, their impact on power quality may not be as large.

All three techniques could interfere with TWACS-based or similar AMR systems. The ripple signal could change the zero crossing instants and surrounding waveforms, leading to corruption of the outbound AMR signal. Any existing TWACS systems must be adapted for islanding detection application.

3.3.4 Conclusion and Discussion

Based on the comparison results, the zero-crossing-distortion technique is finally chosen to create the signals for the islanding detection purpose.

Given that TWACS systems may exist in some of the distribution networks, the researchers face two possible scenarios:

- If no TWACS are present in a distribution system, the implementation of a TWACS-based islanding detection scheme is straightforward and has a very high chance of being successful. In this project, we call such a system "the standalone islanding detection system".
- If a TWACS system exists in the distribution system, the TWACS system has to be adapted for both the AMR and the anti-islanding applications. An ideal solution is to integrate the islanding detection as a new function of the TWACS system. The costs of the islanding detection will be shared with other applications such as AMR and load control. No technical hurdle prevents such integration. Although TWACS is a half-duplex technique, different channels (say, phase A to ground, and phase B to C, et al) are available for inbound and outbound signaling. Simultaneous inbound and outbound signal transmission is possible if the inbound and outbound signals are using different channels. Therefore, the continuously broadcasting of the outbound signal for islanding detection will not block inbound signal transmission.

For both scenarios, the reliability of the signal detection is very important. Unlike other communication applications that operate in power system steady-state conditions, the application of islanding detection must be able to work correctly during power system transients since the occurrence of islanding is most likely followed by transients. The receiver must be able to distinguish between noise and an actual signal. Complications arise when both noise and a signal are present. If a receiver treats the signal as non-existent under such a condition, a false trip of a DG could happen. On the other hand, if noise is mistaken for a signal, the DGs will not be disconnected. Occasional transients on the distribution network may also affect the performance of the detection system. The receiver design thus requires the utmost attention.

3.4 The Proposed Power-Line-Signaling-Based Method

Based on the studies in the above sections, this section proposes the complete power-line-signaling-based islanding detection scheme. The scheme is shown in Figure 3.7.

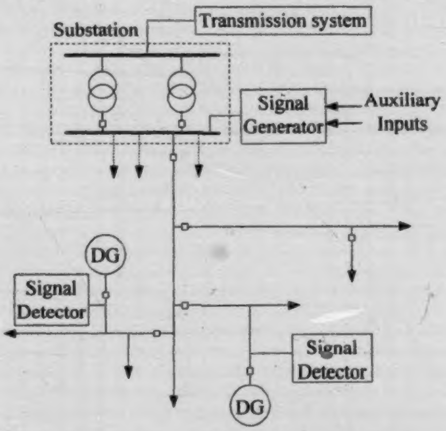

Figure 3.7 The proposed islanding detection scheme.

The scheme includes two devices: a signal generator connected to the substation bus and a signal detector at the terminal of a given DG. The signal generator broadcasts a signal to all distribution feeders with a preset protocol continuously. If the detector of the DG does not sense the signal (caused by the opening of any devices between the substation and the DG) for a certain duration, an island condition is considered to be present, and the DG can be tripped immediately. If the substation bus loses power (such power loss is another islanding condition), the signal generator also loses power and stops broadcasting. So that downstream DGs will also trip. Furthermore, the signal generator has several auxiliary inputs. Any of the inputs can stop the broadcast, resulting in tripping all DGs in the system. This feature is particularly useful when transmission system operators need to trip the DGs. It is also useful when a transmission system island is formed. Since the transmission system is well -equipped with telecommunication means, it can send a stop signal to the signal generator.

This scheme works like a transfer trip scheme. However, since the power line is used as the signal carrier, the opening of any devices can be detected automatically. It works independently of network topology changes (feeder reconfiguration). The scheme is also economical since one SG installed at the substation can satisfy the need of all the downstream DGs. Another important advantage is that the scheme can be tested without actually breaking up the distribution feeders. The main tests could be done by simply stopping the signal generator. In this case, the signal detectors should detect null signal. Later in this section, the methods to generate and to detect the above described signals are presented.

3.4.1 Signal Generator (SG)

Many mature methods are available to send signals through power lines. For islanding detection purpose, the signaling technique should be reliable, low cost and have a quick response. It is also desirable to have minimum interference with power communication schemes that already exist in a distribution system. After extensive evaluation on various schemes, the zero-crossing distortion technique is chosen as the means to broadcast signal.

The structure of the signal generator is shown in Figure 3.8(a). A stepdown transformer (also called a signal transformer) transforms the primary voltage (for example, 25kV or 14.4kV) to a reduced level (say 480V) for thyristor operation. It also limits the short circuit current and the voltage distortion when the thyristor is turned on. Common power transformers can be used for this purpose.

The voltage information at the secondary side of the transformer at point T is used to time the thyristor gating operation. The thyristor is turned on several degrees before its voltage (say, phase A to ground voltage) crosses zero, creating a momentary short circuit. The thyristor automatically turns off after the supply voltage (at point X) reverses its direction. Figure 3.8(b) shows the resulting waveforms. A small distortion exists around the zero-crossing-point of the primary feeder voltage. This voltage distortion is the signal for islanding detection. If the thyristor does not fire, there is no waveform distortion and thus no signal. Auxiliary inputs can be sent to disable the triggering operation. When this occurs, the signal generator will stop broadcasting signals.

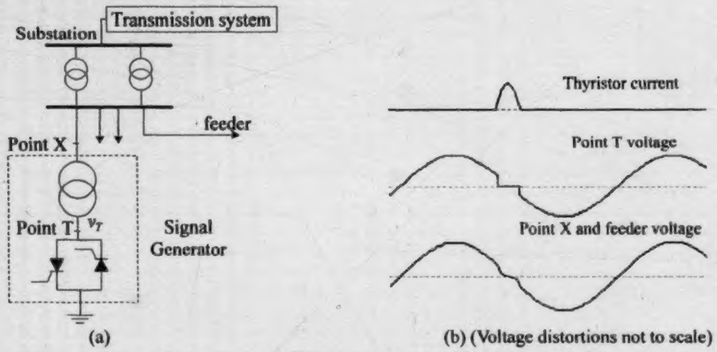

Figure 3.8 The signaling method and waveforms.

To facilitate the signal detection, the anti-islanding signal can be assigned certain patterns. For example, it can be broadcasted for every 2, 3 or 4 cycles. Figure 3.9 shows an example voltage waveform containing a signal every 2 cycles. Also, signals can be created with several channels, say, phase A to the Ground (denoted as A-G channel), B-G, or C-G. Phase-to-phase channels (A-B, B-C or C-A) are also available, in which a thyristor is connected and fired between two phases to create signals on the phase-phase voltage waveform. Two anti-parallel thyristors can be used to fire at the voltage rising and the falling edge respectively, creating different signal patterns.

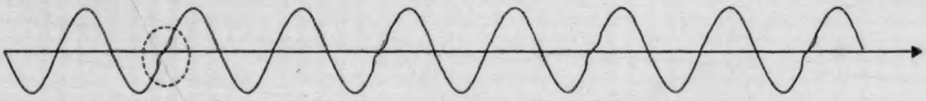

Figure 3.9 A sample voltage waveform containing a signal every two cycles.

3.4.2 Signal Detector (SD)

Signal detectors are installed at the locations in the distribution system where DGs are connected. It senses the three phase voltages. If a signal is not present, the signal pattern is not consistent with the pre-established rule, or the waveform frequency deviates significantly from the power frequency (say, 60Hz), the signal detector will send a signal to trip the DG. Accordingly, a signal detector works like a relay. In fact, the preferred embodiment of the signal detector is to integrate the anti-islanding signal detection function into a microprocessor-based relay, which is used in many DG stations.

A significant feature of the signal detector is that the voltage distortion signal is extracted by subtracting two consecutive voltage cycles (see Figure 3.10). Supposing that the thyristor is fired in a way such that the voltage distortion exists in only one of two consecutive cycles, the difference between these two cycles is the distortion voltage, i.e., the signal. This subtraction method is extremely powerful since it filters out the background distortion in the voltage waveforms. The scheme is therefore essentially immune to background waveform distortions.

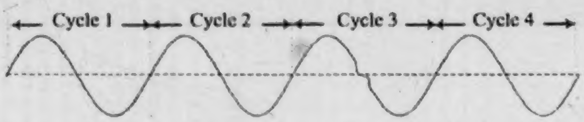

(a) Voltage waveform (signal is at the 3rd cycle)

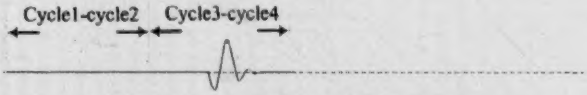

(b) Voltage distortion signal waveform

Figure 3.10 The subtraction method for signal extraction.

After a voltage distortion signal is extracted, additional algorithms are needed to determine whether the distortion signal represents a genuine distortion signal or not. The algorithms will be introduced in Section 3.6.

3.5 Signal Characteristics Analysis and Signal Generator Design

The features of the anti-islanding signals need to be fully understood in order to reliably detect the signals. This section utilizes theoretical analysis and computer simulations to investigate the characteristics of the signals and the important influencing factors.

3.5.1 Simplified Signal Analysis and Signal Generator Design

The case where SG fires between phase A and ground as shown in Figure 3.11 is used as an example to determine the design parameters. The steady state sinusoidal voltage at the secondary side of the signal transformer when there is no signaling can be expressed as

$$v_{TA}(t) = -\sqrt{2/3}V_N \sin(\omega t - \delta) \tag{3.1}$$

where V_N is the rated phase-to-phase voltage at the secondary side of signal transformer. According to superposition principle, the signaling process is equivalent to injecting a negative voltage source $-v_{TA}$ between phase A and the ground at point T. The signaling transient can be calculated with a circuit energized by $-v_{TA}$ as shown in Figure 3.11(b), where L_{self} is the self-inductance of the supply system at point X, and L_T is the signal transformer inductance. In this circuit, the other two phases are approximated as open circuits, so are the loads connected to the feeders. The resistive part of the system impedance and the transformer impedance are also omitted. Since this analysis is conducted for distribution networks ranging from 10 to 66 kV, the omission of the resistive part will not cause significant inaccuracy.

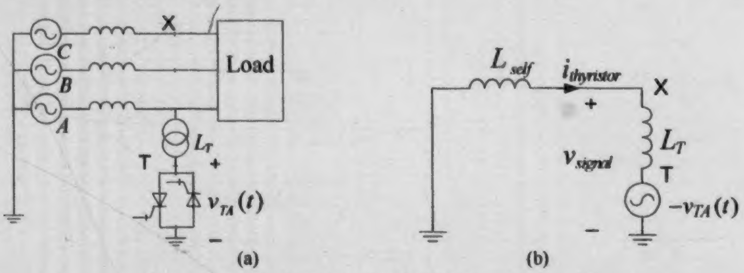

Figure 3.11 The analysis circuit for phase-ground signaling.

If the thyristor is fired ahead of v_{TA}'s zero crossing point by an angle of δ, the thyristor conduction period will be 2δ, and the voltage distortion signal at point X and the thyristor current can be determined as:

$$v_{signal}(t) = \sqrt{2/3}V_N \frac{L_{self}}{L_{self} + L_T}\sin(\omega t - \delta), \quad \omega t \in [0, 2\delta] \tag{3.2}$$

$$i_{thyristor}(t) = \frac{\sqrt{2/3}V_N}{X_{self} + X_T}\left[\cos(\omega t - \delta) - \cos\delta\right] \tag{3.3}$$

where $X_{self} = \omega L_{self}$ and $X_T = \omega L_T$. The corresponding waveforms are shown in Figure 3.12.

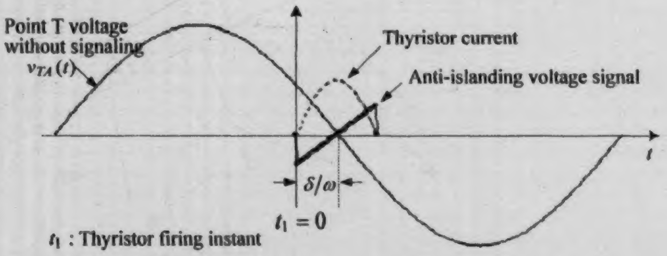

Figure 3.12 The anti-islanding signal and the thyristor current waveforms.

The peak of $v_{signal}(t)$ represents the strength of the anti-islanding signal, which is

$$V_{signal\_peak} = \sqrt{2/3}V_N \frac{L_{self}}{L_{self} + L_T} \sin\delta$$

Defining the signal strength as the ratio of signal peak to the peak of its carrier voltage, we can obtain:

$$k = \frac{V_{signal\_peak}}{V_{PG\_peak}} = \frac{L_{self}\sin\delta}{L_{self} + L_T} = \frac{X_{self}\sin\delta}{X_{self} + X_T} \times 100\% \tag{3.4}$$

If the distribution system in Figure 3.11 is grounded through a reactance X_N, the signal strength will be

$$k = \frac{(X_{self} + X_N)\sin\delta}{(X_{self} + X_N) + X_T} \times 100\% \tag{3.5}$$

Both (3.4) and (3.5) can be converted to the form in Table 3.2 by substituting the impedances with the system fault level and the transformer capacity. If the system neutral is grounded through a resistance R_N, the above analytical method still works. However, the signal strength cannot be calculated using equation (3.5) unless R_N is much smaller than X_{self}.

The above analysis can be used to design the signal generator. There are two key design parameters for the signal generator. One is the size of the signaling transformer and the other is the rating of the thyristor. The signaling transformer is selected to ensure there is sufficient signal strength. The thyristor is selected to meet voltage and current stress requirements.

Table 3.2 summarizes the equations of signal strength P-G and P-P signaling channels. Note that for the P-P signaling, the signal strength is not affected by system grounding condition. These equations can be used to select signaling transformer.

Based on the above analysis, the average and RMS values of the thyristor current can be determined as

$$I_{rms} = \frac{I_{peak}}{\sqrt{N}} \frac{1}{1-\cos\delta} \sqrt{\frac{1}{2\pi}[\delta(2+\cos 2\delta) - 1.5\sin 2\delta]} \tag{3.6}$$

$$I_{average} = \frac{I_{peak}}{N} \frac{\sin\delta - \delta\cos\delta}{\pi(1-\cos\delta)} \tag{3.7}$$

TABLE 3.2 EQUATIONS FOR SIGNAL STRENGTH AT POINT X

Signaling channel	Signal strength k (%)
Phase-Ground	$\frac{\sin\delta}{1+3x_T S_{PG}/S_T}$
Phase-Phase	$\frac{\sin\delta}{1+x_T S_{3ph}/S_T}$
S_{3ph}: Supply system three phase fault level at point X; S_{PG}: Supply system phase-to-ground fault level at point X; S_T: Stepdown transformer capacity (three-phase); x_T: Impedance of the stepdown transformer in percentage.	

where

$$
\begin{aligned}
I_{peak} &= \frac{\sqrt{2/3}(1-\cos\delta)}{V_N[1/(3S_{PG})+x_T/S_T]} \quad \text{(Phase - Ground signaling)} \\
&= \frac{\sqrt{2}(1-\cos\delta)}{2V_N(1/S_{3ph}+x_T/S_T)} \quad \text{(Phase - Phase signaling)}
\end{aligned}
\tag{3.8}
$$

N stands for the interval between two firing events in the unit of number of cycles. A large N such as 4, 5 or 6 can be used to reduce the heating stress on the thyristor. The side effect is that a larger N may delay the response speed of the signal detector.

As an example, a case where a SG is to be installed at a 12kV substation bus whose fault level is S_{PG} = 30.4MVA and S_{3ph} =79.7MVA is considered. If δ =30°, x_T =2%, V_N =480V, $N=4$ (firing at every 4th cycle), the minimum size of signal transformer and thyristor current are listed in Table 3.3.

TABLE 3.3 EXAMPLE SG PARAMETERS

	SD and SG: P-P			SD and SG: P-G		
k	S_T (kVA)	I_{peak} (A)	I_{RMS} (A)	S_T (kVA)	I_{peak} (A)	I_{RMS} (A)
3%	102	943	140	116	1246	185
4%	139	1258	187	158	1661	247
5%	177	1572	234	202	2076	308

3.5.2 Detailed Signal Analysis and Simulations

This section investigates the characteristics of the anti-islanding signal as seen at a DG site. A representative 25kV distribution system shown in Figure 3.13 is used for this purpose. Parameters of the system are listed below.

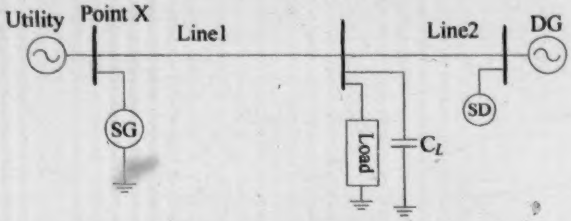

Figure 3.13 The single line diagram of the simulation system.

- Utility: 25kV, impedance 6.25+j14.4 ohm, Y_g connected.
- Feeders: Line1 is 10km and Line2 is 1km; R_1, X_1, R_0, X_0 are 0.2138, 0.3928, 0.3875, 1.8801 ohm/km respectively, and B_1, B_0 are 4.2315 and 1.6058 Microsiemens/km respectively.
- DG transformer: 25k/480V, Yg/Δ connection, 6MVA, impedance of 6%.
- DG: 480V, 5MVA, subtransient reactance of 0.25; Y_g connected.
- Load: R-L load, 2MVA lagging power factor of 0.9.
- Capacitor: 0.8MVar.
- SG: 3-phase transformer 25/0.48kV, 150kVA, impedance 3%; firing angle of 20°; A-B signaling.
- SD: located at the 480V bus of DG transformer; detection channel is B-G (or the Phase-Ground channel with the strongest signal).

A. Signal Equations

The equivalent circuit representing the system is shown in Figure 3.14. For simplified analysis, both the load and the resistive components are ignored. According to the principle of superposition, the anti-islanding signal at the DG site is the response of the system energized by a virtual voltage source $-v_{TAB}$, where $v_{TAB} = \sqrt{2}V_N \sin \omega t$ is the steady state sinusoidal phase A-B voltage. This source is injected between phase A and B at the secondary side of the SG transformer during thyristor conduction. Symbols L_1, L_T, L_{Line1}, L_{Line2} and L_{DGxfmr} represent the positive sequence inductances of the utility system, SG transformer, Line1, Line2, and DG transformer respectively. L_{DG} is the inductance corresponding to the DG subtransient reactance. C represents the shunt capacitance. $L_{L2} = L_{Line2} + L_{DGxfmr}$, $L_{SD} = L_{DG}$.

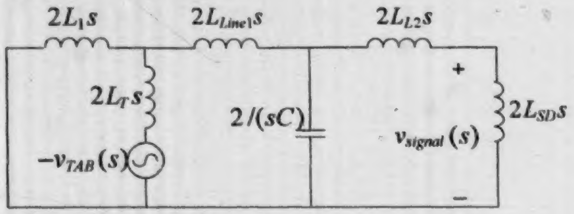

Figure 3.14 The equivalent circuit for signal propagation analysis.

The Laplace transformation of anti-islanding signal is determined to be

$$v_{signal}(s) = -v_{TAB}(s)\frac{L_1}{L_1 + L_T}\frac{L_{SD}}{L_{sum}}\frac{1}{1+(s/\sigma)^2} \tag{3.9}$$

where

$$L_{sum} = L_1 // L_T + L_{Line1} + L_{L2} + L_{SD} \quad , \quad L_{eq} = (L_1 // L_T + L_{Line1}) // (L_{L2} + L_{SD}) \quad ,$$

$$\sigma = \sqrt{1/L_{eq}C} \; . \tag{3.10}$$

According to the above equations, the following conclusions can be drawn:

- The signal at the DG site is initially driven by voltage source $-v_{TAB}(t)$ during the thyristor conduction period. After that, the signal is oscillatory at the natural frequency of the system σ.
- $-v_{TAB}(s)L_1/(L_1 + L_T)$ represents the signal level at the SG connection point X. The signal strength at DG terminal is reduced according to the ratio of L_{SD}/L_{sum}. It can be seen that a very large DG (meaning a small L_{DG} value) will lead to signal attenuation.

Suppose $-v_{TAB}(t) = \sqrt{2}V_N \sin(\omega t - \delta)[u(t) - u(t - \alpha/\omega)]$, where α is the total conduction angle of the thyristor, and $\alpha \approx 2\delta$ according to simulation results; $u(t)$ is the unit step function. The time-domain equation of the anti-islanding signal is derived according to (3.9) as follows (with the detailed procedures shown in Appendix A):

$$\begin{aligned} v_{signal}(t) = \frac{\sqrt{2}V_N K_{SD}}{1-\omega^2/\sigma^2}\{&\sin(\omega t - \delta)[u(t) - u(t-\alpha/\omega)] \\ &+ A_\delta \cos(\sigma t + \theta_\delta)u(t) + A_\beta \cos[\sigma(t-\alpha/\omega) - \theta_\beta]u(t-\alpha/\omega)\} \end{aligned} \tag{3.11}$$

where $K_{SD} = \dfrac{L_1}{L_1 + L_T} \dfrac{L_{SD}}{L_{sum}}$, $A_\delta = \sqrt{\sin^2 \delta + \dfrac{\omega^2}{\sigma^2} \cos^2 \delta}$,

$A_\beta = \sqrt{\sin^2 \beta + \dfrac{\omega^2}{\sigma^2} \cos^2 \beta}$, $\beta = \alpha - \delta \approx \delta$, $\theta_\delta = \tan^{-1}(\omega / (\sigma \tan \delta))$,

$\theta_\beta = \tan^{-1}(\omega / (\sigma \tan \beta))$.

Considering the damping impacts of resistive components in the circuit in Figure 3.14, the anti-islanding signal can be approximately expressed as

$$\begin{aligned} v_{signal}(t) = \frac{\sqrt{2} V_N K_{SD}}{1 - \omega^2 / \sigma^2} &\{\sin(\omega t - \delta)[u(t) - u(t - \alpha/\omega)] \\ &+ e^{-t/\tau}[A_\delta \cos(\sigma t + \theta_\delta) u(t) + A_\beta \cos(\sigma(t - \alpha/\omega) - \theta_\beta) u(t - \alpha/\omega)]\} \end{aligned} \tag{3.12}$$

where τ is a damping time-constant for the σ-frequency components in (3.11).

B. Computer Simulations and Sensitivity Study

Computer simulations have been carried out to study the anti-islanding signals. Representative signal waveforms are shown Figure 3.15.

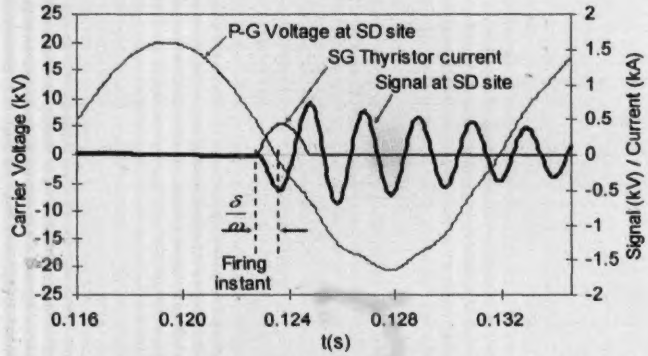

Figure 3.15 The representative signal waveforms.

(Voltages values at 25kV side, current values at 480V side; the same for the rest figures).

To determine which system components have more impact on the characteristics of the signal, key system parameters are varied, including the utility impedance (or fault level), the DG subtransient reactance (or DG capacity), the load level, the line length and the shunt capacitance. The variations of these parameters are shown as percentages of the base case values.

Figure 3.16 presents a series of anti-islanding signals obtained with computer simulations as the shunt capacitance varies from 0.4MVar to 2.75Mvar (or 50% to

344%). The waveform of the thyristor current has little changes as the shunt capacitance varies. The frequency of the anti-islanding signal reduces as the shunt capacitance increases; the strength of the anti-islanding signal, however, has a maximum value around the shunt capacitance of 0.8 Mvar (or, around the calculated $\sigma/(2\pi)$ of 491Hz).

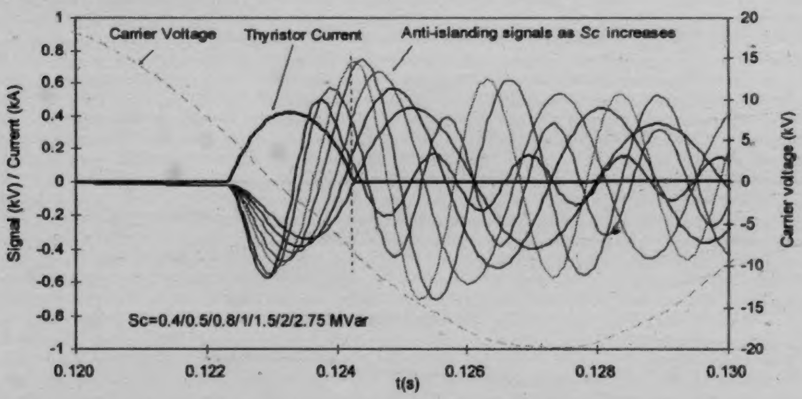

Figure 3.16 The anti-islanding signals corresponding to various shunt capacitances.

Figure 3.17 plots a series of anti-islanding signals calculated by using (3.12) as the oscillation frequency $\sigma/(2\pi)$ varies from 600, 500, 400, 300 to 200Hz due to the increase in the shunt capacitance. τ is assumed to be 0.004 second according to simulation experiences. The variation tendency of the anti-islanding signals in the upper graph coincides with the simulations in Figure 3.16 very well. The lower graph plots the three components of each anti-islanding signal separately: the fundamental component, the σ-frequency oscillating component starting at the thyristor firing instant, and the σ-frequency component starting at the thyristor extinction instant.

According to Figure 3.17, as the σ-frequency reduces, the variation in the magnitude of each component is not quite large. However, the magnitude of the sum of these three components (i.e., the anti-islanding signal) increases and then decreases as the σ-frequency drops from 600 to 200Hz. It is found that the maximum magnitude of the anti-islanding signal occurs when the 2nd positive peak of the oscillating components-1 appears around the positive peak of the fundamental component, i.e., when the 2nd positive peak of the oscillating component-1 appears at the thyristor extinction instant. Denote the σ-frequency corresponding to the largest magnitude of the anti-islanding signal as $\sigma_{\max}$. The above condition implies $2\pi/\sigma_{\max} \approx 2\delta/\omega$, i.e. $\sigma_{\max} \approx \pi\omega/\delta$. This analysis ignores the damping of the σ-frequency component. Therefore the calculated

$\sigma_{\max}$ tends to be slightly higher than the actual value. For a 60Hz system, when $\delta = 20^\circ = \pi/9$, the calculated $\sigma_{\max}/(2\pi) \approx 540\text{Hz}$. This approximately agrees with the simulation result of $\sigma_{\max}/(2\pi) = 491\,\text{Hz}$ in Figure 3.16.

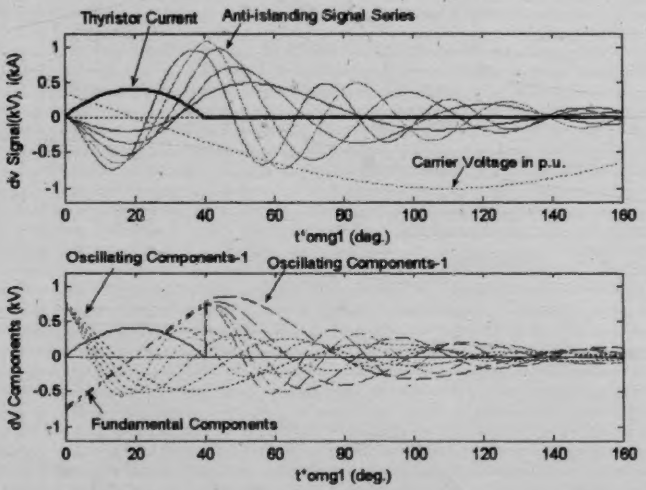

Figure 3.17 The calculated anti-islanding signals of different resonance frequencies.

Key signal characteristics of interest are studied in detail, including the signal peak value, signal attenuation and its oscillation frequencies. Figure 3.18 shows the signal strength *k* at the DG site. It can be seen that the impact of line length and load level is not very significant. The utility impedance has a large impact since it is the main factor influencing the voltage distortion level at the SG site. The impact of the DG subtransient reactance can be significant if the impedance becomes quite small. The impact of shunt capacitance is not straightforward. There is a value where the capacitor produces maximum signal level. Analysis based on Figure 3.17 has shown that this phenomenon is related to the natural frequency of the system, the firing angle, and an associated resonance situation. It is a coincidence in this case that the peak signal level occurs at 100% capacitor value. The signal RMS value is also determined and is found that it has similar variation tendency to the signal peak value.

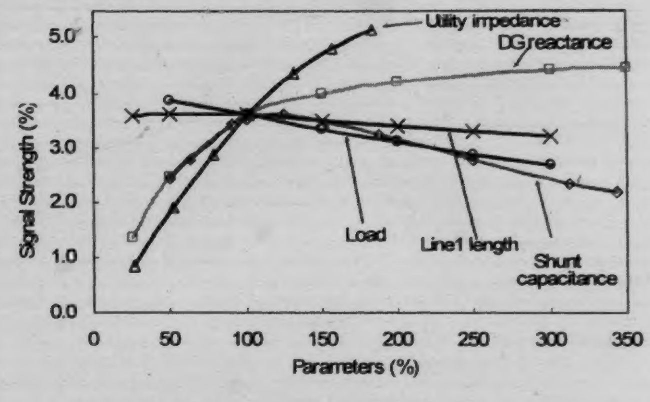

Figure 3.18 The signal strengths k as affected by system parameters.

Figure 3.19 shows the attenuation characteristics of the signal. The attenuation factor is defined as $k_{@DG} / k_{@SG}$. It characterizes the degree of signal reduction when it travels from the substation to the DG site. The attenuation is useful to guide the selection of SG size. The figure shows that the DG subtransient reactance (or DG capacity) is the main factor influencing signal attenuation. For the given system, when DGs capacity is lower than 10MVA, the signal attenuation is insignificant. For larger DG installations, a stronger signal generator may be needed. The result also shows that heavy load together with large shunt compensation can also cause notable signal attenuation. The system impedance has a negligible effect on signal attenuation.

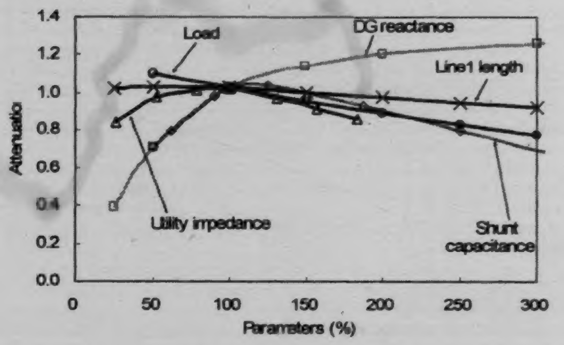

Figure 3.19 The system attenuation as affected by system parameters.

The characteristics of signal frequency are shown in Figure 3.20. This frequency is a critical parameter for the SD algorithm explained later. The frequency is estimated using a duration of 3 cycles of signal oscillation so it represents the dominant natural frequency of the system. The results show that the size of shunt capacitance affects the frequency most, which is followed by the utility impedance. The Line length and DG subtransient reactance have mild effects. The load has little effect. The results also reveal that typical signal frequency is within 200~600Hz.

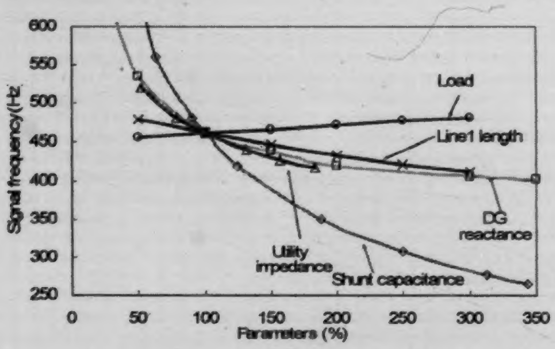

Figure 3.20 The signal oscillation frequency as affected by system parameters.

The case where SD is installed at the HV voltage side of the DG transformer (at 25kV) has also been studied. It was found that the signal strength is increased from 3.6% to 4.4%. As a result, connecting SD at the HV side is a very effective way to enhance signal detectability or to reduce the size of signal generator. On the other hand, the SD installation becomes more expensive since primary voltage PTs are needed. The simulation results have been compared with the calculated results using (3.10). A reasonable agreement is found between the simulation and analytical results. For example, the calculated oscillation frequency at the base parameters is 491Hz, which is very close to the simulation results. Detailed comparison results are shown in Figure 3.21. Main conclusion drawn from the comparative studies is that (3.9) and (3.10) can be used to estimate the key characteristics of the signal.

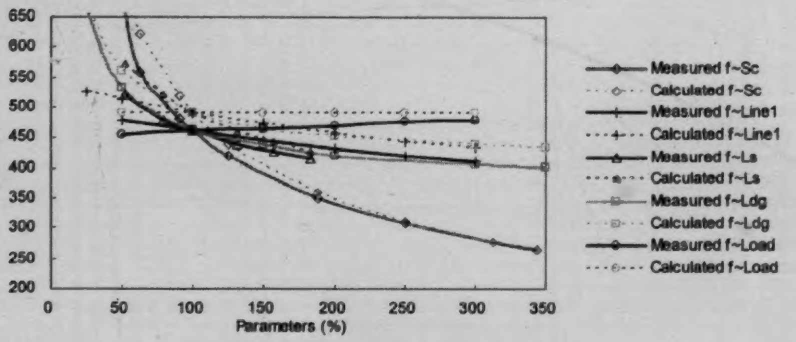

Figure 3.21 The measured vs. the calculated signal frequency.

3.5.3 Signal Propagation across Transformers

In the above discussion, the impact of transformer connection to anti-islanding signal propagation is ignored for the purpose of simplicity. In practice a DG is interconnected to the utility distribution network via a stepup transformer. This transformer is typically delta connected at the low-voltage (LV) side and grounded wye connected at the high-voltage (HV) side for fault current limiting and 3rd harmonic blocking purposes. The wye/delta connected transformers may cause the anti-islanding signal originally broadcasted with one channel to show up in another channel with a different strength. This section will discuss the propagation of signals across transformers.

Figure 3.22 illustrates a Y_g/Δ connected transformer interconnecting a DG to the distribution network. Consider the case that the signal is originally created using phase A to B channel in the distribution network. Suppose the signal strength at the transformer high voltage side is k_{AB}; the transformer HV and LV side line-line voltages are v_{LL1} and v_{LL2} respectively. The signal peak between phase A and B at the transformer HV side is therefore $v_s = \sqrt{2}k_{AB}V_{LL1}$. The A-G and B-G signal peaks are respectively $\frac{1}{2}v_s$ and $-\frac{1}{2}v_s$.

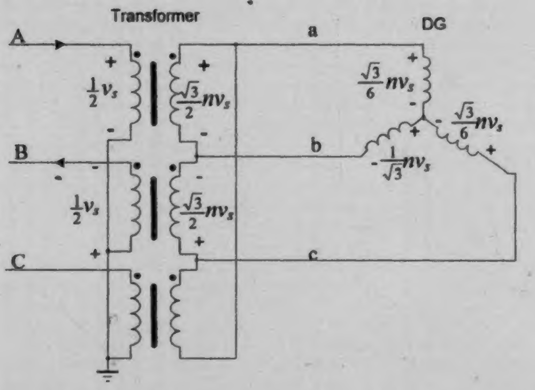

Figure 3.22 Signal propagation across a Y_g/Δ transformer (P-P signaling).

Denote $n = V_{LL2}/V_{LL1}$; the transformer HV to LV turns ratio will be $(V_{LL1}/\sqrt{3}) : V_{LL2} = 1 : (\sqrt{3}n)$. The signals at the LV side can therefore be calculated according to the ratio and the HV side strengths. Based on the results shown in Figure 3.22, the signal strengths detected with phase-phase channels at the transformer LV side are

$$k_{ab} = \frac{\frac{\sqrt{3}}{2}nv_s}{\sqrt{2}V_{LL2}} = \frac{\frac{\sqrt{3}}{2}v_s}{\sqrt{2}V_{LL1}} = \frac{\sqrt{3}}{2}k_{AB}, \quad k_{bc} = \frac{\sqrt{3}}{2}k_{AB}, \quad k_{ca} = 0, \tag{3.13}$$

where k_{ab}, k_{bc} and k_{ca} are the signal strength detected at phase a to b, b to c and c to a channel respectively. The signal strengths of phase to ground channels are

$$k_{bg} = \frac{\frac{1}{\sqrt{3}} n v_s}{\sqrt{\frac{2}{3}} V_{LL2}} = \frac{v_s}{\sqrt{2} V_{LL1}} = k_{AB}, \quad k_{ag} = k_{cg} = \tfrac{1}{2} k_{AB}, \tag{3.14}$$

where k_{ag}, k_{bg} and k_{cg} are the signal strengths detected at phase a, b and c to ground channel respectively.

The case where signal is created using phase A to ground channel at the transformer HV side is studied in Figure 3.23. The signal strengths at the LV side are calculated and the results are summarized in Table 3.4. Please note that the results are based on the transformer connection and phase labelling shown in the above figures. Should the phase labelling changes, for example, from *a*, *b* and *c* into *b*, *c* and *a*, the results need to be adjusted accordingly.

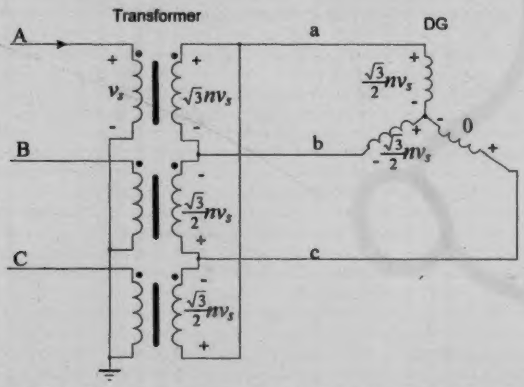

Figure 3.23 Signal propagation across a Y_g/Δ transformer (P-G signaling).

TABLE 3.4 SIGNAL PROPAGATION ACROSS A TRANSFORMER.

Signal Strength Transformer Connection	Primary-side Input	Secondary-side Output	
		P-P Signal Strength	P-G Signal Strength
Yg/Δ	A-B Signaling Signal Strength k_{AB}	a-b, c-a: $\frac{\sqrt{3}}{2}k_{AB}$ b-c: 0	a-g: k_{AB} b-g, c-g: $\frac{1}{2}k_{AB}$
	A-G Signaling Signal Strength k_{AG}	a-b: k_{AG} b-c, c-a: $\frac{1}{2}k_{AG}$	a-g, b-g: $\frac{\sqrt{3}}{2}k_{AG}$ c-g: 0
Yg/Yg	Phase-ground, or Phase-phase signaling	Same signal strengths as the primary side	Same signal strengths as the primary side

3.6 The Signal Detection Algorithms

As mentioned before, after the voltage distortion between two consecutive cycles (denoted as v_{signal}) is extracted, an algorithm is needed to detect whether a signal is actually present or not. Based on the characteristics of the signal at the DG site presented in the previous section, three signal detection algorithms are proposed and investigated. The objective is to choose the best algorithm for field implementation.

3.6.1 RMS-based Signal Detection Algorithm

The first algorithm was proposed at the beginning stage of the research and was adopted in the field tests. This algorithm is illustrated below in Figure 3.24, where v_{signal} denotes the voltage distortion between two consecutive cycles.

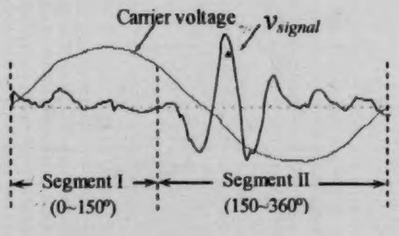

Figure 3.24 The original signal detection algorithm.

This algorithm uses the RMS and peak values of v_{signal} to detect the signal. As shown in Figure 3.24, this algorithm divides one fundamental cycle of distortion signal into two segments. Segment I is from 0° to 150°, and segment II from 150° to 360°. With a firing angle no higher than 30°, the signal will exist in segment II only. The RMS values of both segments are calculated using

$$RMS = \sqrt{\left(\sum_{i=1}^{N_{seg}} v_{signal\_i}{}^{2}\right) / N_{seg}} \tag{3.15}$$

where N_{seg} is the number of all sampled points for one segment. A detection logic can therefore be designed as follows: 1) A normal signal is considered as existent if the RMS and peak values of segment II are higher than a preset set of thresholds and the RMS value of segment I is lower than another threshold. 2) A signal is considered as nonexistent if the RMS of segment II is lower than a preset threshold. 3) If both RMS values of segments II and I are higher than their corresponding thresholds, or the RMS value of segment II is higher than its corresponding threshold but its peak value of segment II is lower than its corresponding threshold, the signal is considered abnormal and a warning is triggered. The field test showed that the average signal RMS strength was about 0.85%. A 0.44% threshold is found to give the best detection results for the system tested.

This algorithm is intuitively straightforward. When applied to actual field signals that contain high noise and low signal levels, its performance is not very good. As a result, two alternative algorithms are proposed.

3.6.2 Spectrum-based Signal Detection Algorithm

One new algorithm attempts to utilize the oscillatory pattern of the signal for detection. This algorithm works by doing Discrete Fourier Transform (DFT) analysis for a portion of the extracted signal. The DFT window is located in the position where the signal is supposed to show up. The window uses the zero crossing point of the carrier voltage as a reference. It has a width of 180° and starts 30° ahead of the voltage zero crossing point (Figure 3.25). If the signal oscillation frequency were known, one could use the magnitude of the resulting harmonic component whose frequency is closest to the signal oscillation frequency as an index to detect the existence of the signal.

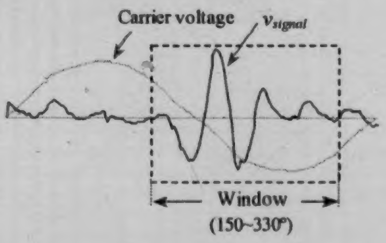

Figure 3.25 The spectrum-based detection algorithm.

In reality, the signal frequency is not known and is system dependent. The above spectrum based algorithm will make the signal detector too system dependent to be practically useful. In addition, the signal frequency may reside between two harmonics. This factor plus the transient nature of the signal waveform make the signal to show up as a group of harmonics in the DFT spectrum. Therefore, it is important to use a group of harmonic components for signal detection. Based on the field experience, reference [6] has shown that the natural frequencies of North American 60Hz distribution systems are between 200Hz to 600Hz. As a result, harmonics with order 4, 6, 8, and 10 are selected as a group to form a composite RMS index as follows:

$$RMS_h = \sqrt{M_{h4}^2 + M_{h6}^2 + M_{h8}^2 + M_{h10}^2} \tag{3.16}$$

where M_{hi} is the magnitude of the h_i^{th} harmonic. Note that due to the width of the DFT window used, only even order harmonics exist. A signal is considered as existent if index RMS_h is above a threshold.

The impact of the signal frequency on the performance of the proposed algorithm has been investigated. A simulated signal waveform with different oscillation frequencies f_i is input to the spectrum-based algorithm

$$v_{input} = \lambda_i \sin(2\pi f_i t)e^{-t/\tau}, \quad t \in [0, 2\pi/\omega] \tag{3.17}$$

where f_i varies from 100Hz to 700Hz, $\tau = 0.0018$ second; λ_i is a normalization ratio such that the actual RMS of the sampled signal is always 1. The normalized signals are plotted below in Figure 3.26 as f_i varies from 700Hz to 100Hz with a step of 100Hz.

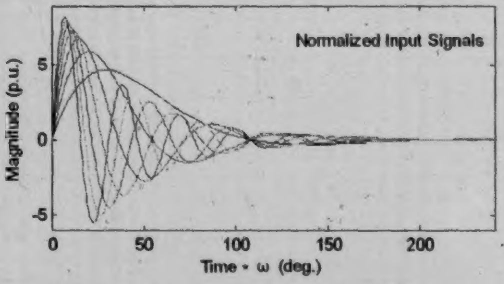

Figure 3.26 The simulated signals of various frequencies.

When the above signals are input to the spectrum based algorithm, the resulting spectrums and RMS_h are examined to verify if RMS_h is an adequate indicator of signal presence. The results are shown in Figure 3.27. Figure 3.27 (a) shows the magnitudes of spectrum components. It can be seen that as f_i varies from 200 to 600Hz, the highest component appears between the 2nd harmonic to 10th harmonic. Which harmonic exhibits peak value is dependent on the signal frequency. If we taken 4th, 6th, 8th and 10th harmonics into account in the RMS_h form of (3.16), most signal peaks will be included. Figure 3.27(b) shows that RMS_h value. It can be seen that RMS_h varies with respect to the signal oscillation frequency f_i. When f_i is within 200~600Hz range, RMS_h has a high response. It suggests that the index is suitable for the intended application. In fact, the RMS_h index filters out low and high frequency noises and could exhibit a better performance than the original RMS and peak based algorithm.

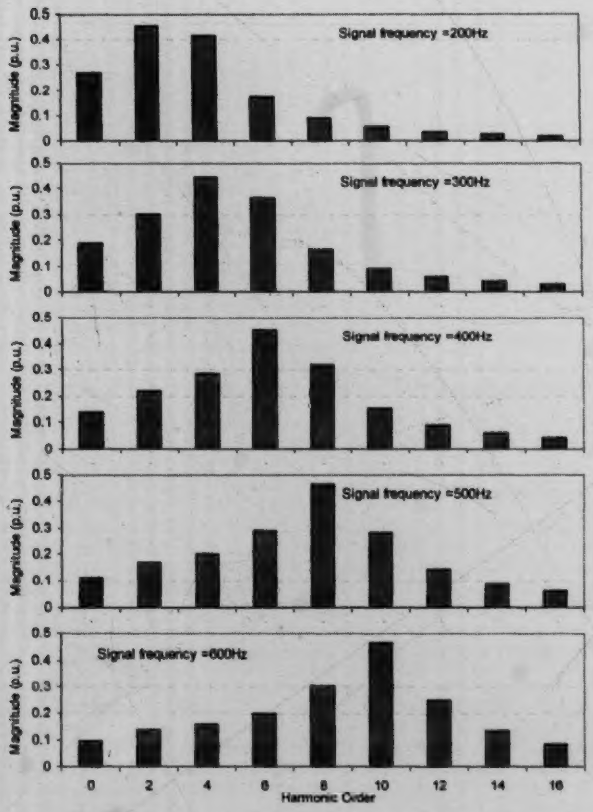

(a) Harmonic magnitudes as affected by signal frequency.

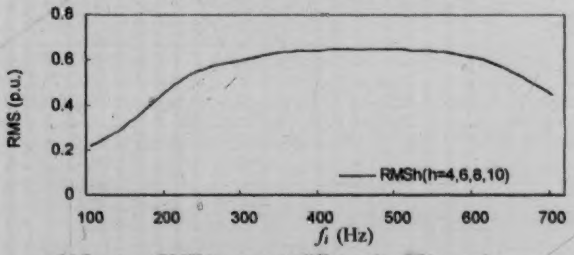

(b) Spectrum RMSh response to different signal frequencies.

Figure 3.27 The detection results of the spectrum-based algorithm.

3.6.3 Template-based Signal Detection Algorithm

The idea of another new index is to compare the distortion waveform with a preset signal template $v_{template}$ using the following correlation equation

$$CR = \sum_i v_{signal\_i} v_{template\_i} \tag{3.18}$$

A higher $|CR|$ index suggests a higher degree of match between the signal and template. A threshold for the *CR* index is applied to determine if a signal exists. An important consideration for this template-based method is how to select an adequate signal template. A system dependent template will generally improve the reliability of detection. But it makes the signal detector too complicated. After studying various options, a windowed sinusoidal waveform shown in Figure 3.28 (a) is selected as the template. The template is aligned to the thyristor firing instant on the voltage waveform. Since the thyristor firing angle is usually fixed (say, 30°), the template position is fixed. Under ideal condition, the frequency of the template sinusoid should be equal to the signal oscillation frequency. This will give almost "perfect" match between the signal and the template. In reality, however, the signal frequency is unknown. To overcome this problem, a set of templates is proposed, each with a different frequency and aligned at the same position. Utilizing the natural frequency data of reference [6], 5 templates with frequencies equal to 5th, 6th, 7th, 8th and 9th harmonics are selected as

$$v_{template} = \eta_i \sin(2\pi f_{template} t)\,, \quad f_{template\_i}\, t \in [0,2.5]. \tag{3.19}$$

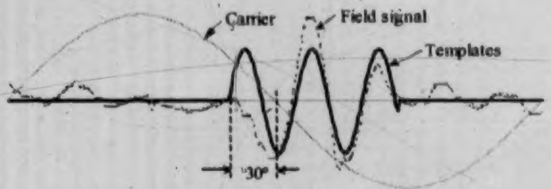

(a) A windowed sinusoidal template;

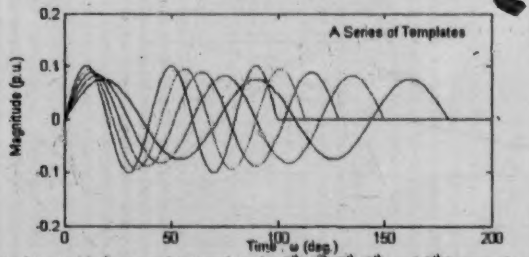

(b) Five templates with frequencies equal to the 5th, 6th, 7th, 8th, and 9th harmonic respectively.

Figure 3.28 The waveforms of signal templates.

Each template is of 2.5 cycles at its own frequency, and is normalized with η_i so that it has a RMS value of 1 (see Figure 3.28(b)). The detection index is

$$RMS_t = \sqrt{CR_{t5}^2 + CR_{t6}^2 + \cdots + CR_{t9}^2} \tag{3.20}$$

where CR_{ti} is the calculation result with the i^{th} template.

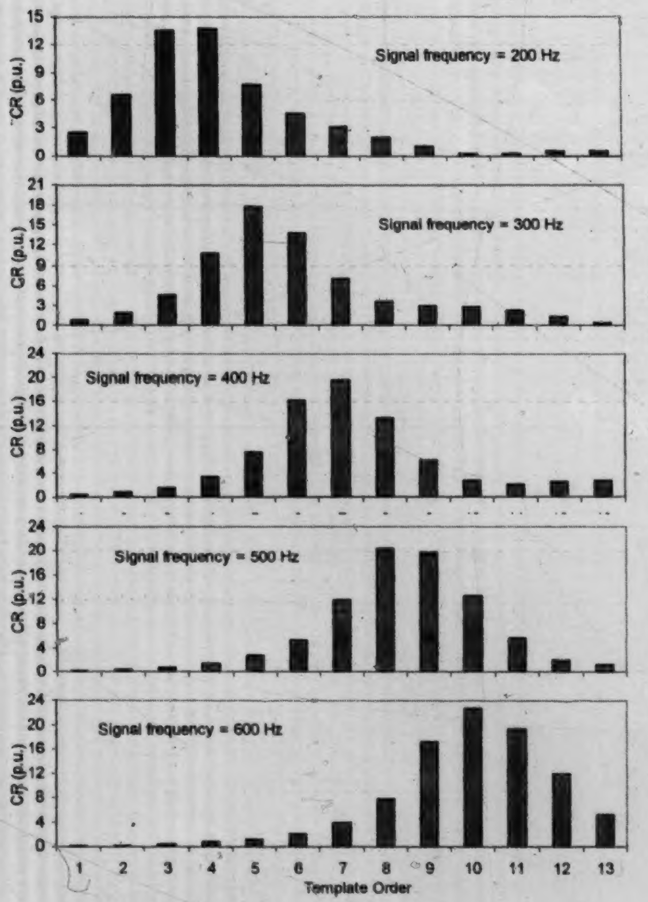

(a) $CR|$ indices computed using different templates.

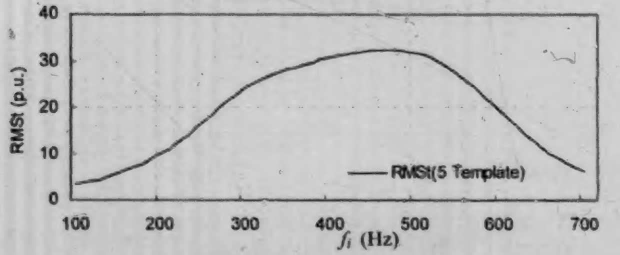

(b) Template RMS_t response to different signal frequencies

Figure 3.29 The detection results of the template-based algorithm.

The impact of signal frequency on the performance of the template-based algorithm has also been investigated as well. The same simulated signal is input to the algorithm. The results are shown in Figure 3.29. Figure 3.29(a) shows the CR index corresponding to different template orders. As expected, the best template that yields the highest CR value varies with signal frequency. For the signal frequency range of 200Hz to 600Hz, the peak CR value is obtained for templates corresponding to the 4th to the 10th harmonics. The CR indices for the 5th to 9th templates are combined to derive an aggregate value RMS_t as shown in (3.20). Figure 3.29(b) shows the RMS_t index. It can be seen that RMS_t index has similar features to those of RMS_h. It can also be used for detection.

Both new algorithms and the old algorithm have been tested using field data in comparison, which eventually decides which algorithm is the best choice. The thresholds were selected based on field test results as well. The findings will be reported in Section 4.3.

3.7 Conclusion

The islanding detection of synchronous DGs is one significant technical barrier for the fast growing DG industry. This chapter presented a new and powerful islanding detection concept and associated scheme. The scheme is similar to the telecomm-based transfer trip scheme. However, the signal is sent through power line, which makes the scheme applicable to any distribution system regardless the availability of telecomm means. More importantly, since the signal passes through any switches, breakers and other openable components connected between the substation and DG sites; the scheme is able to 'detect' automatically the opening of any components. This has resulted in a significantly simplified 'transfer trip' scheme. In addition, the scheme is also economically attractive to DG owners and utilities, especially for systems with multiple DG installations.

This chapter investigated the design considerations for the signal generator. A set of design formulas is established. Typical signal generator parameters are illustrated using actual system data. The proposed scheme can be implemented using other signaling techniques. Developing a signaling technique that can take advantage of the simple requirement of anti-islanding signaling to reduce the cost of signal generator is still a subject worth research.

The chapter further investigated the characteristics of the anti-islanding signal. Key factors that can affect the signal strengthen, attenuation and frequency are identified. Based on the findings, three signal detection algorithms are proposed. The algorithms are tested using simulated waveforms.

Chapter 4. FIELD TESTS OF POWER-LINE-SIGNALING-BASED ISLANDING DETECTION

Field tests were conducted in the spring and fall of 2004 to test the performance of the signal generator and the signal detector. A prototype signal generator and detector were constructed in 2003 at the University of Alberta. They were installed in the distribution system of ATCO Electric Ltd., an Alberta utility company, for field tests and evaluation. The prototypes were tested for more than 6 months in 2004 from January to March and from September to October. A lot of valuable information was collected on the characteristics of signal propagation, performance of signal detection algorithms and even the interference of the proposed scheme with an AMR system.

4.1 Field Tests Setting

The general arrangement of the field test is shown in Figure 4.1. A prototype signal generator (SG) was connected to the 25kV bus of a 216 fault MVA substation through a three-phase 300kVA, 25kV/480V stepdown (signaling) transformer. A prototype signal detector (SD) implemented on a laptop-based LabVIEW platform was installed at a 347V bus of a pipeline pumping station about 10km away.

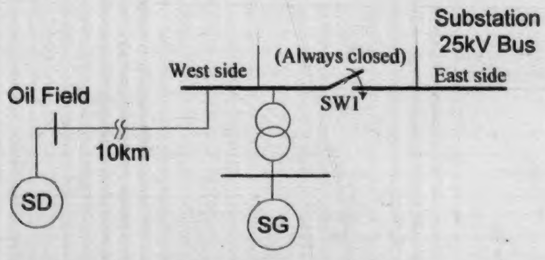

Figure 4.1 The field test arrangement.

A picture of the signal generator installed at the substation is shown in Figure 4.2. The signal generator is designed to fire the thyristor at 5, 10, 15 and 20 degrees at the negative-going voltage zero-crossing point. The signals can be sent between phase to ground or phase to phase. Based on the system parameters, the signal strengths are estimated as 2.5% for phase to ground signaling and 2.1% for phase to phase signaling respectively at δ =20° and for phase to ground signal reception. For the test results reported in the subsequent sections, the SG sent signals using the phase to phase channel and $\delta = 20^\circ$. For this signaling arrangement, the thyristor peak current is estimated as 1382A. It was a concern that such a high current could cause excessive temperature rise if the thyristors are fired too frequently. As a result, a signaling pattern of firing once every 4 cycles was used. The thyristor RMS current is about 168 A.

Figure 4.2 The installation of the signal generator at the substation.

The built-in signal detection algorithm was the RMS and peak based algorithm introduced before in Chapter 3.6.1. The signal detector is designed to operate with the 4-cycle signaling pattern. Four consecutive cycles is defined to be one signaling period. If a signal is absent for 3 continuous signaling periods, i.e. 12 cycles, an "islanding event" is detected. This means that the delay time for islanding detection is 12 cycles or 200ms. If the signal is absent originally for three signaling periods but is detected for next 3 consecutive signaling periods, the event is considered as the starting of DG and a "starting event" is detected. With this design, an individual abnormal signal doesn't cause starting or islanding event. But if the signals are abnormal for 3 continuous periods or the signals are normal but their pattern does not follow the signal generation pattern, a warning event is recorded and 24 cycles of data are saved for offline analysis.

4.2 Summary of Field Test Results

The field tests were conducted in the spring and fall of 2004. The most useful results are obtained during the fall test. Sample voltage and signal waveforms recorded for this test are shown in Figure 4.3. It can be seen that the signal is invisible from the voltage waveform, implying that the signal has little impact on power quality. The signal waveform v_{signal} was extracted by subtracting the 1st cycle by the 2nd cycle, the 3rd cycle by 4th cycle and so on of the carrier (voltage) waveform. Since the voltage waveform has 8 cycles, the signal plot contains 2 signaling periods. Each period has two segments. One of them contains the signal and the other doesn't. For the plot shown in the figure, the signal is in the first segment. The figure also plots $|v_{signal}|$ which is used for signal strength determination and for signal detection.

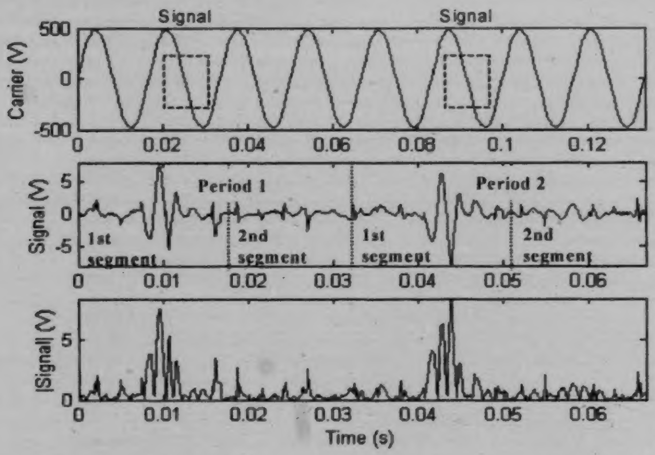

Figure 4.3 Sample waveforms of the carrier voltage and the anti-islanding signals.

Table 4.1 summarizes the main results obtained with the originally-designed RMS-based SD algorithm. The signal generator was turned on for four periods. As expected, all SG turn-off events, which represent genuine 'islanding events', have been correctly detected. The main concern here is if the signal detector could cause nuisance trips of a DG due to inability to detect the existence of the SG signals. It can be seen from Table 4.1 that a total of 4 nuisance "islanding" events occurred. This implies that the signal detector failed to detect the presence of the signal for some of the signaling periods. The threshold used for detection is also listed in Table 4.1. Note that the peak of the carrier voltage is 480V. So the RMS threshold is about 0.3% of the rated voltage peak.

TABLE 4.1 A SUMMARY OF THE FIELD TEST RESULTS.

Test Period	Duration	Threshold RMS (V)	Threshold peak (V)	Was the real "islanding" or SG "starting" event detected?	"Nuisance islanding" events detected	"nuisance starting" events when SG OFF	"warning" events when SG was ON/OFF
I	67 hours	1.5	4.0	Yes	3	many	many/many
II	24 hours	1.5	4.0	Yes	0	many	many/many
III	31 hours	1.5	4.5	Yes	1	many	many/many
IV	24 hours	1.5	4.5	Yes	0	many	many/many

*The waveforms of nuisance islanding events are shown in Appendix B.

4.2.1 Signal Characteristics

Figure 4.4 and Figure 4.5 show the signal strength (the *k* index defined on page 50) and the dominant signal frequency during the test period respectively. The data points are determined as follows: 1) a 16 cycles of waveform representing four signaling periods are selected randomly within every one-hour window; 2) the signal strength for each signaling period is then determined, which yields 4 values; and 3) these four values are averaged to arrive at one data point. So each point of the figure represents one hour. The frequency of the signal is determined by counting the averaged time span between two rising (or falling) edge zero-crossing points. The following conclusions are drawn:

- The average level of the anti-islanding signals is about 1.9%, which is consistent with the estimated level of 2.1%. However, the signal level fluctuates. The cause is not clear at present. More field measurement is needed.
- The signal frequency does not have significant variations during the test period. The frequency is around 430Hz. This characteristic is important for the spectrum and template based signal detection algorithms.

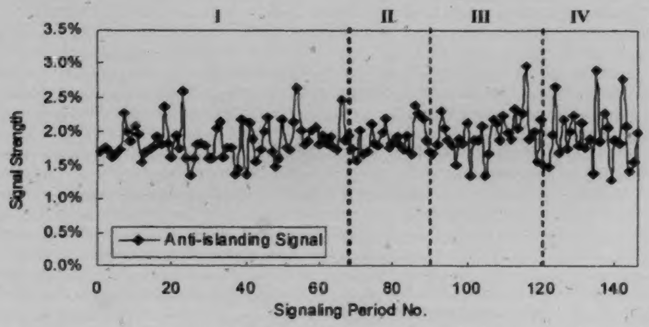

Figure 4.4 The signal strength during the field test period.

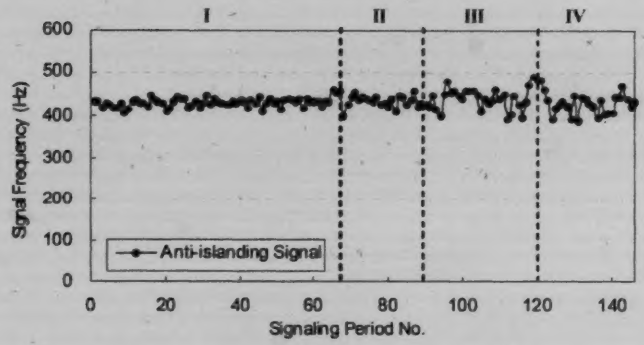

Figure 4.5 The dominant signal frequency during field test period.

4.2.2 Recorded Events

The recorded events were analyzed at University of Alberta power lab to understand the reasons of the signal detector's malfunctions. An example of waveforms that result in nuisance "islanding" events is shown in Figure 4.6. This figure shows that the signals are not strong enough for the 1st, 2nd, and 3rd periods. Therefore, the cause for the above nuisance islanding events is identified as a weak signal along with high noise. The signal peak is only about 5V or 1% in this case. As was mentioned, the average signal strength defined with signal peak is about 1.9% (Figure 4.4). The 1% signal level is too low to be detected by the RMS detection algorithm.

It is not clear, however, why the signal level dropped to 1% from a typical value of 1.9%. Figure 4.6 does confirm that the signal strength varied during the test period. Such a phenomenon needs to be investigated further. One solution to the nuisance "islanding" detection problem is to increase the signal level to about 3% to 4%. Improvement of the signal detection algorithm and/or increasing signaling periods will also help. This subject will be discussed in the next section.

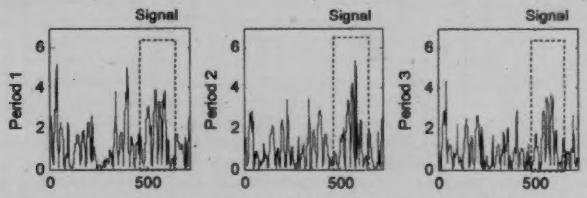

Figure 4.6 A sample of measured anti-islanding signal (Sep. 26, 00:01:22).

The field test also showed that disturbances or noise may present themselves as signals even if the SG is actually offline. In this case, the SD will incorrectly record such events as the starting of the signal generator. This problem is mitigated by improving the verification of the uniformity of the signal pattern for several signal periods. As a result of this improvement, most nuisance starting events have been eliminated as well.

The field test task also evaluated various warning events recorded. Some warning events are determined to be caused by disturbances and one example is shown below in Figure 4.7. The rest are caused by interferences with AMR signals, which will be discussed later in Section 4.4.

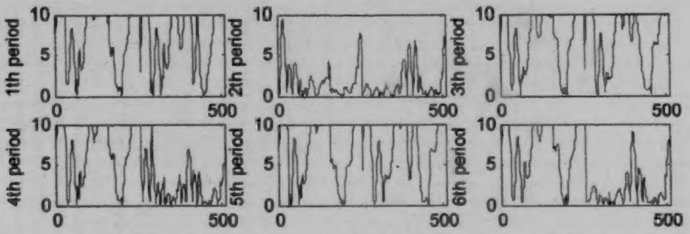

Figure 4.7 A sample warning event caused by disturbances (Oct. 19, 17:19:32).

Main conclusions drawn from this field test are summarized as follows:

- All SG shut off events which represent genuine "islanding" cases have been detected correctly;
- The SD failed to detect the presence of the anti-islanding signal for 4 occasions. This means that the nuisance trips of DG could occur. There is a need to address this issue.

4.3 Evaluation of Three Signal Detection Algorithms

The spectrum and template based signal detection algorithms were proposed in response to the poor performance of the RMS based algorithm. In this section, they are evaluated using about 18,400 signaling periods recorded in the field tests. These periods were recorded because they have low signal levels that lead to warning events or false 'islanding' detection. To test the robustness of the template-based algorithm, the templates are aligned at the instant corresponding to a firing angle of 30°, which is different from the actual firing angle of 20°.

4.3.1 Typical Performance

A set of normal signaling periods in Figure 4.8 is used as an example to show how the algorithms' performance is assessed.

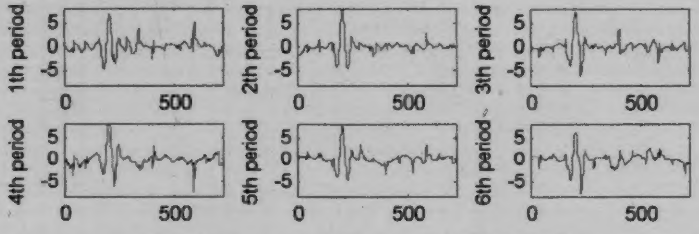

Figure 4.8 A normal signaling event (Sep. 25 22:55:10).

Recall that each signaling period consists of two segments of signal waveforms (see Figure 4.3). One of them contains the signal and the other contains no signal. RMS_h and RMS_t are calculated for both segments. The results corresponding to the signal-containing segment is labelled as 'with signal' and those corresponding to the no-signal segment are labelled as 'without signal'. Figure 4.9(a) and (b) plot the spectra of six segments "with signals" and the corresponding segments "without signals". This figure shows that the energy of the signal-containing segments concentrate in the 4th to 10th harmonics, supporting the design of the spectrum based algorithm. The energy levels of signal-containing segments are much higher than those of segments without signals. The RMS_h results are shown in Figure 4.9(c). For reliable signal detection, the two sets of RMS_h values should be far apart. The vertical separation of the two curves shows the ability of an algorithm to distinguish signals from noises. For the results shown in Figure 4.9(c), there is a clear separation between the segments with signal and those without signal. A detection threshold of, say, 1.2V can be used to detect the signal easily.

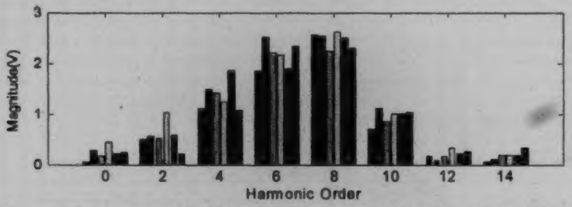

(a) Spectra of six segments "with signals" (Harmonic peaks plotted instead of RMS).

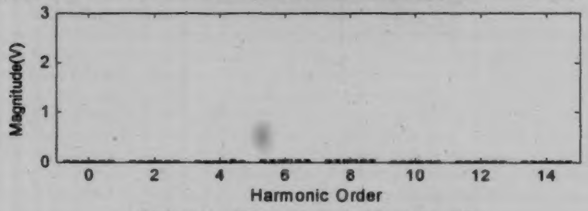

(b) Spectra of six segments "without signals".

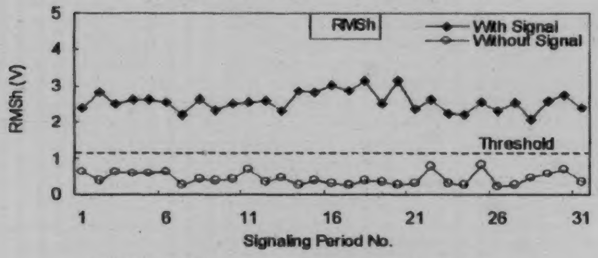

(c) The RMS_h of segments with signals and without signals.

Figure 4.9 The spectra and RMS_h of typical signaling periods.

Figure 4.10 plots the $\sin(\theta_h)$ of signal containing segments, where θ_h is the phase angle of h^{th} harmonic calculated with DFT. It is proposed to use the sign of $\sin(\theta_h)$ corresponding to the highest harmonic to represent the signal polarity.

This will be discussed further in Section 4.5.

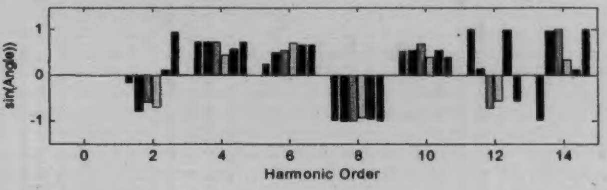

Figure 4.10 The $\sin(\theta_h)$ plot for polarity determination.

For the template-based algorithm, Figure 4.11(a) and (b) show the CR plots of signal and noise-containing segments respectively. The CR bars with signals are much higher than those without signals, and the energy concentrate in the 4th to 9th harmonics. Figure 4.11(c) plots the RMS_t. The curves with signals and without signals are far apart vertically, which means the RMS_t index can reliably detect the presence of signals. A threshold of 15p.u. can be used to detect the signals.

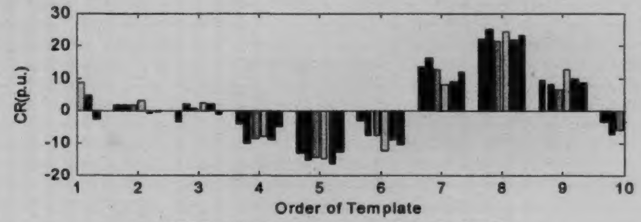

(a) The CR plot of six segments "with signal".

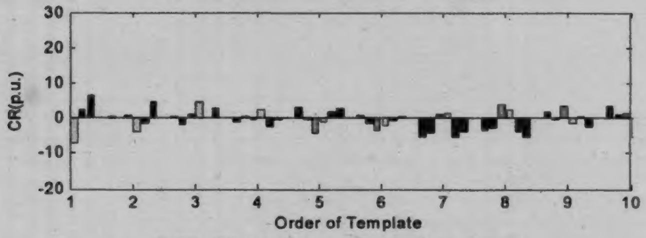

(b) The CR plot of six segments "without signal".

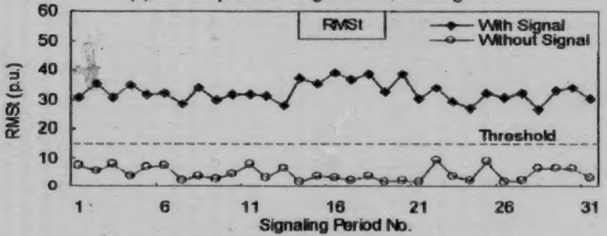

(c) The RMS_t of segments with signals and without signals.

Figure 4.11 RMS_t of signaling/non-signaling cycles from 31 records.

4.3.2 Performance with Nuisance Islanding Events

Waveforms recorded for the 4 false 'islanding' events that could cause nuisance DG trips were analyzed in detail. Figure 4.12 to Figure 4.14 show the signal characteristics when different detection algorithms are applied to the data. According to Figure 4.12, it is very hard to separate the signal-containing data from the non-signal data. This is especially true for event 4. The findings explain why the RMS algorithm will lead to false islanding detection for the signaling periods. In comparison, indices *RMS*$_h$ and *RMS*$_t$ show improved separation between the signals and noises. There will be no nuisance "islanding" detection according to the new algorithms. When these algorithms are used, the false islanding detection events are eliminated.

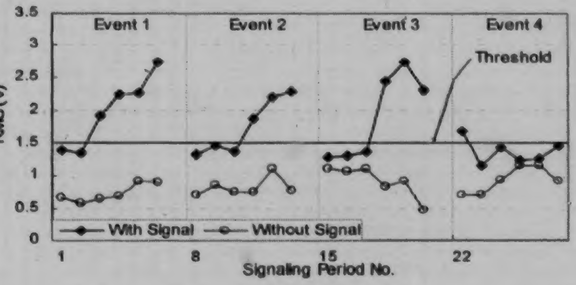

Figure 4.12 Performance of the *RMS*-based algorithm.

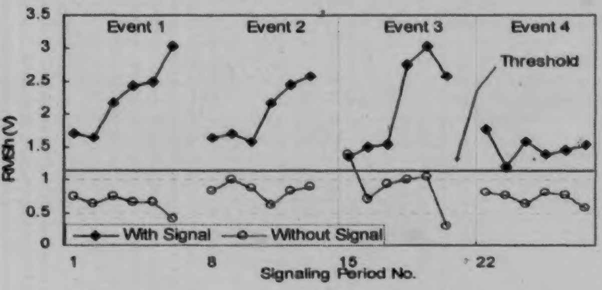

Figure 4.13 Performance of the spectrum-based algorithm.

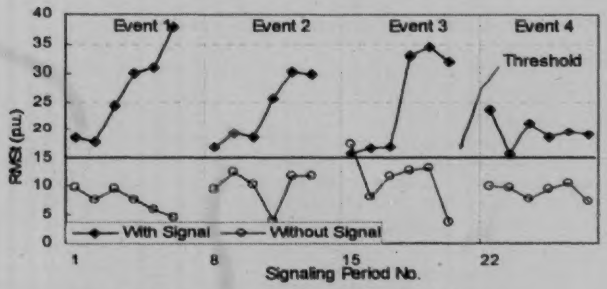

Figure 4.14 Performance of the template-based algorithm.

4.3.3 Statistical Performance Analysis

To understand the statistical performance of three detection algorithms, all 18,400 signaling periods are played back to the algorithms. These periods were recorded throughout the test periods and were determined to be containing normal signals. The results are shown in Figure 4.15 to Figure 4.17. To avoid crowding caused by massive amount of data points, the plots just show the points sampled from the original results at a rate of 1 sample per 12 data points. It can be seen that the signal strength is generally constant for the test duration. However, there is a large fluctuation of signal strength for period IV. Some of the high signal cases were analysed and the cause was found to be AMR interference (see Section 4.4.2). For the period III, the signal level is lower than average. The causes have not been found.

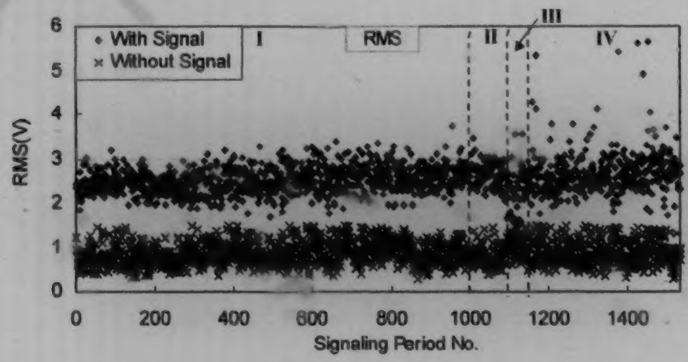

Figure 4.15 Statistical performance of the *RMS*-based algorithm.

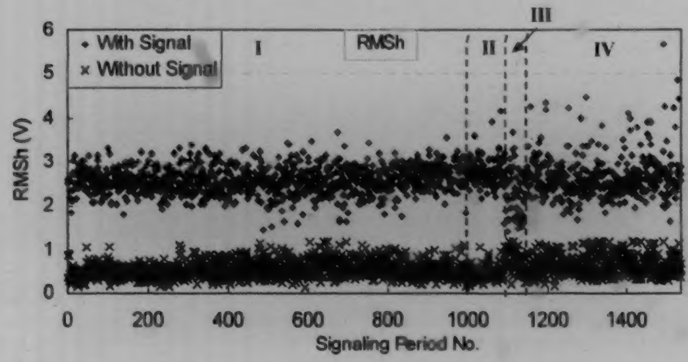

Figure 4.16 Statistical performance of the spectrum-based algorithm.

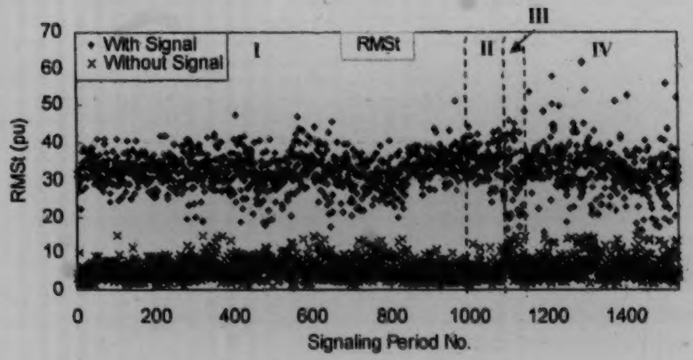

Figure 4.17 Statistical performance of the template-based algorithm.

To quantify the signal detection capability of different algorithms, an index of signal to noise ratio is determined. The ratio is defined as

$$\text{Signal Noise Ratio} = \frac{RMS_{withSignal}}{RMS_{nonSignal}} \tag{4.1}$$

Figure 4.18 shows the statistical distribution of the ratio index. According to the figure, the average signal to noise ratios of *RMS*, *RMS*$_h$ and *RMS*$_t$ are about 3, 4.5 and 6 respectively. A higher ratio means that the corresponding algorithm can detect the signal more reliably. The results confirm the observation that the RMS based algorithm has the poorest performance. Note that although the ratio of *RMS*$_t$ has the highest average, it distributes in a wider range than the other two ratios. In the worst case, the ratio of *RMS*$_t$ drops to 2.8 and is close to the worst case of *RMS*$_h$.

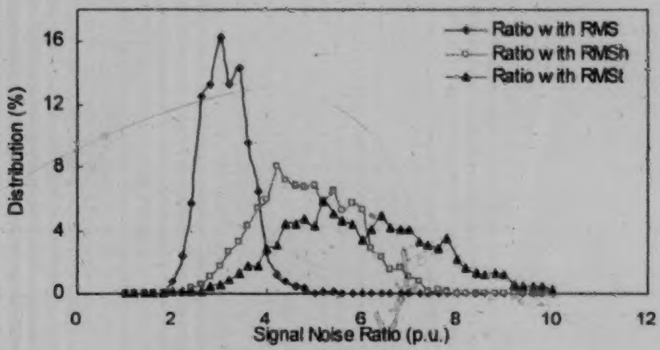

Figure 4.18 The distribution of signal to noise ratios.

Based on the above results, we can conclude that the spectrum and template based algorithms have better performance than the RMS algorithm. There is no significant performance difference between the spectrum and template based algorithms. Either of them can be selected for implementation. However, the algorithms have different computational burden, which becomes a deciding factor.

4.4 Interferences between Islanding Detection and AMR

The potential interference between the anti-islanding and the AMR schemes becomes a natural concern. Understanding the nature and degree of inference is critical to the acceptance of the proposed anti-islanding scheme by industry. Fortunately, the ATCO Electric is the first utility company that deployed the waveform distortion based AMR scheme. As a result, the project had the opportunity to evaluate the interference concern. The test set up for study of interferences between anti-islanding and AMR schemes is shown in Figure 4.19.

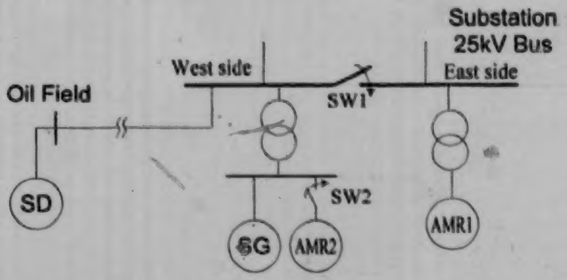

Figure 4.19 Parallel operation of anti-islanding and AMR schemes.

(According to ATCO record, SW1 remains closed during the field test; SW2 was open when SG is ON.)

The AMR system was running concurrently with the SG during test periods II and IV. The AMR system was also running in each gap between two SG operating periods. Note that the AMR system also sends signals occasionally even if no meter reading takes place. The purpose is to calibrate time for the revenue meters. Test periods I and III were run under such condition. For all test periods, the channels used by the AMR were essentially random. The AMR operation status is listed in Table 4.2. Large quantities of AMR signals were found from SG II-OFF-1, and from III-OFF to IV-ON period.

TABLE 4.2 AMR OPERATION TIME SCHEDULE

SG	I-ON	I-OFF	II-ON	II-OFF	III-ON	III-OFF	IV-ON	IV-OFF
AMR	Passive	Active	Active	Active	Passive	Active	Active	Active

*AMR active means AMR signals have been detected during this period, but not necessarily throughout the whole section.

4.4.1 AMR Signal Characteristics

Figure 4.20 is a chart representing the signal levels of both AMR and SG during the testing period. It is plotted with data points which were chosen approximately every 2 hours. The following conclusions are drawn from this chart.

- The average level of SG signals is 1.9%, and the average level of AMR signals is 3.4%.
- The level of SG signals appears to stay relatively constant, while the AMR signal level varies drastically with time. This may be caused by the change of AMR signal channel. This subject will be discussed further in the next section.
- When both SG and AMR signals are detected during the 2nd and 4th SG ON period, the level of AMR signals greatly decreased from the average level. This is because both AMR1 and AMR2 were operating when SG was off, while only AMR1 was operating when SG was on.

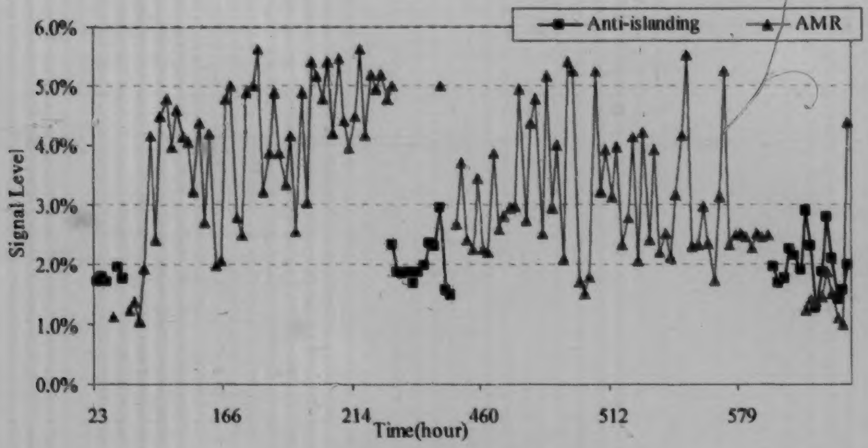

Figure 4.20 SG vs AMR signal strength.

Besides the signal level, the SG signal phase location in a fundamental cycle of voltage waveform is also examined. According to field test results, the SG signal starts at around 160° of the fundamental cycle of Phase A to ground voltage and the signal transient lasts about 90°. A sample signal is shown in Figure 4.21.

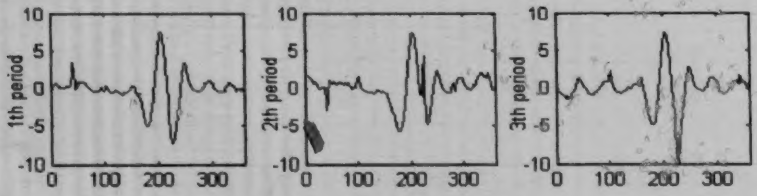

Figure 4.21 A sample anti-islanding signal.
(Y axis: vsignal in V; X axis deg.; Sep. 30, 13:50:36).

The AMR signals, however, showed up in different phase locations. Sample results are presented in Figure 4.22. The results indicate that the AMR was using different channels for signaling during the test periods. Therefore the phenomenon of varying AMR signal level (at the channel measured by SD) becomes understandable. It's also observed that the AMR signal levels dropped approximately by half during the parallel tests periods no matter which phase location the AMR signals assumed. It is inferred that when SG was OFF, both AMR1 and AMR2 were active; while during the parallel tests when SG was ON, only AMR1 was operating and this caused the AMR signal level to drop by half.

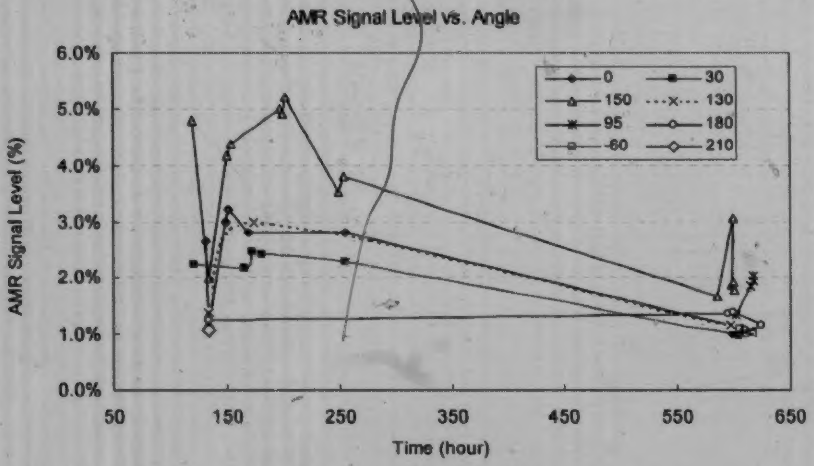

Figure 4.22 AMR signal strength vs. phase angle.

4.4.2 AMR and Islanding Detection Signal Interference

Main findings from the tests are as follows:

- When the SG is ON, an AMR signal appearing at a different waveform location from the anti-islanding signal caused SD to detect warning events. A number of warning events were captured during the period IV and an example was shown in Figure 4.23.

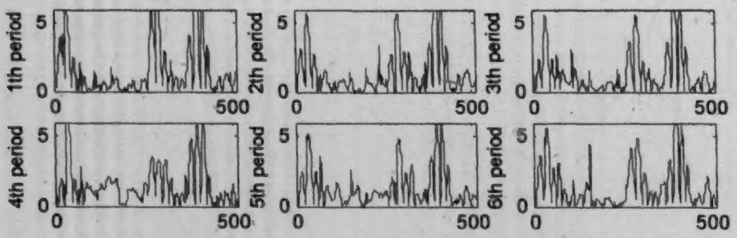

Figure 4.23 A warning event caused by AMR signals (Oct.19 17:12:32).

- When the SG is ON, an AMR signal appearing at the same waveform location as the anti-islanding signal (say, around the negative-going zero-crossing point) can amplify or weaken the detected anti-islanding signals. If an AMR signal and an anti-islanding signal are generated at the same position of two adjacent cycles, the subtraction of these two cycles will show no signal or very weak signal. As a result, the anti-islanding signal may not be detected. If an AMR signal and an anti-islanding signal are generated at the same position of the same cycle, this will strengthen the anti-islanding signal. The fluctuating anti-islanding signal level recorded in period IV is due to this cause. In an example in Figure 4.24 below, the signals appearing in the first half plotting window are AMR signals due to its varying polarity and firing angle. The signals in the second half window are anti-islanding signals. Analysis showed that the anti-islanding signal was missing in the 2nd, 3rd and 5th period because of the AMR signal interference.

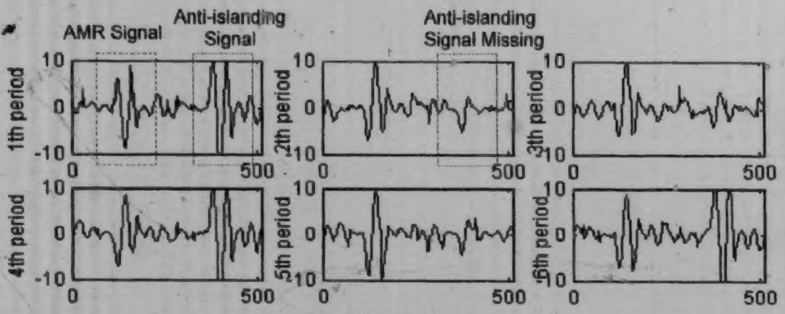

Figure 4.24 A record with both SG and AMR ON.

(Y axis: vsignal in V; X axis: sample points. Oct.20 01:19:40).

- Theoretically, the AMR signals could cause nuisance DG trips by 'erasing' the anti-islanding signal. For such events to happen, the AMR signal must have a pattern complement to that of the anti-islanding signal so that the subtraction of two waveform cycles result in null signals for 3 continuous signaling periods. This is a low probability event and it was not encountered in the field.

- When the SG is OFF, AMR signals resulted in warning and even starting events. This is due to the fact that the signal detector treats the AMR signal as the anti-islanding signal mistakenly. Examples are shown in Figure 4.25 and Figure 4.26.

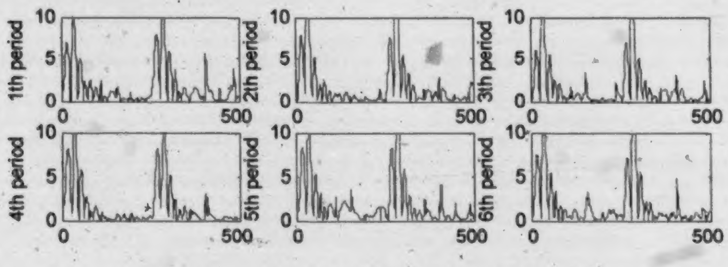

Figure 4.25 A warning event caused by AMR signals (Sep. 27, 08:31:19).

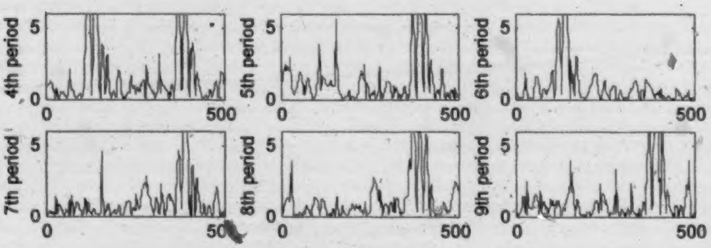

Figure 4.26 A sample nuisance starting event (Oct. 21, 18:37:48).

In summary, the impact of the AMR signal on the proposed anti-islanding scheme is insignificant. This is because the AMR has not caused nuisance "islanding" detection when the SG is ON. It only caused warning events. Furthermore, if a SG is put into operation to send anti-islanding signals, a lack of a SG signal means islanding has happened. The AMR signal won't be able to reach the DG site either. As a result, AMR signal cannot sustain an island. So we can conclude that the AMR is very unlikely to cause interference to the anti-islanding scheme.

It is likely that the anti-islanding signal will affect the operation of the AMR system. The experience of the ATCO Metering Department during the test did not suggest that such interference has happened. The AMR system worked smoothly during the entire field test. One of the explanations may be that the AMR signal at 4% is much stronger than the anti-islanding signal that is at 1.9%. However, a lot more field tests are needed to confirm if the anti-islanding signal is indeed troublesome to AMR. Should interference exist, one of the solutions is to let the AMR signal transmitter broadcast both meter reading and anti-islanding signals but using different signaling channels.

4.5 Complete Signal Detection Algorithms

This section introduces the complete signal detection algorithms developed using spectrum or template based detection criteria. The algorithms can be briefly described as follows.

- The algorithms check each cycle of transient signal independently. Each cycle of signal is divided into two segments. Segment I of (150°~330°) is where a signal supposed to show up, and Segment II of (0°~150°) ∪ (330° ~360°) is supposed to contain no signal. The RMS_h (or RMS_t) of Segment I and *RMS* value of Segment II are checked. If the RMS_h (or RMS_t) is below a certain threshold, a code 00 is generated; if the RMS_h (or RMS_t) is above the threshold, and the *RMS* value is below another threshold, a code 01 is generated; if the RMS_h (or RMS_t) is above the threshold, while the *RMS* value is also above another threshold, a code 11 is generated;

- Suppose the SG fires every four cycles, and two cycles of transient signals will be obtained for one signaling period. By putting the code of these two cycles together, a four-digit code is generated. If the sum of four digits is 0, there is considered to be no signal; if the sum is 1, there is determined to be a signal; if the sum is above 1, it is regarded as abnormal condition.

- When signal turns from present to absent for 3 continuous signaling periods, an islanding condition is determined; when the signal turns from absent to present for 20 continuous periods, and the code remains the same, a SG starting event is determined; when the code are abnormal for 3 continuous periods, a warning event is determined.

The indices of signal polarity studied in section 4.3.1 are abandoned in the final algorithm due to their unsatisfactory precision. In order to reliably determine SG starting events, a long delay of 20 periods are used instead of checking the uniformity in signal polarities.

4.6 Conclusion

This chapter presented field results and their analysis for the proposed DG islanding detection scheme. The field test arrangement and device settings were explained. The main findings from the field test study are

- The proposed scheme performed successfully during the field test. The four false islanding events encountered during the test were eliminated using improved signal detection algorithms.

- The measured average SG signal level was about 2%, agreeing with theoretical results. This signal level was about 40% lower than the level of the AMR signal. As a result, there is still room to improve the signal detection reliability for the proposed scheme. The field test experience suggested that a signal level of 4% was probably the best compromise between reliable signal detection and the cost of signal generator. Power quality is not a concern at this signal level.

- The investigation of the interference between the AMR and anti-islanding schemes showed that the AMR system was unlikely to cause problems to the anti-islanding scheme. Although field experience suggested that the anti-islanding scheme did not interfere with the AMR system, more field tests are needed to clarify this issue.

- The analysis identified a number of potential improvements to the signal detection algorithms. We intend to develop a new algorithm based on the experience gained from this test.

Chapter 5. THE SCALABLE ISLANDING DETECTION SCHEME

This chapter presents an important improvement of the above power-line-signaling based islanding detection scheme to increase the original scheme's flexibility and adaptability. With this improvement, the signal-generation device can be located at any place between the substation and the DG sites. As the device moves downstream, the signal coverage area shrinks while the flexibility of implementation increases. This feature is called the scalability of the scheme. For different DG interconnection scenarios, the signaling device can be located to meet the minimum requirement for the signal-coverage area. In this way, even if only a few DGs are interconnected in the distribution network, the power-line-signaling-based islanding detection can still be economically practical. In the improved scheme, the signaling device needs to monitor its connection status to the main supply by examining an extra current signal. The contents presented in this chapter have been published in [73].

5.1 The Idea of Scalable DG Islanding Detection

The original power-line-signaling-based scheme continuously broadcasts a voltage distortion signal (i.e., an anti-islanding signal) downstream from the substation and, therefore, transforms the detection of islanded DGs into the checking of signal continuity at DG sites. As shown in the sample distribution system in Figure 5.1, one signal generator (SG) installed at the substation secondary bus (Site-1) satisfies the needs of all the downstream DGs (DG1, DG2, and DG3…). The costs of the SG can be shared among the DG owners. However, depending on the ownerships of the substation and feeders, there are some practical issues to overcome. Because of deregulation, different companies may own the substation and its feeders. It can be difficult for a distribution company to install a device in the transmission substation. So the flexibility in locating the SG is an important feature. If there is only a limited number of DGs near the end of a feeder, it would be advantageous to install the SG just upstream of these DGs as the SG transformer's size could be reduced. The size of this transformer is closely related to the fault level at its location (see Section 3.5.1). When the SG is installed at the substation, a large signal transformer is often needed.

Our proposed solution is to locate the SG downstream of the substation when only a few DGs are interconnected in the distribution network. As shown in

Figure 5.1, when only two DGs, DG1 and DG2, exist, the SG can be moved from Site-1 to Site-2. In this way, the anti-islanding signal broadcast downstream by the SG has a smaller coverage area, which still contains DG-1 and DG-2. This arrangement avoids the need to access the substation, and a smaller signal transformer can be used. This feature of moving the SG downstream and having a variable coverage area and cost is called the scalability of the power-line-signaling-based scheme and makes the anti-islanding scheme more adaptable to various DG interconnection scenarios.

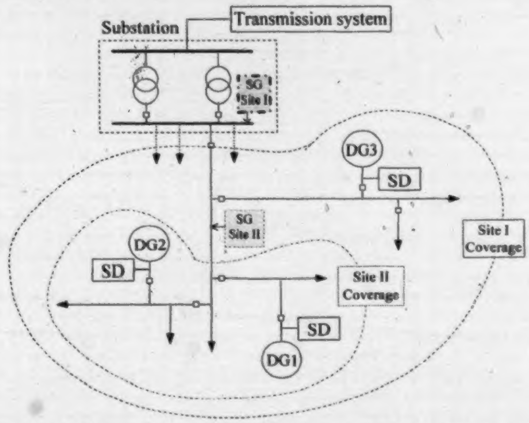

Figure 5.1 A sample system using power-line-signaling based islanding detection.

As the SG is moved away from the substation secondary bus, a new problem arises: how can we know if the SG is still electrically connected to the main supply? This condition must be monitored at all times. Once the SG is determined to be isolated from the main supply, it must stop broadcasting immediately and therefore trip all the downstream DGs.

We propose to detect the SG connection status to the main supply by monitoring the transient current signal flowing in the line at the upstream side of the signal generator. This current signal is created as a byproduct of the voltage distortion signal generation process. Figure 5.2 shows the architecture of the signal generator in the improved scheme. The same stepdown transformer and thyristors as those in the original scheme are used to create the voltage distortion signals. Moreover, a current transformer (CT) is installed at the SG upstream side, monitoring the line current. When the thyristor is fired to create a voltage distortion signal, a transient current signal flows through the CT. If the SG is connected to the main supply, this transient current will have a pulse-like shape (see Figure 5.3). If the SG is disconnected from the main supply, the shape of this current waveform will be different. The transient current waveform can therefore be used for monitoring the SG connection status to the main supply. The transient current signal detector in Figure 5.3 extracts the transient current using the subtraction method introduced in Section 3.4.2, and then determines the SG connection status using the algorithm investigated later in Section 5.2.2.

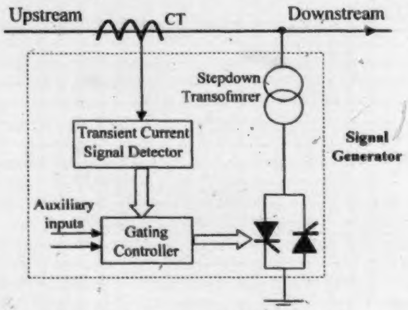
Upstream
CT
Downstream
Stepdown Transofmrer
Transient Current Signal Detector
Signal Generator
Auxiliary inputs
Gating Controller

Figure 5.2 The architecture of the new signal generator (one phase illustration).

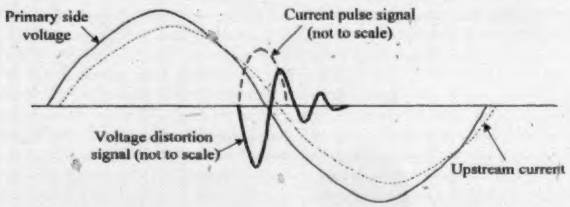
Primary side voltage
Current pulse signal (not to scale)
Voltage distortion signal (not to scale)
Upstream current

Figure 5.3 Transient voltage and current signals with SG connected to the main supply.

The improved power-line-signaling-based scheme has been developed to suit various DG interconnection scenarios and to reduce costs. The signal generator can be installed at any place between the substation secondary bus and the DG sites. There are three possible arrangements.

1) The SG is installed just outside of the substation and connected to the sending end of a particular feeder. This arrangement is suitable for the scenario where many DGs are connected downstream and does not require access to the substation.
2) The SG is connected at any point along distribution feeders. A typical application of this arrangement is to connect the SG at the upstream of an area with many DG installations.
3) The SG is connected at the DG site. In this arrangement the SG can be directly installed at the DG terminal and does not require a stepdown transformer. Checking of the voltage distortion signal is not necessary. This arrangement is of low cost and is suitable for the scenario where only one DG exists.

With the above arrangements, the upstream current pulse must be checked to determine if the SG is connected to the supply system.

5.2 Detection of SG Connection to the Main Supply

The main challenge for the proposed scheme is to determine whether or not the SG is connected to the main supply according to the upstream transient current signals. When the SG is connected to the main supply (see Figure 5.4(a)), the upstream transient current is a pulse-like signal. When the SG becomes isolated from the main supply, the shape of the transient signal will be different. In a simple case that the SG is at the feeder sending-end, this signal simply disappears when the SG becomes isolated. In another case where a shunt capacitor is connected to the feeder before the SG (see Figure 5.4(b)), the capacitor might mimic the main supply and contribute to a large transient current even when the SG is isolated from the main supply. The main objective of this section is to identify the SG connection status in the second case. Computer simulations were performed to search for a criterion.

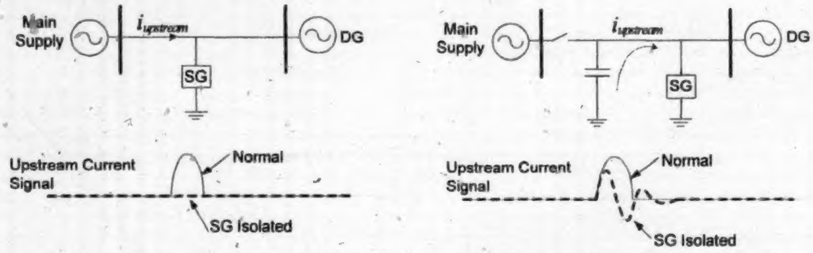
Main Supply
$i_{upstream}$
DG
SG
Upstream Current Signal
Normal
SG Isolated
Main Supply
$i_{upstream}$
DG
SG
Upstream Current Signal
Normal
SG Isolated

(a) SG at feeder sending-end; (b) Shunt capacitor connected before SG.

Figure 5.4 Illustration of possible influence of shunt capacitors.

5.2.1 Base Case Computer Simulations

Figure 5.5 presents a sample distribution system adopting the improved islanding detection scheme. Shunt capacitors are connected to the feeder before the SG. This system was simulated using PSCAD software and the parameters are listed below.

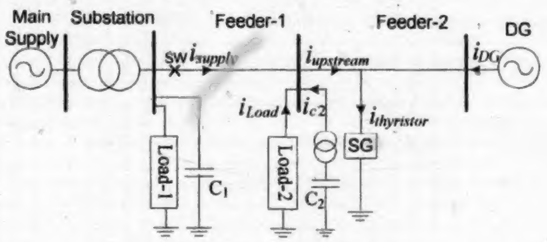
Main Supply
Substation
Feeder-1
Feeder-2
DG
SW
i_{supply}
$i_{upstream}$
i_{DG}
i_{Load}
i_{c2}
$i_{thyristor}$
SG
Load-1
C_1
Load-2
C_2

Figure 5.5 The PSCAD simulation system.

- Transmission system: 3-phase, 230kV, 60Hz; three-phase-to-ground fault level is 5976 MVA; reactively grounded via a 1.5 ohm resistor.
- Substation: 230/25kV; 3-phase-to-ground fault level at the 25kV bus is 500 MVA.
- Feeders: segment 1 and 2 are both of 5km, and have parameters of R_1 =0.168 ohm/km, X_1 =0.379 ohm/km, R_0 =0.474 ohm/km, X_0 =1.164 ohm/km, $C_1 = C_0 = 0$ μS/km.
- Load and shunt at the substation: Load-1 is 20MVA with a lagging power factor of 0.95; each phase of Load-1 is modeled with a resistor in parallel with an inductor. Capacitor-1 is 5MVar. Both load-1 and Capacitor-1 are Yg connected.
- Load and shunt along the feeder: Load-2 is 2MVA with a lagging power factor of 0.95; each phase is modeled with a resistor in parallel with an inductor. Capacitor-2 is 0.6Mvar. Both Load-2 and Capacitor-2 are Yg connected and fed via a 25/0.6kV, Yg/Yg connected transformer.
- DG: 5MVA, subtransient reactance of 0.25; the DG transformer is 25/0.48kV, Yg/Δ connection, 6MVA, Z=5%.
- SG: the interface transformer is 25/0.48kV, 350kVA, Z=2.5%, Yg/Yg connected; the firing angle is 30°, a phase A to Ground (A-G) signaling channel is used. SG is installed at the sending-end of Feeder-2.

In simulations, an island was created by opening the switch SW at the sending end of Feeder-1. In the normal condition, this switch was closed. If for any reason this switch was opened, the SG became isolated from the main supply, and the DG was islanded. The SG was operated in both conditions, and the system responses to SG firing were simulated and are presented in Figure 5.6 and Figure 5.7, respectively.

In the normal condition (Figure 5.6), the SG upstream transient current signal is a positive pulse drawn mainly from the main supply and is close to the thyristor current waveform. However, in the SG isolated condition (Figure 5.7), the DG supplies the majority of the thyristor current; the SG upstream current signal is composed mainly of the transient current flowing through capacitor-2 and is in oscillating form.

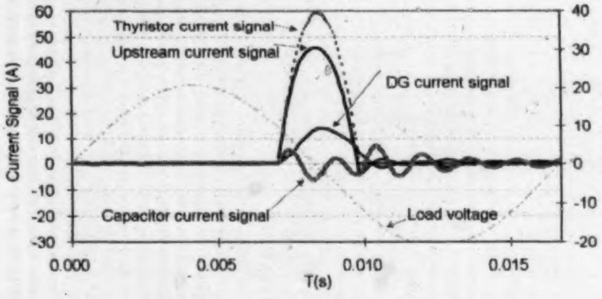

Figure 5.6 The system responses to SG firing in normal condition.

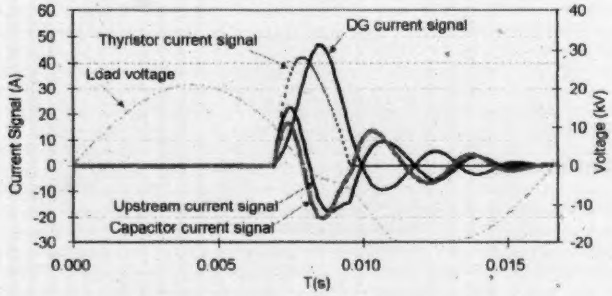

Figure 5.7 The system responses to SG firing in SG isolated condition.

Discrete Fourier Transform (DFT) was performed to investigate the differences between the SG upstream current signals in the normal and SG isolated conditions. The input signals to DFT were of 2-cycle length, and were sampled at a rate of 256 points/cycle. The same settings are used for DFT later in this section unless otherwise specified. The spectra of the upstream current signals are shown Figure 5.8. In the normal condition, the upstream current signal contains abundant harmonic components (from the DC to the 7th harmonic) with a reduced energy level as the harmonic order increases. In the SG isolated condition, the energy of the upstream signal concentrates around the 5th harmonic. The most distinct difference between the normal and isolated condition signals is that the former contains much larger low-frequency components (from the DC to the 1.5th interharmonic).

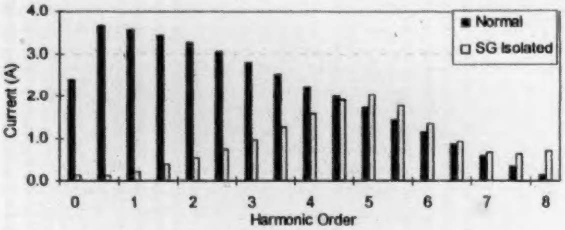

Figure 5.8 Spectra of the upstream current signals.

5.2.2 Theoretical Analysis and the Detection Criterion

This section verifies the findings in Section 5.2.1 by providing a through theoretical analysis and then develops a method for determining the SG connection status to the main supply.

Take the signal generator between phase A and the ground as an example. According to the superposition principle, the transient caused by thyristor firing can be analyzed with a network energized by a virtual voltage source $-v_{TA}$. The source $-v_{TA}$ is injected at the thyristor position to replace the thyristor during its conduction, and v_{TA} is the steady-state sinusoidal voltage across the thyristor when no signaling occurs. Denote

$$v_{TA}(t) = -\sqrt{2/3}U_N \sin \omega t \, , \tag{5.1}$$

Where U_N is the rated phase-to-phase voltage, and ω is the fundamental angular speed.

Figure 5.9(a) shows the analysis circuit for the simulation system in Figure 5.5, where L_s and L_{DG} are, respectively, the self-inductance of the main supply plus feeder-1, and the self-inductance of the DG plus feeder-2; L_{SG} is the inductance of the SG stepdown transformer; R_L is the load-2 resistance; C is the shunt C2 capacitance. Load-1 and shunt C1 are ignored since they are in parallel with a very small main supply inductance, i.e., with almost an ideal voltage source. In the studied system, $(\omega L_s):(\omega L_{DG}):(\omega L_{SG}):R:(\omega C)^{-1}$ = 6:40:45:329:1042.

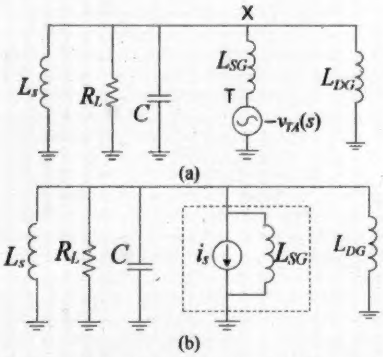

Figure 5.9 Analysis of the upstream transient current signal.

According to Thevenin's theorem, the circuit in Figure 5.9(a) is equivalent to the circuit in Figure 5.9(b) energized by a current source i_s in parallel with an inductor L_{SG}. If the thyristor is fired at instant $t_1 = -\delta / \omega$, the current source will be

$$i_s(t) = \sqrt{2/3}\,\frac{U_N}{\omega L_{SG}}\left[\cos \omega t - \cos \delta\right],\ (i_s \geq 0). \tag{5.2}$$

Both the voltage and current sources are active only during the thyristor conduction period, which occurs from instant $-\delta/\omega$ to approximately δ/ω according to computer simulations. The waveforms of the virtual voltage and current sources are plotted in Figure 5.10(a). The spectrum of such a current source is calculated using the DFT and is plotted in Figure 5.10(b) for $\delta = 30°$. This figure shows that this current source contains abundant harmonic components from the DC to the 7th harmonic, and that the energy level reduces as the harmonic order increases.

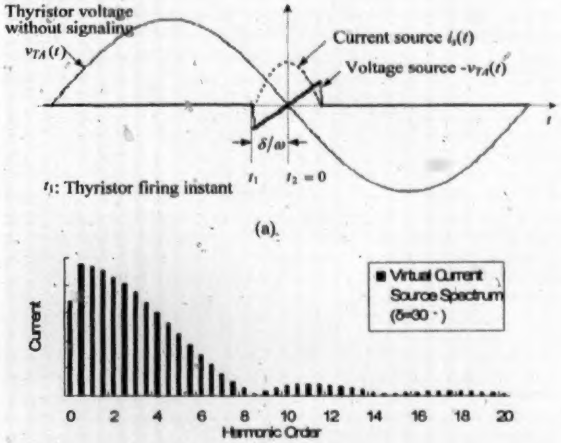

(a)

(b)

Figure 5.10 The virtual voltage and current source (a) waveforms and (b) spectrum.

Frequency domain analysis was performed to explain how the harmonic components of the virtual current source flow in the network. The supply system inductance L_s, DG inductance L_{DG}, load resistance R_L and capacitance C compose a parallel current-dividing circuit. The different frequency responses of the inductive, resistive and capacitive components determine the distribution of harmonic currents among them. The findings are as follows:

- Resonance occurs in the system at frequency

  $$\sigma = 1 / \sqrt{L_{eq} C} \tag{5.3}$$

  where L_{eq} is the system equivalent inductance, and L_{eq} equals

$L_s \,//\, L_{DG} \,//\, L_{SG}$ in the normal condition and $L_{DG} \,//\, L_{SG}$ in the SG isolated condition.

- In the normal condition, $L_{eq} \approx L_s$. The simulated system is resonant at a very high frequency of the 15th harmonic. Therefore, the major components of the current source (the DC to the 7th harmonics) are divided mainly among the low-pass filters of L_s, L_{DG} and L_{SG}. The portion of the current flowing through L_s constitutes the upstream current signal.
- When the SG is isolated from the main supply, $L_s = +\infty$, $L_{eq} \approx L_{DG}$. The system is resonant at a lower frequency of the 5th harmonic. Large currents around the 5th harmonic flow through L_{DG} and C. The very low frequency component in the current source, such as the DC component, flows through L_{DG} and L_{SG}. Since the upstream current flows through C and R_L, it contains components around the 5th harmonic, and no DC component.

Frequency domain analysis of the circuit in Figure 5.9(b) was also performed using computer and MATLAB software. The obtained upstream current signal spectra are shown in Figure 5.11 and are very close to the results obtained through the time domain simulations shown in Figure 5.8. This finding verifies the validity of the frequency analysis. The only difference in the results is that the resonance in the SG isolated condition occurs at the 5th instead of the 6th harmonic according to time domain simulations. This difference is due to the approximations made in the frequency domain analysis.

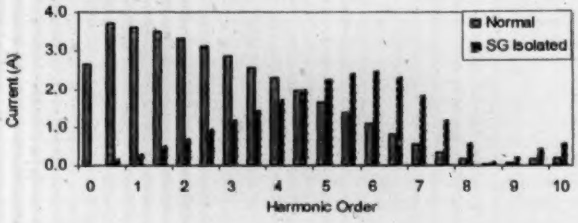

Figure 5.11 Spectra of upstream current signals calculated with MATLAB.

Based on theoretical analysis, the low frequency (the DC to the 1st) harmonic components decrease sharply when the SG becomes isolated from the main supply. These components can therefore be used to construct a criterion for detecting the SG connection status to the main supply. In view of the workload, the DC component in the upstream current, I_{DC}, is chosen as the method used for detecting the connection status of the SG to the main supply. When I_{DC} is higher than a preset threshold, the SG is regarded as connected to the main supply. Otherwise, the SG is regarded as isolated from the main supply and should stop broadcasting immediately.

5.2.3 Sensitivity Study

Sensitivity studies were performed using the sample distribution system and PSCAD software to test the validity of I_{DC} detection criterion. The following key system parameters were varied to determine their impacts on the DC criterion: the shunt capacitor C2 size, the 25kV substation fault level, the DG capacity, the load-2 capacity, the feeder length, and the distance from the SG site to the substation. The variations were shown as percentages of the base parameter values.

Figure 5.12 plots the variation of the DC criteria with respect to the shunt capacity in both the normal and SG isolated conditions. As is shown, the shunt capacity has a negligible impact on the DC criteria. A large vertical separation exists between the two curves corresponding to the normal and isolated conditions. This finding is of significant importance as the main purpose of this research was to find a reliable islanding detection method in the presence of large shunt capacitors.

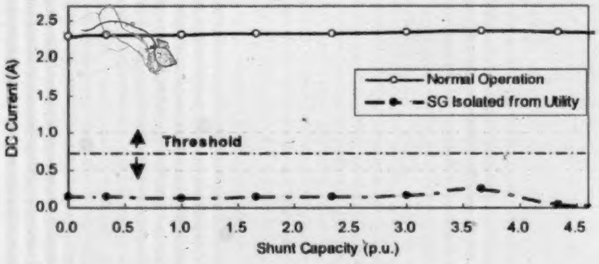

Figure 5.12 The shunt capacitor's impact of on the DC detection criterion.

Figure 5.13 shows the impact of the other system parameters. The substation fault level and DG capacity affect I_{DC} in opposite ways. In the normal condition, I_{DC} increases as the substation fault level rises and decreases as the DG capacity rises. In SG isolated condition, the I_{DC} is small and relatively constant. Therefore, with a low substation fault level or high DG capacity, the difference between I_{DC} values in the normal and SG isolated conditions would be small. However, the difference would still be large enough to support reliable detection according to the study of an extreme case where the substation and DG fault levels are equal (25MVA). Similarly, long distribution feeders or a large distance from the SG to the substation reduces the supply system fault level at the SG site and increases the detection difficulty, but cannot cause unreliable detections. A heavy load-2 slightly increases the I_{DC} in the SG isolated condition. However, even in the extreme case, in which the load is equal to the DG capacity, the SG isolated condition can still be clearly differentiated from the normal condition.

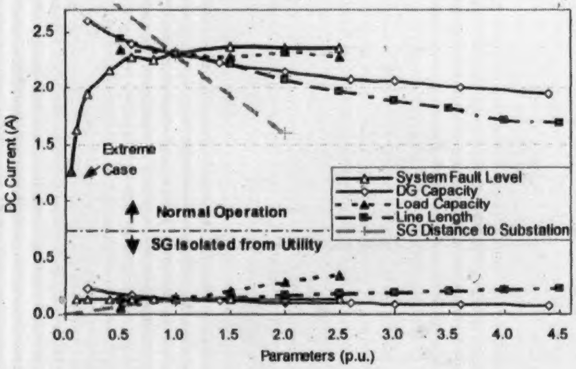

Figure 5.13 Sensitivity study of the DC detection criterion.

Figure 5.12 and Figure 5.13 show that a large difference exists in the upstream DC criteria in the normal and SG isolated conditions. For the studied system, a threshold can be set between 0.5A to 1A to reliably detect the SG isolated condition in various system configurations.

According to the simulations, in order to generate a voltage signal of 3% strength at the DG site, the required SG transformer size is 850kVA when the SG is at the substation secondary bus. This size reduces to 350kVA when the SG is moved to the site shown in Figure 5.5. Therefore, moving the SG downstream can reduce the SG transformer related cost in the studied system.

In the above studies, grounded-Y connected capacitors were investigated for the purpose of simplicity. Actually, ungrounded-Y connection of shunt capacitors is commonly practiced in the industry. Therefore, simulations were also conducted with both C-1 and C-2 ungrounded-Y connected instead of grounded-Y connected. The obtained upstream current spectra were plotted in Figure 5.14 in comparison with those in the base case. It's found that the change in capacitor grounding makes negligible differences to the upstream current signal.

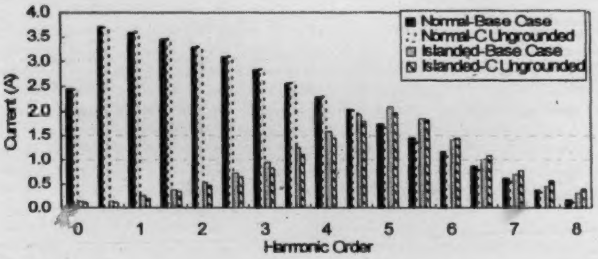

Figure 5.14 Upstream current signal spectra under two capacitor grounding patterns.

The capacitor C-1 and C-2 ungrounded case can be analyzed using a sequential circuit in Figure 5.15. As is seen, the change in capacitor connection only affects the zero-sequence part of the circuit. The upstream transient current signals in this circuit are calculated using MATLAB program. The results coincide with those in Figure 5.14 and are omitted here.

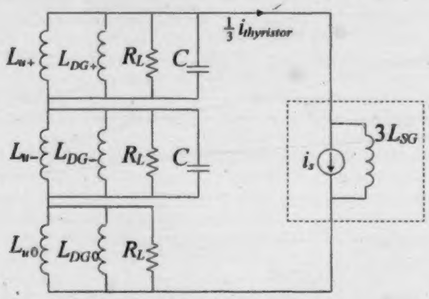

Figure 5.15 The sequential circuit for transient current analysis.

5.3 Experimental Tests

Laboratory experiments were performed in University of Alberta to confirm the effectiveness of the DC current criterion for islanding detection. The test system was constructed by scaling down the voltage level of a 25kV distribution system to 208V and reducing all its impedances by a ratio of 19.5. This ratio of 19.5 was determined according to impedance values of components in the 25kV system and available components in the lab. The original 25kV system has the same structure as the one in Figure 5.5, except that Load-1 and C-1 do not exist. The 25kV system parameters are listed below.

- The distribution system: 25kV, 60Hz, three-phase fault level of 39.8MVA.
- The distribution feeder1 and feeder 2: both of 10km, R_{self} =0.2717 ohm/km, X_{self} =0.8886 ohm/km.

- DG: 5MVA, subtransient reactance of 0.25; the DG transformer is 6MVA, with impedance of 5%.
- Load-2: 1MW, lagging power factor of 0.9; each phase is modeled with a 625 ohm resistor in parallel with a 3.4H inductor.
- Capacitor-2: three-phase capacitor – size varies.
- Signal generator: the transformer of 150kVA, Z=5%; firing angle of 25°.

Figure 5.16 plots the upstream current signals in the 25kV system when the shunt capacity in the 25kV system varies in a large range from 0 to 1.93 MVar. In the normal condition, the upstream current signal either is a positive pulse or contains a positive pulse. In the SG isolated condition, the signal is always oscillatory. According to the signal spectra in Figure 5.17, in normal condition, the upstream signal contains relatively steady DC and 0.5th harmonic components. However, in SG isolated condition, the DC component in the upstream current signal is almost zero. Figure 5.18 plots the DC current components as the shunt capacity varies, showing that the DC current criterion can be used to clearly distinguish the SG normal and isolated conditions with a threshold such as 0.12A.

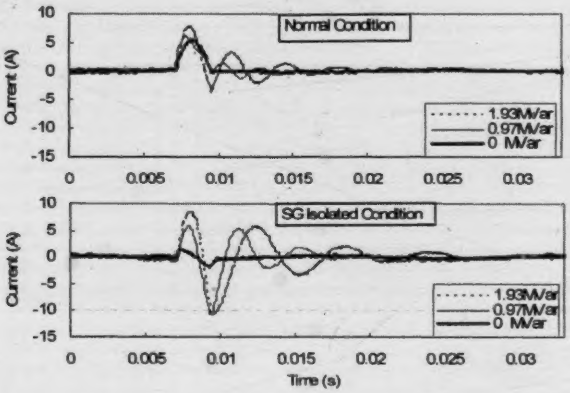

Figure 5.16 The upstream current signals in normal and SG isolated conditions.

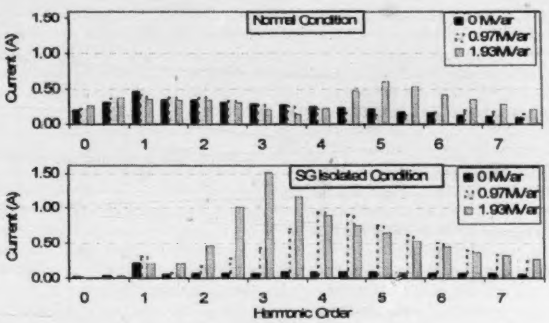

Figure 5.17 The spectra of upstream current signals obtained in laboratory tests.

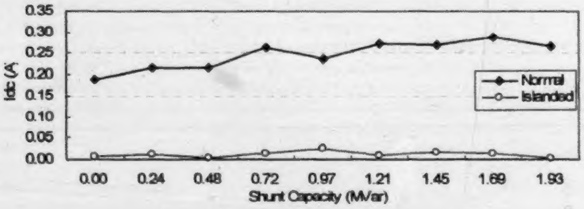

Figure 5.18 The DC criteria in laboratory tests.

In Figure 5.18, the normal-condition DC current criterion slightly rises from 0.2A to 0.3A as the shunt capacitance increases. This tendency is different from the relatively constant DC level in Figure 5.12 because the SG firing angle in the tests was not ideally fixed. In the tests, the thyristor firing pulse was created according to the zero-crossing instant on the thyristor voltage waveform. When the system compensation level was high, harmonic resonance occurred in the system, causing large harmonic distortion and discrepancy in the zero-crossing instant on the thyristor voltage waveform and that on the fundamental voltage waveform. Therefore, the actual SG firing angles, which is defined relative to the thyristor fundamental voltage, was slightly different from the designed value. Overall, the tests verified the effectiveness of the DC current detection criterion and demonstrated the feasibility of the improved islanding detection scheme.

5.4 Design of the Signal Generator

In the improved power-line-signaling based scheme, the design of the signal generator needs to meet the requirements for both the voltage signal strength and the thyristor voltage and current ratings. The formulas for the signal transformer size and thyristor ratings in Section 3.5.1 still apply. Moreover, to facilitate the detection of its connection status, the signal generator must be able to draw a large enough DC current from the main supply in the normal condition. The analysis below shows that this requirement can be naturally met for signal generators installed at the distribution level.

According to (3.4), (3.7) and (3.8) in Section 3.5.1, the DC current drawn from the main supply by the SG in the normal condition equals

$$\begin{aligned} I_{DC} &= \frac{2\sqrt{6}k_v S_{PG}}{\pi N U_N}\left(1-\frac{\delta}{\sin\delta}\cos\delta\right) \text{ (SG : Phase – Ground)} \\ &= \frac{\sqrt{2}k_v S_{3ph}}{\pi N U_N}\left(1-\frac{\delta}{\sin\delta}\cos\delta\right) \text{ (SG : Phase – Phase)} \end{aligned} \quad (5.4)$$

where k_v is the designed voltage signal strength defined with the voltage signal peak; S_{PG} and S_{3ph} are the supply system phase-ground fault level and three-phase fault level at the SG installation site, respectively; N is the interval between two firing events in the unit of the number of cycles. Please be noted that $I_{DC} = 2I_{avg}$ as the DC component is calculated in a window of $N/2$ cycles. Therefore, for fixed voltage signal level k_v and firing angle δ, I_{DC} is proportional to the system fault level. Given the typical phase-ground fault level of 25kV systems from 20 to 150MVA, $k_v = 5\%$, $\delta = 30^\circ$ and $N = 4$, the calculated I_{DC} ranges from 1.5 to 10.9A (SG between phase-ground).

In order to determine whether the aforementioned DC current is discernible or not, we compare it with the normal load current flowing on the line. If the load capacity is proportional to the system fault level, the load current can be calculated using

$$\begin{aligned} I_{load} &= S_{PG}/(\lambda U_N/\sqrt{3}) \qquad \text{(SG : Phase – Ground)} \\ &= \sqrt{3}S_{3ph}/(\lambda U_N) \qquad \text{(SG : Phase – Phase)} \end{aligned} \quad (5.5)$$

In (5.5), λ is a constant of, say, 20, which means that the system fault level is 20 times of the load capacity. The ratio of the DC signal to the load current (RMS value) is calculated as follows:

$$\begin{aligned} k_I &= \frac{I_{DC}}{I_{load}} = \frac{2\sqrt{2}k_v\lambda}{\pi N}\left(1-\delta\frac{\cos\delta}{\sin\delta}\right) \text{ (SG : Phase – Ground)} \\ &= \frac{\sqrt{6}k_v\lambda}{\pi N}\left(1-\delta\frac{\cos\delta}{\sin\delta}\right) \text{ (SG : Phase – Phase)} \end{aligned} \quad (5.6)$$

With the above assumptions, the current ratio k_I is determined by k_v, λ, N and δ and is independent of the system fault level. Given the above values, $k_I = 2.1\%$ (and 1.8%) for phase-ground (and phase-phase) signaling.

Our field measurement experiences with voltage distortion signals were referred to for evaluating the calculated DC current signal strength. In the test introduced in Chapter 4, voltage signals with average RMS strength of 0.85% could be reliably detected. Therefore, a DC current signal with a RMS strength of 2.1% (or 1.8%) has a good chance of being reliably detected. This result means that a signal generator installed at the distribution network can draw a large enough DC current for detection of its connection status to the main supply.

5.5 Conclusion

This section proposed an important improvement to a power-line-signaling-based islanding detection scheme by increasing its adaptability to different DG interconnection scenarios. With the improvement, the signal generator can be located at any place between the substation and the DG sites. The signal generator installation no longer requires access to the substation, and this feature is convenient for the distribution utility. In a typical arrangement, the signal generator can be connected at the upstream of an area with DG installations. In this way, the costs of the signal generator can be reduced and shared among the DG owners.

In the improved scheme, the signal generator must have the ability to detect its connection status to the main supply. The signal generator does so by examining its upstream transient current signal created during the signaling process. The level of the DC component contained in this transient signal is used as the criterion for determining the connection status. A high DC current means that the SG is connected to the main supply, while a low DC current means that the SG is isolated from the supply. The computer simulations and experimental tests all showed that this criterion can work reliably in various system conditions.

Chapter 6. HARMONIC IMPEDANCE MEASUREMENT USING THYRISTOR-CONTROLLED SHORT-CIRCUITS

In this chapter, the thyristor-controlled-fault is applied to design an effective and easy-to-implement method for measuring power system harmonic impedances. The method uses a thyristor to create a controlled short circuit at the measurement point. The short circuit produces a pulse current and a voltage distortion, which are then used to estimate the system impedance. The strength of the current pulse is controlled through the thyristor firing angle so that enough signal energy is available for precise measurement, and yet the disturbance is small enough not to cause power quality problems. The method can be implemented into a portable impedance measurement device. Computer simulations and lab tests were used to verify the effectiveness of the method. This chapter also establishes a criterion for determining the frequency range of reliable measurements using the proposed device. The parameter setting of the device is discussed. The results in this chapter have been published in [74].

6.1 Introduction

Harmonic impedances represent the frequency responses of power networks. The impedance data are highly useful for harmonic propagation study. In recent years, the impedance data of supply systems have also been needed for setting the anti-islanding protection relays of distributed generators [10]. In many applications, the system or load impedances need to be measured online. For example, the measured impedance results are used to verify network models or to identify harmonic sources.

6.2 Review of Existing Methods

Many impedance measurement methods have been proposed in the literature. All have to rely on voltage and current variations at the metering point due to the nature of the problem. Several different classifications exist for these measurement methods. For example, according to the variables used for measurement, the methods can be classified into two types. One type uses variations in the steady-state voltage and current harmonics, while the other uses transient signals on the voltage and the current waveforms caused by a disturbance [46]. The transients-based methods are suited for obtaining fast results due to the short duration of the transient signals. The transient current usually has an abundant harmonic spectrum; therefore, obtaining frequency characteristics in a wide-band frequency range is easy. A high-speed data acquisition device is a prerequisite for using the transient-based method.

In this research work, the methods are classified into two types according to the equipment used to create voltage/current variations or disturbances.

1. One type utilizes the existing facilities of the power system to be measured. Examples include methods that use natural variations in steady-state voltage/current harmonics, or variations caused by switching an existing equipment (e.g., a nonlinear load or capacitor banks) [46][47]. Methods using transients caused by switching of existing equipments (e.g., capacitor banks or transformers) for measurement are also classified into this type [48][49][50].
2. The second type of methods relies on dedicated disturbance generators for measurement. Some methods inject steady-state noncharacteristic harmonic currents into the system for measurement [51]. Other methods inject transient currents for measurement. For example, reference [9] proposes using an inverter to inject current spikes into the supply system for impedance measurements.

The second type of method is more expensive than the first type but has more general applications since it is independent of the availability of the disturbance sources in the system to be measured. The measurement device contains all the hardware needed for the required task. Furthermore, the second type of method provides much better control of the disturbances generated. This type of method can adjust the disturbance spectrum and disturbance strength to improve measurement accuracy for different system conditions and locations; this type of method can also maintain the disturbance within a level that will not disrupt normal system operations. Therefore, a measurement can be performed at any time in a continuous manner. Such dedicated impedance measurement devices are especially useful for distributed generator (DG) applications. In [53] and [54], for example, the supply impedances are measured at the DG interconnection sites continuously so that the impedance-based DG anti-islanding relays can work properly.

Dedicated disturbance generators provide technical advantages in harmonic impedance measurement. However, the proposed disturbance generators, such as the converter in [9], are expensive and complex to implement. Therefore, a new simple one needs to be developed.

In this chapter, we propose a new portable device along with the algorithms for harmonic impedance measurement. The device is simpler than those in [9][53]. It utilizes a thyristor to create a controlled short-circuit at the measurement point. The resulting current pulse and voltage distortion are used for impedance measurement. The strength of the current pulse is controlled through the thyristor firing-angle so that sufficient disturbance energy is always available for impedance extraction independent of the condition at the measurement location. The firing-angle is also controlled to ensure the generated disturbance is not too strong to cause power quality problems in the system. This method can be easily implemented into a portable and low-cost device.

6.3 The Proposed Measurement Scheme

The proposed device utilizes voltage and current disturbance signals to measure harmonic impedances. Therefore, the principle of transient-based measurement will be reviewed before introducing the proposed device.

6.3.1 Transient-Based Harmonic Impedance Measurement

Consider a linear network in Figure 6.1 disturbed by an external event. Transient signals show up on the terminal voltage and current waveforms and decay to an indiscriminable level i.e. zero after a period. These signals are recorded during the whole transient process and are denoted as $dv(t)$ and $di(t)$, respectively. According to the Fourier Transform of non-periodical signals,

$$dV(j\omega) = Z(j\omega) \cdot dI(j\omega), \tag{6.1}$$

where $dV(j\omega)$ and $dI(j\omega)$ are the Fourier transform of $dv(t)$ and $di(t)$, respectively, and $Z(j\omega)$ is the harmonic impedance of the network.

In digital applications, the transient signals within a window of length T_1 are sampled at an interval of ΔT. Discrete signals $dv[k\Delta T]$ and $di[k\Delta T]$ are obtained. The following equation is obtained through the Discrete Fourier Transform (DFT):

$$dV[jn\omega_1] = Z[jn\omega_1] \cdot dI[jn\omega_1], \tag{6.2}$$

where $\omega_1 = 2\pi / T_1$, $dV[jn\omega_1]$ and $dI[jn\omega_1]$ are the Discrete Fourier Transform (DFT) of $dv[k\Delta T]$ and $di[k\Delta T]$, respectively, and $Z[jn\omega_1]$ is the network harmonic impedance at frequency $n\omega_1/(2\pi)$.

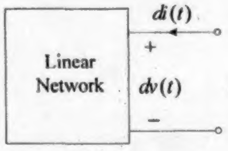

Figure 6.1 A linear network and its transient responses.

Equation (6.2) implies that the harmonic impedance of a network can be measured by using the DFT of the transient voltage and current signals. The following details should be noted.

1) The transient signals in (6.1) and (6.2) are caused by an external disturbance instead of state changes in the network itself. The steady states of the network remain unchanged before and after the transients.

2) The transient process is completed within the sampling window of T_1 length.

3) Anti-aliasing filters are required before sampling if the frequency range of the transient signals exceeds $0.5\Delta T^{-1}$.

This chapter proposes a novel device to create transient signals and measure the harmonic impedance. A complete scheme including signal generation, signal acquisition and impedance calculation is devised and is introduced below. The device is intended for harmonic impedance measurement in 1) distribution systems such as 12.5kV or 25kV, and 2) customer-level low-voltage (LV) systems below or equal to 480V. As well, the device can be adapted to single-phase and unsymmetrical multi-phase systems.

6.3.2 The Proposed Device for Single-Phase Syst[illegible]

The proposed device for a single-phase system is described below.

A. Transient Signal Generation

The proposed device adopts a waveform distortion technique, which was originally designed for power line communication, to create the transients signals [5]. Figure 6.2 illustrates this device for the measurement of a LV system. A thyristor in series with a small inductor is connected between the driving point and the ground, and is identified as the signal generator (SG). The thyristor is turned on at a certain degree (denoted as the firing angle) before the driving point voltage crosses zero, creating a temporary fault. This results in a thyristor current pulse flowing from the system. This current firstly increases and then decreases after the driving point voltage reverses its direction. As the current reaches zero, the thyristor shuts off automatically. Transient signals also show up on the driving point voltage and line current waveforms and are used for impedance measurement. The interface inductor is used to limit the magnitude of thyristor current, especially when capacitor banks are connected nearby. The inductor also limits the level of voltage distortion at the driving point. By adjusting the thyristor firing angle and using a proper inductor, the generated transient signals can have strong enough energy for precise measurement. Also, the impact of the transients on load operation can be controlled in a negligible range. This process will be discussed in Section 6.6. To facilitate detection, the thyristor is fired for every 2 or 4 cycles. When the thyristor is not fired, no transients are imposed on the system.

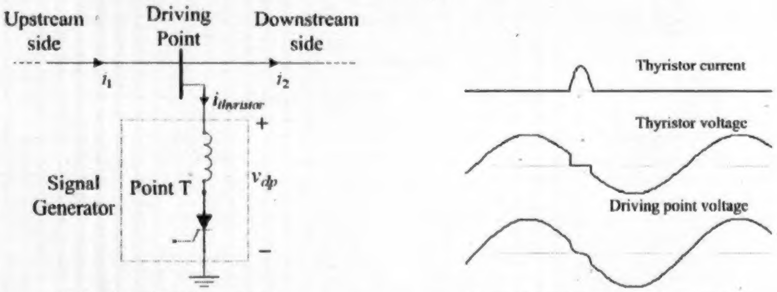

(a) transient signal generator (b) waveforms containing transients

Figure 6.2 The proposed harmonic impedance measurement method.

For the measurement of distribution systems, the interface inductor will be replaced by an interface transformer. This transformer reduces the voltage for thyristor operation, and its leakage inductance also functions as an interface inductance. A common power transformer used by a consumer can be adopted for this purpose. There's a minimum requirement on the transformer size such that strong enough current signals can be injected. However, if there is no such transformer available, an extra transformer will be needed.

B. Transient Signal Acquisition

An important concern in transient-based harmonic impedance measurement is how to extract the transient signals from the recorded voltage and current waveforms. In the proposed device, this extraction is done by subtracting two consecutive cycles of a waveform. According to test results, the generated transient signal usually dies out within one cycle [5]. The thyristor is fired so that a transient signal exists in only one of two consecutive cycles. Therefore, the difference between two consecutive cycles is the transient signal. This subtraction method is illustrated in Figure 6.3 using the waveform of the driving point voltage.

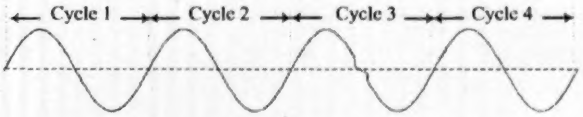

(a) Voltage waveform (signal is at the 3^{rd} cycle)

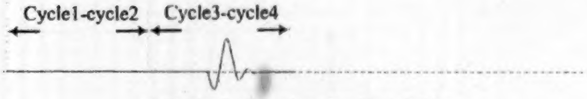

(b) Voltage distortion signal waveform

Figure 6.3 The subtraction method for signal extraction.

The advantage of the subtraction method is that it can effectively filter out the fundamental component and the harmonics, since their levels remain almost unchanged within a short period of two cycles. The proposed method is therefore essentially immune to fundamental and harmonic noises.

C. The Measurement Algorithm

The DFT is performed for the extracted transient signals. dV_{dp}, $dI_{thyristor}$, dI_1 and dI_2 represent the DFT of the voltage transient at the driving point, the DFT of the thyristor current $i_{thyristor}$, the DFT of the upstream transient current, and the DFT of the downstream transient current, respectively. The supply system harmonic impedance Z_s, the driving point impedance Z_{dp} and the load impedance Z_{load} can be calculated as follows:

$$
\begin{aligned}
&Z_s(f) = -dV_{dp}(f)/dI_1(f) \\
&Z_{dp}(f) = -dV_{dp}(f)/dI_{thyristor}(f) \qquad (6.3) \\
&Z_{load}(f) = dV_{dp}(f)/dI_2(f) \ .
\end{aligned}
$$

6.3.3 The Proposed Device for Three-phase Systems

The proposed device for three-phase systems is introduced as an example of measurement in multi-phase systems. In this case, the SG needs to be installed at multiple locations to create transient events using different channels. For example, it can be connected between phase A and the ground (denoted as the A-G channel), B and the ground and C and the ground. Phase-to-phase channels of A-B, B-C, C-A are also available. The multiple transient events need to be created in a short time in order to minimize the system variations during the measurement interval. The firing channels can be switched manually, or automatically using several thyristors (see Figure 6.4).

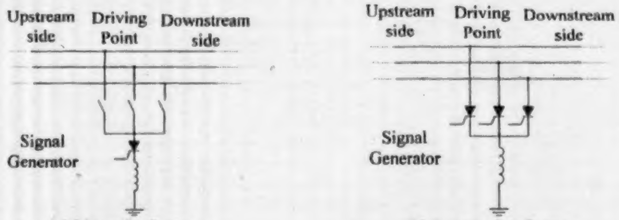

(a) Manual scheme (b) Automatic scheme.

Figure 6.4 Examples of SG topology for measuring three-phase systems.

After multiple events are created and recorded, the following equation set is constructed for different frequency f:

$$
\begin{bmatrix} dI_{a1}(f) & dI_{b1}(f) & dI_{c1}(f) \\ \vdots & \vdots & \vdots \\ dI_{am}(f) & dI_{bm}(f) & dI_{cm}(f) \end{bmatrix}
\begin{bmatrix} Z_{aa}(f) \\ Z_{ab}(f) \\ Z_{ac}(f) \end{bmatrix}
=
\begin{bmatrix} dV_{a1}(f) \\ \vdots \\ dV_{am}(f) \end{bmatrix}
$$

or

$$[dI(f)]_{m\times 3}[Z_a(f)]_{3\times 1} = [dV_a(f)]_{m\times 1} \ , \qquad (6.4)$$

where $Z_{aa}(f)$ represents the phase A self-impedance at frequency f; $Z_{ab}(f)$ and $Z_{ac}(f)$ are the mutual impedances between phase A and B, and phase A and C, respectively; $dI_{am}(f)$ and $dV_{am}(f)$ are the DFT of phase A current and voltage transient signals of event m at frequency f; m is the number of events, and $m \geq 3$.

A least-square solution of (6.4) can be calculated as follows, provided that the matrix $[dI(f)]_{m\times 3}$ is well-conditioned [55]:

$$[\mathbf{Z}_a(f)]_{3\times 1} = \left([\mathbf{dI}(f)]^T [\mathbf{dI}(f)]\right)^{-1}{}_{3\times 3} [\mathbf{dI}(f)]^T{}_{3\times m} [\mathbf{dV}_a(f)]_{m\times 1}. \tag{6.5}$$

The harmonic impedance measurement is completed by calculating the solution at different frequencies.

Based on the above discussion, the proposed device and measurement scheme have the following advantages:

- The device generates controllable transients by adjusting the firing angle so that enough strength is available for accurate measurement independent of the condition at different locations. As well, the impact of the transients on system operation is maintained in an acceptable range.

- The SG device is simple and inexpensive since it requires no power electronic component with gate-turn-off ability. It can be constructed as a portable device for measuring LV systems.

- The proposed scheme is immune to background harmonics.

6.4 Computer Simulations and the Finalized Algorithm

Computer simulations were performed to test the proposed scheme, and the results are presented in this section.

6.4.1 Simulations in a Single-Phase LV System

Simulations were done in a customer-level 120V 60Hz single-phase system as shown in Figure 6.5. Transients were created by using a SG firing angle δ of 5°. The waveforms of the driving point voltage, the transient on the driving point voltage, and the thyristor current are plotted below in Figure 6.6, which shows that the transient caused by firing died out within one cycle. The distortion on the waveform of the driving point voltage was unnoticeable by the naked eye, and the peak distortion was very small (5V, or 3% of the rated peak). Therefore the influence of the SG firing on the load operation can be ignored. A DFT was performed for the transient signals, and Figure 6.6 also shows the spectrum of thyristor current. The current energy reduced substantially as the frequency went high, and the bandwidth was about 7000Hz. Since the sample rate is 20kHz, which is higher than twice of 7000Hz, an anti-aliasing filter was not needed.

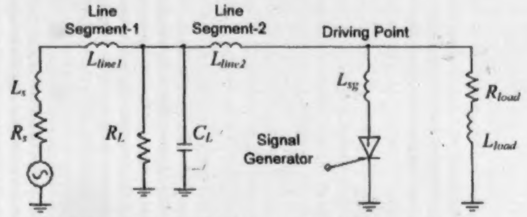
Line Segment-1
Line Segment-2
Driving Point
L_{line1}
L_{line2}
L_s
R_s
R_L
C_L
L_{sg}
Signal Generator
R_{load}
L_{load}

R_s=0.06ohm, L_s=0.08mH, L_{line1}=0.01mH, L_{line2}=0.02mH,
R_L=R_{load}=7.2ohm, C_L=178.43uF, L_{sg}=0.2mH, L_{load}=9.2mH;

Figure 6.5 The 120V single-phase simulation system.

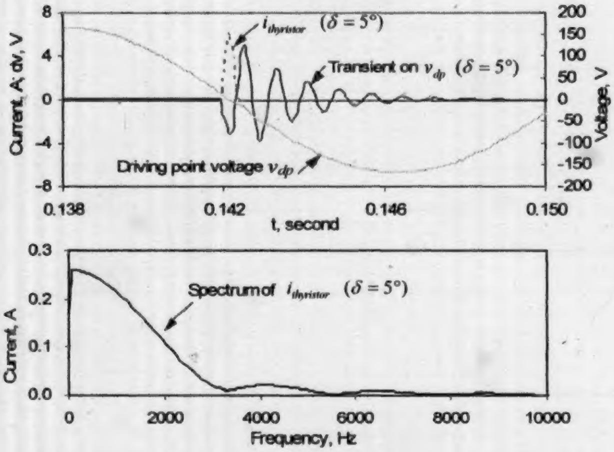

Figure 6.6 The 120V system responses during SG firing.
(The driving point voltage, voltage transient, thyristor current waveform and spectrum.)

Figure 6.7 presents the measured system harmonic impedance. It coincides very well with the real impedance, which is calculated according to the system parameters.

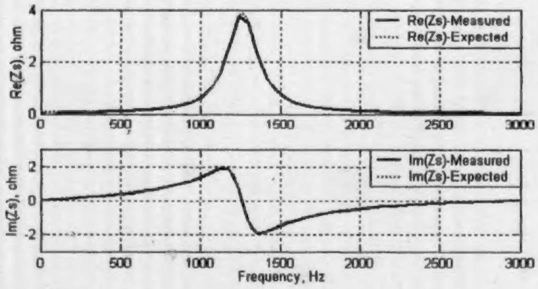

Figure 6.7 The measured vs. expected supply system harmonic impedance.

The measured load impedance, however, is no longer accurate when the frequency rises above 1500Hz. These results are presented in Figure 6.8. Since the load impedance is much larger than the system impedance at high frequencies, only a small fraction of the high-frequency transient current flows through the load. This makes the load impedance measurement inaccurate at high frequencies.

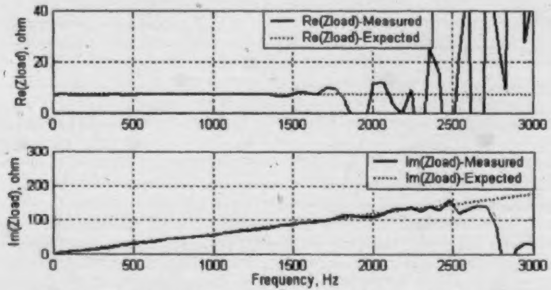

Figure 6.8 The measured vs. expected load harmonic impedance.

Sensitivity studies were done on the composition of the load vs. the supply system. It was found that when the load had a leading power factor and its impedance dropped as frequency increased, accurate measurements could be achieved for both the system and the load impedances. However, generally, the proposed method is intended for measuring system harmonic impedances or driving point impedances.

6.4.2 Simulations in a Three-Phase System

Simulations were also carried out in a 25kV 60Hz distribution system to test the proposed scheme for three-phase systems. The 25kV system shown in Figure 6.9 has the same structure as the 120V system in Figure 6.5 except that the 3-phase 25kV system has phase-coupled segment-1, segment-2 is of zero length, and a 3-phase interface transformer replaces the interface inductor L_{sg}. The parameters of the 25kV system are $R_s = 6.25$ ohm, L_s =0.0382H, $R_l = R_{load} = 281$ ohm, $C_l = 1.698$uF, L_{load} =0.36H, segment-1 has L_{self} =0.024H, $L_{mutual} = 0.013$ H, $R_{self} = 2$ ohm; the interface transformer is of 100kVA and Z =3%.

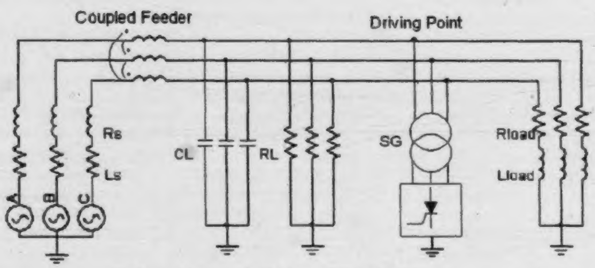

Figure 6.9 The 3-phase 25kV simulation system.

Transient events were created with three channels of A-G, B-G and C-G. Two firing angles of 10° and 20° were used for each channel. Compared to the firing angle in simulations for the 120V system, bigger firing angles were adopted here in order to achieve enough signal strength. Figure 6.10 shows the system responses during the SG firing, including the driving point voltage, the transient voltage and the thyristor current. As the firing angle increases from 10° to 20°, the thyristor current pulse became twice as wide. Low energy points showed up on the spectra of the thyristor currents within 0~3000Hz. This result may affect the measurement precision.

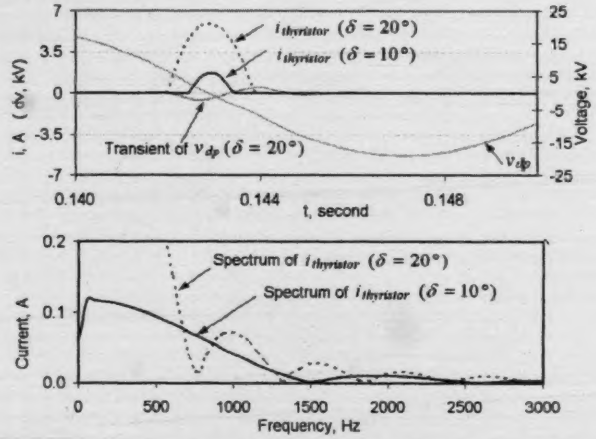

Figure 6.10 System responses during SG firing; the spectra of thyristor currents.

Transient events created with one firing angle and three different channels (A-G, B-G and C-G) were used for measurement of driving point impedances. The results corresponding to a firing angle of 10° and 20° were presented in Figure 6.11 and Figure 6.12 respectively. The measurements were compared with precise values obtained using the equations in Appendix C. Besides impedances, the condition number of matrix $[\mathbf{dI}(f)]_{3\times m}$ was also monitored. This number describes the status of a matrix, and a low value (say, 20 for the 3-phase simulation system in this section) indicates a well-conditioned matrix. The observations are presented below.

1) With both firing angles, the measured impedances coincided very well with the expected values except at several frequencies. The errors were caused by the low energy levels of the thyristor currents at these frequencies. The spectra in both figures reveal these levels.

2) The errors corresponding to $\delta = 10^{\circ}$ were located at different frequencies from those corresponding to $\delta = 20^{\circ}$, because the low energy frequencies on the thyristor current spectrum of $\delta = 10^{\circ}$ were shifted from those on the spectrum of $\delta = 20^{\circ}$.

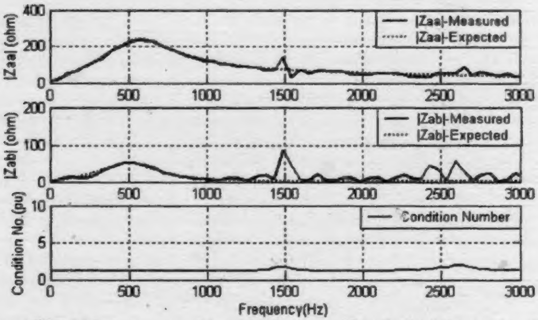

Figure 6.11 Measurement results using events with a single firing angle of 10°.

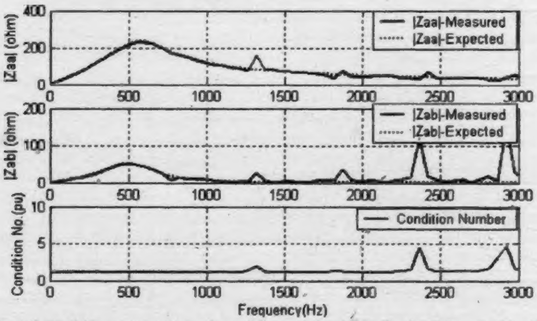

Figure 6.12 Measurement results using events with a single firing angle of 20°.

Based on observations 1) and 2), it was proposed that if all the six transient events created with both firing angles (10°and 20°) and three different channels were used together to construct (6.4), they might compensate for each other at their low energy frequencies and produce better solutions. This proposal was verified, and Figure 6.13 showed that the errors were largely reduced when both firing angles were used. Also, the current matrix was well-conditioned within 0~3000Hz and the impedance solutions were numerically reliable.

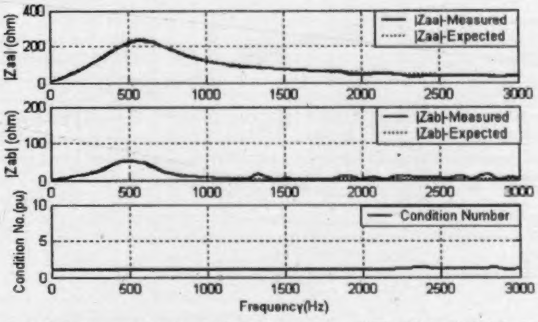

Figure 6.13 Measurement results using events created with both firing angles.

Study was also carried out to determine the channels required for creating transients that could compose a well-conditioned matrix $[\mathbf{dI}(f)]_{3\times m}$. Theoretical analysis and simulations showed that

1) Different transient events created using the same channel form linearly dependent rows of matrix $[\mathbf{dI}(f)]_{3\times m}$. Therefore, at least three different channels are required to reliably measure non-symmetrical three-phase systems. Otherwise, the matrix $[\mathbf{dI}(f)]_{3\times m}$ will be ill-conditioned.

2) Arbitrary combinations of three different channels are sufficient for measurements except for (a) the combination of A-B, B-C and C-A and (b) combinations of two phase- ground channels and one phase-phase channel using the above two phases (e.g., A-G, B-G and A-B).

In practical applications, transients can be created by using multiple firing angles and a proper combination of multiple channels to obtain reliable results.

6.5 Lab Experiment Results

A lab experiment was performed to test the proposed device. Figure 6.14 shows the configuration of the three-phase 120V 60Hz test system. The circuit inside the dotted-line box represents an unknown network to be measured. Voltage probes for measurement were connected between the supply-end and load-end of this network. The three-phase voltage drops on this network and the currents flowing through it were recorded. The scheme developed in Section 6.3.3 was applied to the measurement.

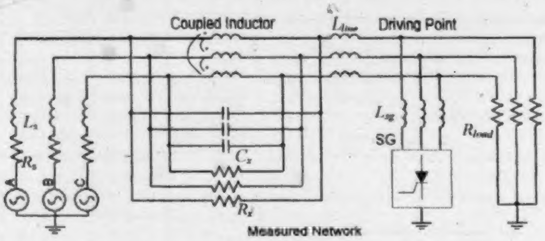

R_s and L_s are unknown; Coupled Inductor L_{self}= 0.6mH, L_{mutual}= -0.25mH, C_x=40uF, R_x=24.3 ohm, L_{line}=1mH, L_{sg}=5mH, R_{load}=83.3 ohm.

Figure 6.14 The 3-phase 120V experimental system configuration.

The currents and voltages were measured by using probes with ratios of 100mV/A and 1/100, respectively. Each current probe was hooked on 2 coils of wires for better precision. A National Instrument device, NI-DAQ 6020E, sampled the probe outputs at a rate of 256 points/cycle and performed A/D conversion with a resolution of 12 digits and input range of +5/-5V.

6.5.1 Experiment Results

Transient events were created with four firing angles of 15°, 20°, 25° and 30°. Three channels of A-G, B-G and C-G were used for each firing angle. All the created 12 events were used together for measurements.

Figure 6.15 shows the measured Z_{aa} and Z_{ab} vs. the expected impedances. The expected values were calculated by assuming all the components were linear and ideal and by using their parameters measured at 60Hz. The following results were obtained:

1) The measured $|Z_{aa}|$ and $|Z_{ab}|$ reasonably predicted the expected impedances within 0~1600Hz (0~25th harmonic). As the frequency went higher than 1600Hz, the measurements started to deviate from the expected values and became unreliable;

2) Discrepancies were found in the measured and expected $|Z_{aa}|$ at the resonance points around 900Hz. The assumption of ideal components, which was used for calculating the expected impedances, was not strictly true and therefore contributed to the errors.

3) The zoomed area of $|Z_{aa}|$curve had no particularly high error around 60Hz. This showed that the proposed method has a good suppression of

fundamental noises.

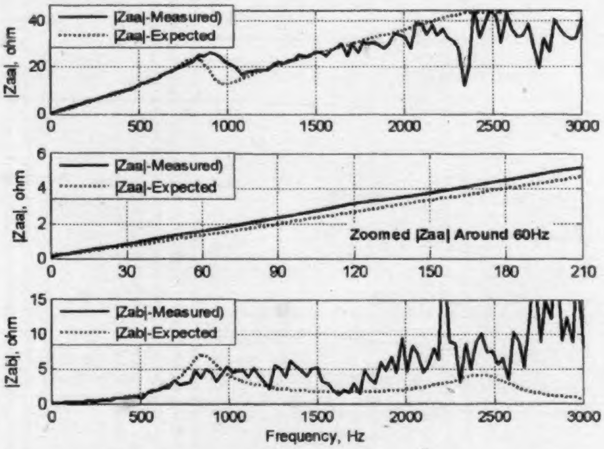

Figure 6.15 The 3-phase 120V experimental system measurement results.

The lab tests demonstrate that with the proposed scheme, reliable measurements can be achieved in a wide range of frequencies. In practical applications, a specific range of reliable measurements is desirable. A criterion is derived below to predict such a range according to the hardware setting of the tests.

6.5.2 Criterion for Reliable Measurements

The cause of unreliable measurements was analyzed in order to develop a criterion for reliable results. As the frequency increases, the strength of the transient current signals decreases substantially. It was suspected that as the energy of current signals dropped to a level comparable to that of quantization noises, the signals would be corrupted and the measurement would become unreliable. This expectation is verified below, and the criterion is developed.

The magnitude of the quantization error is determined by the following factors.

- The current probe ratio k_{probe}=0.1V/A × 2 =0.2V/A.
- The NI-6020E input range V_{in}=5-(-5)=10V;
- The NI-6020E A/D resolution n =12 digit;

According to the definition of A/D resolution, the smallest discriminable current equals

$$I_{\min} = (V_{in} / 2^n) / k_{probe} = 0.0122\text{A}. \tag{6.6}$$

The maximum quantization error in the time-domain current signals equals half of the resolution

$$I_{error} = I_{\min} / 2 = 0.0061\text{A}. \tag{6.7}$$

The quantization error in the frequency-domain current signals can be affected by the precision of the DFT calculation. However, this effect was ignored in the lab tests since a high-precision microprocessor was used. Therefore, the quantization error after DFT calculation is still 0.0061A.

The following equation should hold true in order to generate reliable results for single-phase systems:

$$|dI(f)| > I_{error} \tag{6.8}$$

Consider the measurement of a three-phase system where transient events are created by using three channels of A-G, B-G and C-G. In order to yield a reliable least-square solution for (6.4), at least half of the twelve events for measurement (created with four firing angles and three channels) should have their 3-phase largest current strength higher than I_{error}; i.e., half of the events should have

$$\max_{i=a,b,c} |dI_i(f)| > I_{error}. \tag{6.9}$$

The criterion in (6.9) was used to predict a range of reliable measurements. The range is plotted in Figure 6.16 where an indicator of 1 means 'reliable' and 0 means 'unreliable'. This range agrees very well with the results in Figure 6.15. Therefore, the criterion (6.9) is shown to be effective.

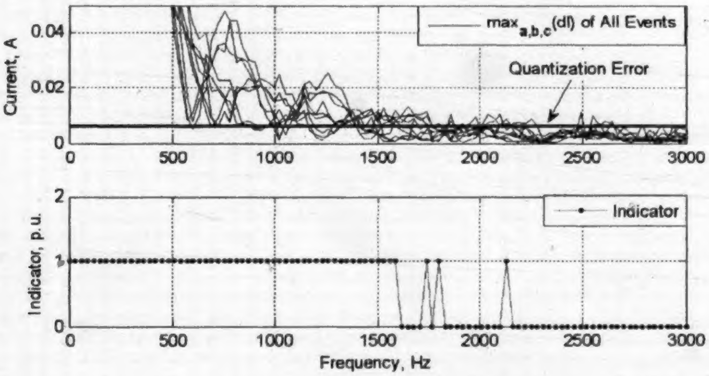

Figure 6.16 The criterion for reliable measurements.

6.6 SG Setting for Practical Applications

This section explains how to set the SG parameters in practical applications to meet the requirements for both signal strength and power quality. First, the transient caused by SG firing is analyzed to determine its strength. Take the thyristor firing between phase A and the ground as an example. Suppose the steady-state voltage across the thyristor when no firing occurs is $v_{thyristor}(t) = -\sqrt{2/3}V_N \sin(\omega t)$, where ω is the fundamental angular speed, and V_N is the rated line-line voltage. The process of a controlled short-circuit is equivalent to temporarily injecting a virtual voltage source $e_{vitual} = -v_{thyristor}(t)$ between point T and the ground. According to the linear superposition principle, the transient response of the system is calculated with a zero-initial-state network energized by a temporary source $e_{virtual}$ (see Figure 6.17(a)). For the sake of simplicity, the loads connected at downstream side are treated as open-circuits due to their large impedances. Therefore, only the path from the phase A supply to the SG is considered in Figure 6.17(b).

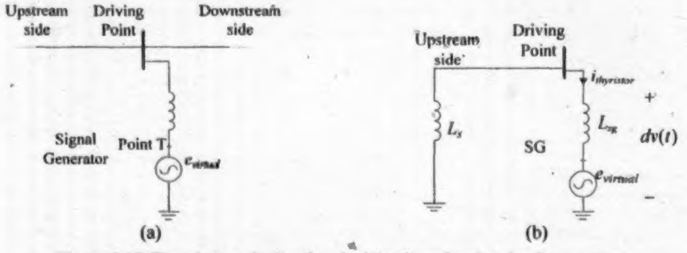

Figure 6.17 Transient analysis using the injection of a virtual voltage source.

Suppose the supply system impedance is mainly inductive (L_s). Denote the SG inductance as L_{sg}. All the variables including V_N are converted to values at the high voltage side if a SG transformer is applied. After the thyristor is fired at instant $\omega t = -\delta$, the thyristor current is determined by the charging process of two inductors in series:

$$i_{thyristor}(t) = \frac{\sqrt{2/3}V_N}{\omega(L_{sg} + L_s)}(\cos\omega t - \cos\delta),\quad \omega t \in [-\delta, \delta]. \tag{6.10}$$

The thyristor current is part of a sinusoidal waveform and lasts approximately 2δ. The peak of this current shows up at instant $t = 0$ and equals

$$i_{thyristor\_peak} = \frac{\sqrt{2/3}V_N}{\omega(L_{sg} + L_s)}(1 - \cos\delta) \tag{6.11}$$

The voltage transient at the driving point is

$$dv(t) = \sqrt{2/3}V_N \frac{L_s}{L_s + L_{sg}} \sin\omega t, \quad \omega t \in [-\delta, \delta]. \tag{6.12}$$

The peak of the voltage distortion is

$$dv_{peak,\%} = \frac{\max(|dv(t)|)}{\sqrt{2/3}V_N} = \frac{L_s}{L_{sg} + L_s}\sin\delta \times 100\%. \tag{6.13}$$

Denote the system three-phase fault level as S_{3ph}, the interface transformer capacity as S_{sg} and the transformer impedance in percentage as x_{sg}. (6.11) and (6.13) are transformed to

$$\begin{aligned} i_{thyristor\_peak} &= \frac{\sqrt{2/3}(1-\cos\delta)}{V_N(x_{sg}/S_{sg} + 1/S_{3ph})} \\ dv_{peak,\%} &= \frac{\sin\delta}{1 + x_{sg}S_{3ph}/S_{sg}} \end{aligned} \tag{6.14}$$

For 25kV distribution systems in North America, the $i_{thyristor\_peak}$ should be at least 5A for strong enough current injection; the $dv_{peak,\%}$ should be maintained below 5% to make the disturbances to load operation negligible. Equation (6.14) can be used to configure the SG interface transformer (or inductance) and the firing angle according to various system conditions.

A SG for measurements of 25kV distribution systems is configured as an example. The typical system three-phase fault level is within 40 ~300 MVA. The maximum SG firing angle is usually 30°. In order to achieve peak thyristor currents no lower than 5A, the 3-phase SG interface transformer should be no smaller than 59kVA (assuming x_{sg}=5%). Suppose a 150kVA, x_{sg}=5% customer transformer is adopted. When the system fault level within 40~300 MVA, the SG firing angle needs to be adjusted to meet both requirements on current strength and voltage disturbance. As the firing angle increases from 5° to 30° with a step of 5°, the peak voltage transient vs. the peak thyristor current is plotted in Figure 6.18. When the curves are within the "operable region" where the peak voltage transient is below 5% and the peak thyristor current is higher than 5A, the requirements for both signal strength and power quality are satisfied. A wide region meets the requirements presented above.

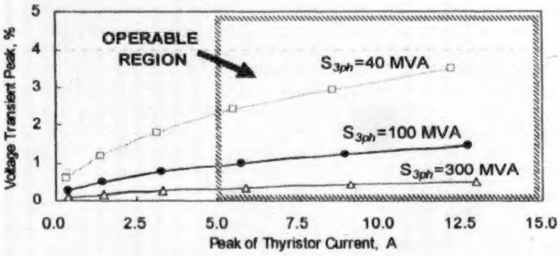

Figure 6.18 The peak voltage transient vs. the peak thyristor current.

For the measurement of LV systems, a typical system impedance is used to determine the SG parameters. For example, the typical system impedance for 120V systems is 0.06+j0.03 ohm at 60Hz. A small inductor of 0.2mH can be adopted for the SG device to make it portable. Its fundamental impedance is almost the same as that of the supply system. The firing angle can be set as 5°. The resulted peak voltage transient is about 3%, and the peak thyristor current is 6A, meeting requirements on both the signal strength and the power quality. If the system impedance is different from the typical value, the firing angle can be adjusted to obtain transient signals with a suitable strength.

6.7 Impedance-Measurement-Based DG Islanding Detection

As mentioned above, the grid impedance measured at DG terminals have been used for DG islanding detection. According to the European standard EN50330-1, when the grid impedance increases over 0.5Ω, the DG is regarded to have become isolated from the utility and should be tripped. For this special application, the fundamental harmonic impedance value will be enough. Therefore we limit our discussion in this section to fundamental harmonic impedances. We can use the impedance measurement device proposed in this chapter to monitor system impedances and detect islanding (see Figure 6.19).

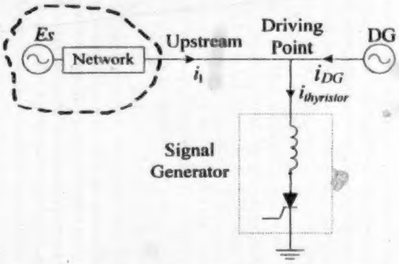

Figure 6.19 Grid impedance measurement for DG islanding detection. .

The SG can be installed right at DG terminal before the DG step-up transformer. In this way, the SG does not need to reduce the voltage for thyristor operation. The SG is composed of a current-limiting inductor and a (pair of) thyristor. Such a SG is easy to implement and suits all types of DGs.

In order to measure the supply impedances for DG anti-islanding protection, the SG interface inductance can be set as 20 times of the typical supply system inductance. A firing angle of 30° is used in the typical condition. In this way, the voltage distortion caused by SG firing is very small compared to the voltage at the measuring point. One firing angle of 30° is enough for the measurement since only the fundamental impedance is of interest.

Both impedances, the system impedance Z_s and the driving point impedance Z_{dp} measured at DG terminal, will increase after islanding occurs and can be used for islanding detection. However, the system impedance varies much more obviously than the driving point impedance and therefore is a more reliable index for islanding detection.

$$Z_{dp} = \begin{cases} Z_{\text{utility}} // Z_{DG} \approx Z_{utility} & \text{(Normal)} \\ Z_{DG} & \text{(Islanded)} \end{cases} \tag{6.15}$$

$$Z_s = \begin{cases} Z_{\text{utility}} & \text{(Normal)} \\ Z_{load} // Z_{shunt} & \text{(Islanded)} \end{cases}, \tag{6.16}$$

where $Z_{utility}$, Z_{DG}, Z_{load} and Z_{shunt} represent the impedances of the utility, DG, load and shunt capacitors in the network.

Chapter 5 also proposed to use the DC current drawn from the upstream by thyristor firing for islanding detection. Table 6.1 lists all the possible indices for DG islanding detection. The DC current indices are simpler than impedance indices since they do not require voltage signals and do not involve Fourier Transform. The DC component in upstream current is more effective in detecting islanding than the DC component in thyristor current.

TABLE 6.1 CANDIDATE INDICES FOR DG ISLANDING DETECTION.

Location / Variable	Driving Point	Upstream
Impedance	Z_{dp} (h=1)	Z_s (h=1)
Current	DC component in thyristor current pulse	DC component in upstream transient current

6.8 Conclusions

This chapter proposed an effective new method for measuring the system harmonic impedances. It utilizes a thyristor to create a controlled short-circuit at the driving point. Transient current and voltage signals are generated and used for harmonic impedance measurement. The strength of transient signals is adjusted through the thyristor firing angle so that accurate measurements are supported, and the disturbances to the load operation are negligible. This method can be easily implemented in a low-cost and portable device.

A complete measurement scheme was developed to operate the proposed device. The transient signals were created by using multiple firing angles to improve the precision at the frequencies with low transient current energy. In order to measure nonsymmetrical three-phase systems, signals were generated with specific combinations of different firing channels. The transient signals were extracted through a subtraction which largely suppressed the fundamental and harmonic noises.

Simulations and lab tests verified the effectiveness of the proposed method. A criterion was established for predicting the range of reliable measurements.

The proposed device can be applied to DG islanding detection by monitoring the system impedances at DG terminals.

Chapter 7. FAULTED LINE IDENTIFICATION IN NONEFFECTIVELY GROUNDED SYSTEMS

In noneffectively grounded electric power systems, the supply system is either ungrounded, high resistance grounded, or resonant grounded. Noneffective grounding is commonly practiced in the power distribution systems of some European and Asian countries. It is also adopted in continuous process industries in North America, such as the textile and mining industries. When a single-phase-to-ground fault occurs, such a configuration allows the distribution system to continue to operate without tripping immediately. Later when the fault is located, it can be cleared at a convenient time, resulting in minimized losses. Typically, the faulted line must be identified and cleared within a required time frame of 30 minutes to 2 hours. However, identifying the faulted line among a number of lines connected to the same bus is a significant challenge due to the small ground fault currents produced in the above systems. Many faulted line identification methods have been developed, but their performances have been unsatisfactory.

This chapter proposes a novel method that can help to overcome this difficulty. This method utilizes a thyristor to create a controlled grounding of the system neutral. A strong current signal flows through the faulted line and is used for identifying the faulted line. This chapter presents a theoretical analysis, computer simulations, and lab experiments for the proposed method. The results are very promising. The contents in this chapter have been published [75].

7.1 Introduction

This section introduces the characteristics of noneffectively grounded systems experiencing a single-phase-to-ground fault. Consider the ungrounded system in Figure 7.1(a), with many distribution feeders connected to the same bus. The loads of such a system are typically ungrounded. Suppose a ground fault occurs to phase A of one distribution line. The fault current will flow through a loop composed of the fault path, the distribution lines, the distribution line to the ground shunt capacitors, and the ground. Since the line shunt capacitors have very large impedances, the single-phase-to-ground fault current is very small, and the system phase-to-neutral voltages remain almost symmetrical. Therefore, the system can operate without tripping the faulted line immediately.

On the other hand, the fault causes obvious changes to the ground voltages in the system. As the phase A to the ground voltage drops to almost zero, the system neutral to the ground voltage rises to close to the rated phase-to-ground voltage, while the phase B (or C) to the ground voltage rises to up to $\sqrt{3}$ times of their normal values (see Figure 7.1(b)). The rise in the neutral voltage can be used as an indication of the ground fault. The over-voltages between an unfaulted phase and the ground may cause insulation failure and expansion of the fault to a phase-ground-phase fault. For this reason, the single-phase-to-ground fault must be located and cleared in a timely manner.

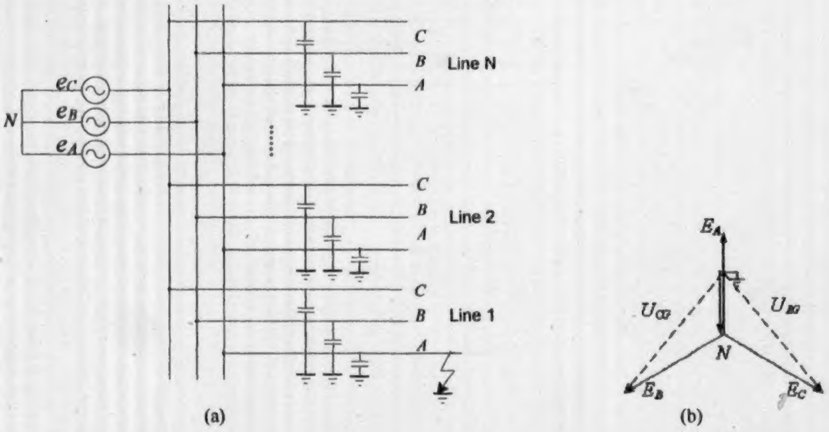

Figure 7.1 The analysis circuit for created transient current signals.

Identifying the faulted line among a number of lines connected to the same bus, however, has been recognized as a difficulty for many years because the ground fault causes very small fault currents. Many efforts have been made to develop reliable and accurate faulted line identification techniques. The existing methods have their limitations, and their performances are unsatisfactory. These methods will be reviewed in the next section.

As the distribution networks have expanded in recent years, more distribution lines, especially underground cables, have been installed in distribution networks. These new lines have greatly increased the distribution system's total shunt capacitance and, therefore, also increased the single-phase-to-ground fault current. As a result, single-phase to ground faults are more likely to extend to phase-ground-phase faults. Therefore, identifying the faulted line accurately and in time becomes more important. A reliable faulted line identification method is urgently needed.

7.2 Review of Existing Identification Methods

The difficulty in identifying the faulted line has motivated a great deal of research work since the 1980's. The developed methods are classified into the following three types, which are discussed later separately.

Steady-state-based methods identify the faulted line according to the system characteristics after a single-phase-to-ground fault reaches its steady state.

Transient-based methods work according to the transient signals caused by the single-phase-to-ground fault.

Active methods perform changes in the faulted system and thereby create signals for identifying the faulted line.

7.2.1 Steady-State-Based Methods

The following steady-state based methods have been developed to identify the faulted line.

A. Zero-sequence fault-current-based method

This basic method for identifying the faulted line in ungrounded or high-resistance grounded systems works by examining the steady-state fault current flowing through each line [57][70]. As shown in Figure 7.2, a ground fault causes a zero-sequence fault current to flow through each line. On an unfaulted line, the fault current charges the line shunt capacitor and leads the zero-sequence voltage. On the faulted line, the zero-sequence fault current at the sending-end equals the sum of the zero-sequence currents flowing to all the unfaulted lines and has a reversed direction. Therefore, ideally the faulted line has the largest zero-sequence current among all the lines, which is also lagging the zero-sequence voltage. This method acquires the zero-sequence CT outputs as the steady-state fault currents, and combines the magnitude and phase features of the faulted line zero-sequence current for identifying the faulted line.

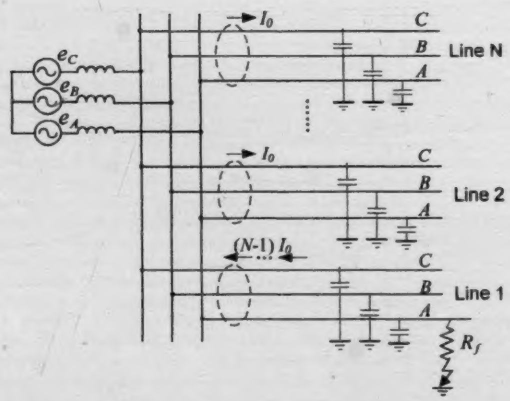

Figure 7.2 Faulted line identification based on steady-state zero-sequence currents.

The disadvantage of this method is that ground fault currents are weak signals, especially when the fault resistance is high. System noises, such as zero sequence CT errors, may seriously influence the identification accuracy. The complexity in distribution network configurations and operation modes also exacerbates the problem. It has been found that when only a few feeders are connected to the system with their lengths varying in a large range, this method tends to yield the wrong results.

B. Zero-Sequence 5th Harmonic-Current-Based Method

In resonant grounded systems, the system neutral is grounded via an arc-suppression coil that compensates for the system total line shunt capacitance at the fundamental frequency. In these systems, on either the faulted or an unfaulted line, the sending-end fundamental zero-sequence current equals the capacitor charging current of this line. Therefore, the fundamental zero-sequence fault current can no longer be used to identify the faulted line.

This method proposed using the 5th harmonics contained in zero-sequence fault currents for identification in resonant grounded systems [60]. At the 5th harmonic frequency, the arc suppression coil is no longer in resonance with the total line shunt capacitance. The faulted line can be identified as the one in which the largest 5th harmonic zero-sequence current is flowing through, and this 5th harmonic current is lagging the 5th harmonic zero-sequence voltage.

Compared to the fundamental zero-sequence current, the 5th harmonic zero-sequence currents are even weaker signals. Industry practices show that this method has a very poor signal noise ratio and low reliability.

C. $I_0 \sin\phi$ *(or Reactive Zero-sequence Power Flow) Based Method*

This method is a variation of the zero-sequence-current-based method and is applicable to ungrounded or high-resistance grounded systems [59]. It utilizes the projections of zero-sequence currents on the bus zero-sequence voltage, i.e., $I_0 \sin\phi$, as the detection criteria, where I_0 is the zero-sequence current of each line, and ϕ is the angle that I_0 is lagging the zero-sequence voltage. According to Figure 7.2, if the largest $I_0 \sin\phi$ has a positive sign, this $I_0 \sin\phi$ corresponds to the faulted line; otherwise, if the largest $I_0 \sin\phi$ is zero or negative, then the fault occurs at the distribution bus. Suppose the zero sequence voltage on the distribution bus is 1 p.u., then this method is equivalent to using the zero-sequence reactive power on each line for detection.

D. Zero-sequence Active-Power-Flow-Based Method

This method is designed for resonant grounded systems [61][62]. In these systems, a resistor is connected in series with the arc-suppression coil to suppress any overvoltages that may occur due to the shunt resonance (see Figure 7.3). This resistor is connected in normal conditions and shorted after a delay when a ground fault occurs. The existence of this resistor makes the faulted line to supply a zero-sequence active power to the grounding path, while the zero-sequence powers flowing through other unfaulted lines are mostly reactive. This method examines the zero-sequence active power flow on each line, and identifies the faulted line as the one corresponding to the largest active power flow.

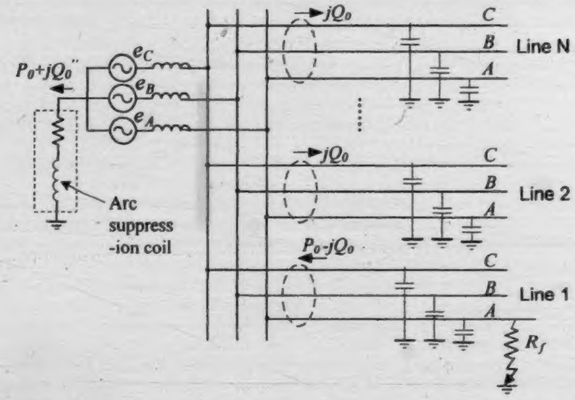

Figure 7.3 Faulted line identification based on zero-sequence active power flow.

This method uses fundamental components instead of the 5th harmonics for detection. However, since the fault current is mainly reactive, the active powers are small portions of the fault power flows and are weak signals. Therefore, the accuracy of this method is still a problem.

The steady-states-based identification methods have the common problem that the steady state criteria for identification are weak signals. These methods have low signal noise ratios and may be affected by noises such as CT errors.

7.2.2 Transient-Based Methods

In view of the disadvantages of steady-states-based methods, researchers seek to use the transient signals that show up during the ground fault processes to locate the faulted line. Due to the drop in the faulted phase to the ground voltage and the rise in the unfaulted phase to the ground voltages, which are caused by the ground fault, the fault transient currents contain high frequency discharging and charging components of the line shunt capacitors. These transient currents last for a short duration (say, 0.5~ 1.0 cycle) and typically have larger magnitudes than the steady-state fault currents. The following research efforts have been made to make use of the transient signals.

A. Detection Based on First Half-Wave's Polarity

This method utilizes a polarity relationship between the transient voltage and the current waveforms to detect the faulted line in radial distribution networks [63]. During the first half-wave of the zero-sequence voltage, the zero-sequence current on the faulted line has an opposite polarity to that of the zero-sequence voltage, while the zero-sequence current on an unfaulted line has the same polarity as the zero-sequence voltage. Therefore, the faulted line can be identified according to the direction of the transient zero-sequence current.

This method was proposed early in the 1950's. However, since the polarity relationship of this method exists for only a short duration and is non-repeatable, the reliability of this method is poor and its applications are very limited.

B. Detection Based on Transient Signals in Selected Frequency Band

In recent years, studies have been conducted to utilize the frequency-domain information of transient signals to detect the faulted line. Reference [64] proposed utilizing the transient signals within a selected frequency band (SFB) to detect the fault. For ungrounded systems, the SFB is defined as a low frequency range

($0 \sim \omega_L$) where all the distribution line impedances are capacitive. For resonant grounded systems, SFB is defined as a narrower range ($\omega_L' \sim \omega_L$) to eliminate the influence of the arc-suppression coil. Within SFB, the faulted line has the largest capacitive current flowing to the sending-end, while an unfaulted line has a capacitive current flowing from the sending-end to the load. The faulted line can be determined according to the magnitude and polarity of the zero-sequence currents. Also, the following two criteria can be used for identifying the faulted line:

$$\begin{aligned} q(t) &= i_0(t) du_0(t) / dt \\ E(t) &= \int_0 q(\tau) d\tau \end{aligned} \quad , \qquad (7.1)$$

where $q(t)$ and $E(t)$ represent the reactive power flow and reactive energy, respectively. For the faulted line, $q(t)$ and $E(t)$ should be negative, while for other lines, they should be positive.

The main oscillation components contained in ground fault transients are within the SFB. This fact implies that the majority of the energy emitted during ground fault transients will be used for identification.

According to field tests, this method correctly identified the faulted line in most faults. However, a small portion (1.7%) of the faults was not sensed due to either low hardware sensitivity or weak transient strength.

C. Wavelet-Analysis-Based Methods

Efforts were made to use wavelets to analyze transient signals and to derive indices for locating the fault [65][66]. In these trials, however, the derived indices had no clear physical meanings, and the technical soundness of the methods were not verified. No field tests were reported for these methods.

Although the transient signals caused by ground faults are typically much stronger than the steady state signals, transient-based detections have common shortcomings. First, transient signals last for only a short duration and are non-repeatable, so that the signal capture difficulty is increased. Second, transient signal strengths are dependent on the fault's occurring instant and are highly random. Ground faults occurring around voltage zero-crossing points will cause much weaker transients than faults occurring at voltage peaks. This problem reduces the reliability of transient-based identification methods.

7.2.3 Active Methods

In recent years, new methods have been developed which work by injecting specific current signals, or modifying the system grounding pattern temporarily. These methods are regarded as promising solutions for the identification of single-phase ground faults.

A. Pulse-Current-Based Method

The pulse-current-based method is widely adopted in industrial systems in North America [17][67]. This method utilizes a pulsing circuit to momentarily increase the fault current on a rhythmic basis by intermittently short-circuiting some of the grounding resistor. The pulsing current can be easily detected at any point in the circuit due to the noticeable flicker of the Ground Current Detector ammeter. The pulse can be timed such that the increased ground fault current is on 30% of the time.

B. Parallel-Resistor-Injection-Based Method

Reference [68] proposed temporarily inserting a resistor between the neutral and ground when a ground fault occurs in resonant grounded systems. This resistor will greatly increase the active power flow from the faulted line to the neutral and, therefore, improve the reliability of the steady-state active-power -flow-based method. This resistor will be tripped once the faulted line is identified, and its conduction time is less than 1 second.

Although this method improves the steady-state active-power-based method, it still utilizes a weak signal of the active flow for identification. This problem limits the accuracy of the method, and false detections were recorded in field tests.

C. Interharmonic-Current-Injection-Based Method

This method injects an interharmonic current between the neutral and ground to the system. This interharmonics current will flow mainly through the faulted line and, therefore, can be used to identify the faulted line. To reduce the implementation difficulty, the interharmonics source can also be connected across the secondary open-delta winding of the PTs monitoring the line-to-ground voltages with the primary side Yg connected [69] [58].

The performance of this method may be affected by the harmonic pollution in the system. If harmonics exist around the injected interharmonics frequency, they may interfere with the detection. According to field experiences, in some heavily polluted industrial systems in China the interharmonic-current-based methods are not satisfactory. Sometimes the faulted line still needs to be identified by switching off the distribution lines one by one.

7.2.4 Conclusion

Active methods are promising solutions for faulted line identification since they can generate strong signals for identification. For these methods, strong enough signals must be created without losing the fault current limiting advantage of noneffectively grounded systems. However, the existing studies do not discuss the disturbance caused by active methods to load operation.

This chapter presents a novel method that temporarily grounds the system by using a thyristor-controlled grounding device. A small but discernable transient current signal will flow through the faulted line and can be used for identification. Compared to the existing active method, this method has a simple structure and does not require a dedicated interharmonics generator. The device is designed so that a strong current signal is injected for identification without causing a serious disturbance to the load operation.

7.3 The Proposed Method Based on Thyristor-Controlled Grounding

For noneffectively grounded systems, identifying the line experiencing a single-phase ground fault is very difficult due to the small steady-state fault current available for identification. The cause of the small fault current, in turn, is that the system is not effectively grounded. In this chapter, we proposed to temporarily convert a noneffectively grounded system into an effectively grounded system by using a controllable grounding device connected between the neutral and ground. A large fault current pulse will appear if a ground fault exists in the circuit. This fault current will flow mainly through the low-impedance loop composed of the faulted line, the fault path, and the ground (see Figure 7.4). We can use regular current transformers (CTs) installed at the sending-end of each feeder to acquire the line current waveforms and send them to a central signal detector. The detector extracts the transient current signal flowing through each line and can therefore identify the faulted line. The detector will display the identification result as an alarm signal and can be implemented into a microprocessor-based device. This scheme suits all types of noneffectively grounded systems. The proposed controllable grounding device and the signal detector are discussed below in detail.

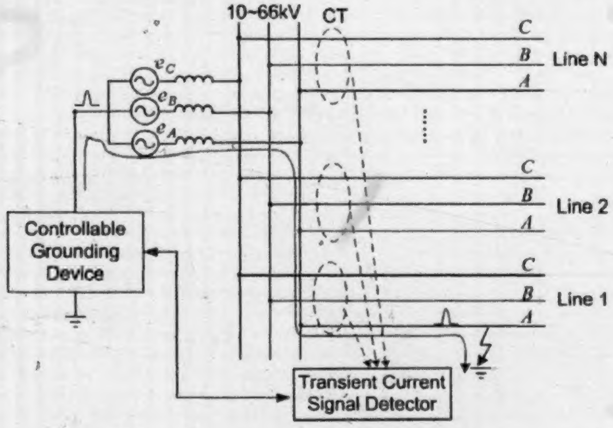
10~66kV
CT
e_C
e_B
e_A
C
B
A
Line N
C
B
A
Line 2
C
B
A
Line 1
Controllable Grounding Device
Transient Current Signal Detector

Figure 7.4 Illustration of the proposed scheme.

7.3.1 Controllable Grounding Device

A thyristor-based device is used to create controllable short-circuits between the system neutral and the ground. The device consists of a stepdown transformer and a thyristor (see Figure 7.5 (a)). When a single-phase-to-ground fault occurs and reaches its steady state, the neutral-to-ground voltage rises to a level close to that of the rated phase-to-ground voltage. The stepdown transformer reduces the neutral voltage to a low level for thyristor operation; its leakage impedance also limits the magnitudes of the transient current pulse and the voltage distortion. The SG stands by during system normal operation. Once a ground fault is detected according to the neutral voltage rise, the thyristor will be fired several degrees before the zero-crossing-point of the neutral voltage, creating a temporary short-circuit. A transient current pulse (see Figure 7.5(b)) flows through the faulted line and then back to the ground.

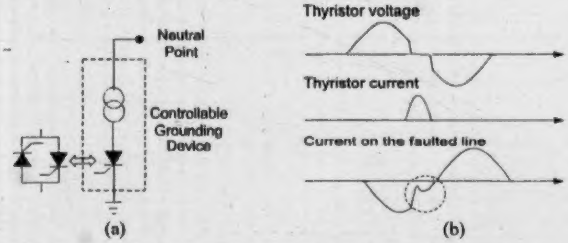
Neutral Point
Controllable Grounding Device
Thyristor voltage
Thyristor current
Current on the faulted line

(a) (b)

Figure 7.5 The controllable grounding device (a) structure and (b) system responses.

In another configuration of the proposed method, the grounding device makes use of potential transformers (PTs) connected at the distribution bus monitoring phase-ground voltages. The PT primary side is grounded Y connected, and the grounding device is connected to the open-delta winding at the secondary side (see Figure 7.6). With this configuration, a grounding device does not require a dedicated stepdown transformer and is cheaper; its installation does not involve the distribution transformer and is therefore much easier. With both configurations the proposed method works in a similar way. This chapter mainly investigates the first configuration in Figure 7.5. The conclusions can be roughly applied to the second configuration.

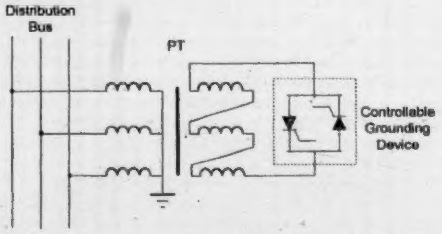

Figure 7.6 The controllable grounding device connected at PT secondary side.

The thyristor-based scheme has a number of advantages. First, the strength of the transient current pulse is controlled through the thyristor firing angle, so that it is strong enough for reliable identification and yet not to cause power quality problems. This will be explained further in Section 7.5. Second, important features can be endowed to the transient current pulses. For example, the pulse can be either positive or negative depending on whether the thyristor is fired across the voltage falling or rising edge. The current pulses can be generated at a frequency of every 2, 4 or 8 fundamental cycles. By manipulating the angle, polarity and frequency of the thyristor firing, a series of current pulses with distinct features can be generated (say, positive pulse—negative pulse—positive pulse). This feature makes the generated transient signals insensitive to random noises.

7.3.2 Transient Current Signal Detector

The signal detector extracts the transient current signal at the sending-end of each line and identifies the faulted line. An important feature of the detector is that the transient current signal is extracted by subtracting subsequent cycles of the current waveform. Suppose the thyristor is fired for every 4 cycles (see Figure 7.7); the difference between the first 2 cycles containing the pulse and the second 2 cycles without the pulse is the desired transient current signal. This subtraction method can effectively eliminate the background distortions contained in the current waveforms. The proposed scheme is therefore immune to influences of harmonics that already exist in the systems.

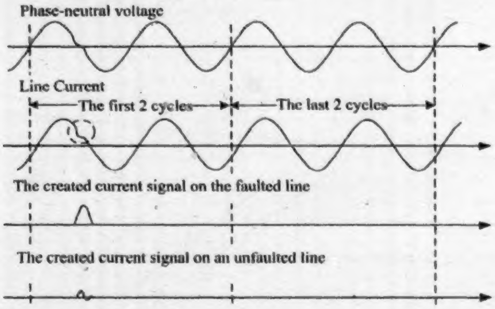
Phase-neutral voltage
Line Current
The first 2 cycles
The last 2 cycles
The created current signal on the faulted line
The created current signal on an unfaulted line

Figure 7.7 The extraction of transient current signals.

After the transient current signals flowing through all the lines are extracted, an algorithm is needed to identify the faulted line. This algorithm is investigated below in Section 7.5.

7.4 Study of Signal Characteristics

This section investigates the characteristics of the created transient current signals in preparation for constructing a faulted line identification criterion. Both theoretical analysis and computer simulations are performed to study the faulted line signal and an unfaulted line signal in comparison.

7.4.1 Theoretical Analysis

This section firstly analyzes the steady-state system with ground fault, and then investigates the transient signals caused by thyristor firing.

A. A Steady-state System with a Single-Phase Ground Fault

Take an ungrounded system (see Figure 7.1(a)) as an example for analysis. Suppose a single-phase ground fault occurs to phase A of one line. The fault is equivalent to the injection of a virtual voltage source $e_{virtual} = -e_{AN}(t)$ between phase A and ground, where $e_{AN}(t)$ is the phase A to ground voltage in normal system condition. The changes caused by the fault can be analyzed using a circuit in Figure 7.8 energized by the virtual voltage source $-e_{AN}(t)$. L'_{s1} and L'_{s2} are respectively the positive-sequence system inductance plus the faulted line inductance (for the segment from the sending-end to the fault point) and the negative-sequence system inductance plus the faulted line inductance; L_{s0} is the zero-sequence supply system inductance; C_0 is the single-phase zero-sequence shunt capacitance of each line (supposing each line has the same value); N is the number of distribution lines; R_f is the fault resistance. The loads are omitted in this circuit. The reason is their positive- and negative-sequence circuits can be regarded as open-circuits compared to L'_{s1} and L'_{s2}, and their zero-sequence circuits are open since the loads in noneffectively grounded systems is typically ungrounded.

In this figure, the zero-sequence shunt capacitance NC_0 has very large fundamental impedance value. Therefore, the fault current is very small; the fault mainly causes changes in zero-sequence voltages, not phase-to-neutral voltages. According to Figure 7.8, the neutral voltage equals

$$\dot{V}_{NG} = \dot{E}_{AN}\frac{j(-X_{C\Sigma})}{j(-X_{C\Sigma})+R_f}\text{, or } V_{NG} = E_{AN}\left|\frac{j(-X_{C\Sigma})}{j(-X_{C\Sigma})+R_f}\right| \tag{7.2}$$

where V_{NG} and E_{AN} are the RMS of $v_{NG}(t)$ and $e_{AN}(t)$ respectively, $X_{C\Sigma}=1/(3NC_0\omega_1)$ and ω_1 is the fundamental angular-speed. L'_{s1} and L'_{s2} are omitted due to their small values when a high R_f is studied (say, above 100 ohm). According to (7.2), the neutral voltage drops as the fault resistance goes high.

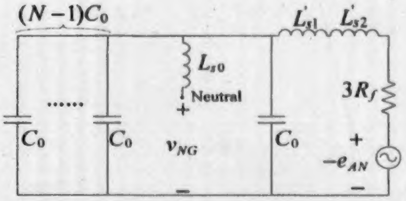

Figure 7.8 The analysis circuit for neutral voltage rise caused by ground fault.

In resonant grounded system, an arc-suppression coil is connected between the neutral and ground, and is tuned so that it is in resonance with the shunt capacitance $3NC_0$ of all the lines. The neutral voltage rise in a faulted resonant grounded system can be calculated using

$$V_{NG} = E_{AN}\left|\frac{(-jX_{C\Sigma})\,//\,j(\omega_1 L_{res})}{(-jX_{C\Sigma})\,//\,j(\omega_1 L_{res})+R_f}\right| \tag{7.3}$$

where L_{res} is the inductance of the arc-suppression coil. Therefore, the neutral voltage in a faulted resonant grounded system remains equal to the rated phase-to-neutral voltage as the fault resistance varies.

B. Transient Current Signal

The transient current signals created by the controllable grounding device are analyzed as follows. A temporary short-circuit created by thyristor firing is equivalent to the injection of a virtual voltage source $e_{virtual} = -v_{NG}(t)$ between the neutral and the ground in Figure 7.1. Therefore, the created transient signals can be calculated using a sequence circuit energized by $e_{virtual}$ as shown in Figure 7.9(a), where L_{SG} is the signal-generator transformer leakage inductance. Figure 7.9(b) is derived from Figure 7.9(a) and shows the real instead of sequential transient current signals. In Figure 7.9(b), L'_{s1} and L'_{s2} are ignored. i_{Rf} is the transient current flowing through the fault resistance; i_{3C_0} is the current flowing through the three-phase shunt capacitances of each line. According to the power industry practice in China, zero-sequence CTs are installed at the sending-end of each line and are available for identifying the faulted line. The triples of these CT outputs are studied for the purpose of simplicity. Therefore, the transient current signal on the faulted line and that on an unfaulted line are respectively $i_{faulted}$ and $i_{unfaulted}$, and

$$\begin{cases} i_{faulted} = i_{Rf} + i_{3C0} \\ i_{unfaulted} = i_{3C0} \end{cases}. \tag{7.4}$$

Figure 7.9(b) is further transformed to Figure 7.9 (c), which is energized by a virtual current source, according to Thevenin's Theorem. Assuming the thyristor is fired ahead of v_{NG} 's rising-edge zero-crossing-point by an angle of δ (denoted as the firing angle) at $t = 0$, the virtual voltage source is

$$e_{virtual} = -v_{NG}(t) = -\sqrt{2}V_{NG}\sin(\omega_1 t - \delta),\ \ t \geq 0. \tag{7.5}$$

The virtual current source is

$$i_s(t) = I_m[\cos(\omega t - \delta) - \cos\delta],\ \ t \geq 0, \tag{7.6}$$

where $I_m = \sqrt{2}V_{NG} / X_{SG}$, $X_{SG} = \omega_1 L_{SG}$. The transient current i_{Rf}, i_{3C_0}, and the thyristor current are respectively

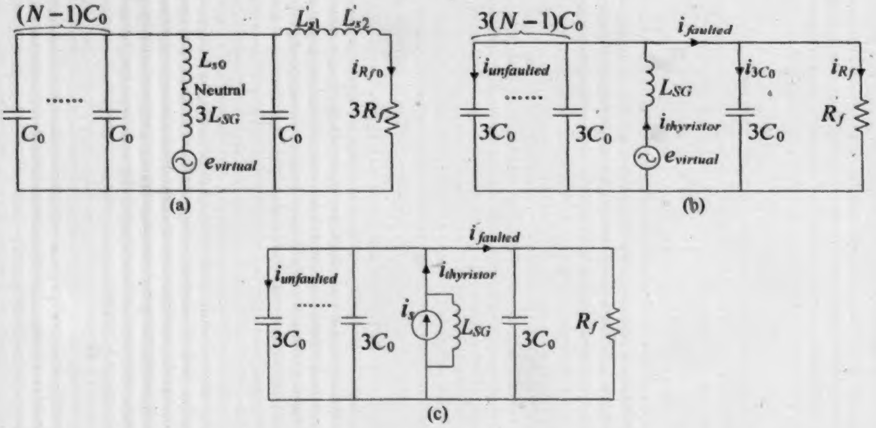
$(N-1)C_0$
L'_{s1}
L'_{s2}
L_{s0}
Neutral
$3L_{SG}$
$e_{virtual}$
i_{Rf0}
$3R_f$
C_0
C_0
C_0
(a)
$3(N-1)C_0$
$i_{faulted}$
$i_{unfaulted}$
L_{SG}
$i_{thyristor}$
$e_{virtual}$
i_{3C_0}
i_{Rf}
R_f
$3C_0$
$3C_0$
$3C_0$
(b)
$i_{faulted}$
$i_{unfaulted}$
$i_{thyristor}$
i_s
L_{SG}
$3C_0$
$3C_0$
$3C_0$
R_f
(c)

Figure 7.9 Analysis of transient current signals in an ungrounded system.

$$\begin{aligned} i_{R_f} = {} & I_m R_f^{-1}/Y_\Sigma\{-\sin(\omega_1 t-\beta) \\ & +e^{-\tau t}[-\sin\beta\cos\sigma t+(\sigma C_\Sigma)^{-1}(X_{SG}^{-1}\cos\beta+(2R_f)^{-1}\sin\beta-Y_\Sigma\cos\delta)\sin\sigma t]\}, \end{aligned} \tag{7.7}$$

$$\begin{aligned} i_{3C_0} = {} & I_m X_C^{-1}/Y_\Sigma\{-\cos(\omega_1 t-\beta) \\ & +e^{-\tau t}[\cos\beta\cos\sigma t+(\sigma C_\Sigma)^{-1}(X_{SG}^{-1}\sin\beta-(2R_f)^{-1}\cos\beta)\sin\sigma t]\}, \end{aligned} \tag{7.8}$$

$$\begin{aligned} i_{LSG} = {} & I_m X_{SG}^{-1}/Y_\Sigma\{\cos(\omega t-\beta)-e^{-\tau t}[\cos\beta\cos\sigma t+\sigma^{-1}(\omega\sin\beta+\tau\cos\beta)\sin\sigma t]\} \\ & -I_m\cos\delta\{1-e^{-\tau t}\sigma^{-1}(\tau\sin\sigma t+\sigma\cos\sigma t)\}, \end{aligned} \tag{7.9}$$

$$i_{thyristor} = i_s - i_{LSG} \quad (\text{or } i_{thyristor} = i_{R_f} + N\, i_{3C_0}), \tag{7.10}$$

where $X_{SG}=\omega_1 L_{SG}$, $I_m=\sqrt{2}V_{NG}/X_{SG}$, $X_C=(\omega_1 3C_0)^{-1}$, $C_\Sigma=3NC_0$, $Y_\Sigma=\sqrt{R_f^{-2}+(X_{SG}^{-1}-\omega_1 C_\Sigma)^2}$, $\tau=1/(2R_f C_\Sigma)$, $\sigma=\sqrt{(L_{SG}C_\Sigma)^{-1}-\tau^2}$, and $\beta=\delta+\sin^{-1}\left(R_f^{-1}/Y_\Sigma\right)$.

Equations (7.7)~(7.10) are valid only during the first thyristor conduction. According to these equations, the $i_{thyristor}$, $i_{faulted}$ and $i_{unfaulted}$ all contain components of two angular speeds: ω_1 and σ . When σ is real, i.e., $R_f > \frac{1}{2}\sqrt{X_{SG}X_{C\Sigma}}$, the σ -components are in oscillatory form; when σ is imaginary, i.e., $R_f < \frac{1}{2}\sqrt{X_{SG}X_{C\Sigma}}$, the system is over-damped, and the σ -components are exponentially damped without oscillations. In typical cases of $R_f << X_C$, $i_{faulted}$ contains a much larger fundamental component than $i_{unfaulted}$ does. This feature can be used for identifying the faulted line.

The above analysis can be applied to resonant grounded or high-resistance grounded systems by adding an extra grounding path of a grounding resistance or an arc-suppression coil between the neutral and ground. The analysis circuits for a resonant grounded system is shown below in Figure 7.10(a). This circuit can be transformed to Figure 7.10(b), which has similar structure to Figure 7.9(c) except that a new component $L_{eq} = (L_{SG}^{-1} + L_{res}^{-1})^{-1}$ replaces L_{SG}. Therefore the current signals in Figure 7.10 are derived by referring to (7.7)~(7.9) as follows

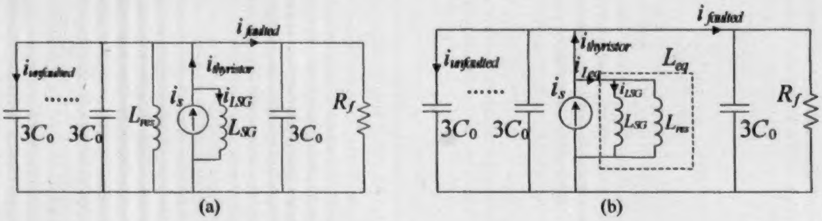

Figure 7.10 The analysis circuit for created transient current signals.

$$\begin{aligned} i_{R_f} = I_m R_f^{-1} / Y_\Sigma \{ & -\sin(\omega_1 t - \beta) \\ & + e^{-\tau t}[-\sin\beta\cos\sigma t + (\sigma C_\Sigma)^{-1}(X_{eq}^{-1}\cos\beta + (2R_f)^{-1}\sin\beta - Y_\Sigma\cos\delta)\sin\sigma t] \}, \end{aligned} \tag{7.11}$$

$$\begin{aligned} i_{3C_0} = I_m X_C^{-1} / Y_\Sigma \{ & -\cos(\omega_1 t - \beta) \\ & + e^{-\tau t}[\cos\beta\cos\sigma t + (\sigma C_\Sigma)^{-1}(X_{eq}^{-1}\sin\beta - (2R_f)^{-1}\cos\beta)\sin\sigma t]\}, \end{aligned} \tag{7.12}$$

$$\begin{aligned} i_{Leq} = & I_m X_{eq}^{-1} / Y_\Sigma \{\cos(\omega t - \beta) - e^{-\tau t}[\cos\beta\cos\sigma t + \sigma^{-1}(\omega\sin\beta + \tau\cos\beta)\sin\sigma t]\} \\ & - I_m \cos\delta\{1 - e^{-\tau t}\sigma^{-1}(\tau\sin\sigma t + \sigma\cos\sigma t)\} \end{aligned}, \tag{7.13}$$

$$i_{thyristor} = i_s - i_{Leq} X_{SG}^{-1} X_{eq}, \tag{7.14}$$

where $X_{eq} = \omega_1 L_{eq}$, $Y_\Sigma = \sqrt{R_f^{-2} + [1/(\omega_1 L_{eq}) - \omega_1 C_\Sigma]^2}$, $\sigma = \sqrt{(L_{eq} C_\Sigma)^{-1} - \tau^2}$, and $\beta = \delta + \sin^{-1}\left(R_f^{-1}/Y_\Sigma\right)$.

When the system is resonant grounded, the thyristor current contains not only ω_1 and σ frequency components, but also a DC component. Suppose the system is precisely resonant grounded, i.e., $X_{C\Sigma} = X_{Lres}$, the steady-state component in $i_{thyristor}$ is

$$i_{thyristor}^{steady} = I_m\left[- L_{eq} / L_{res} \cos\delta - R_f^{-1} / Y_\Sigma \sin(\omega_1 t - \beta)\right]. \tag{7.15}$$

Equations for transient current signals in high-resistance grounded systems are omitted here.

7.4.2 Computer Simulations

Computer simulations were performed to verify the above analysis using the PSCAD software and the following system:

- Supply: 10kV, 50Hz, 3-phase-to-ground fault level of 200MVA; the system is either ungrounded, or grounded via a 1000 ohm high resistor, or resonant grounded via a 4.25H arc-suppression coil.
- Distribution lines: totally 8 overhead lines, each of 20km; R1=0.6 ohm/km, X1=0.39 ohm/km, R0=0.71 ohm/km, X0=1.93 ohm/km, B1=3.86 µSimens/km, B0=1.55 µSimens/km.
- Load: each line has a 3-phase load of 1MW, PF=0.9, ungrounded-Y connected; each phase of the load is modeled with a resistance of 80 ohm in series with an inductance of 0.12H.
- Single-phase-to-ground fault: occurs to phase A at the sending-end of one line.
- Controllable Grounding Device: the stepdown transformer is of 5.77/0.277kV, Z=3.5%, 65kVA.

The simulation results for the ungrounded system with $R_f = 250$ ohm and $\delta = 150°$ are shown in Figure 7.11 as an example. In this example case, the oscillation frequency $\sigma \approx 14\omega_1$, and $X_{C\Sigma} : R_f : X_{SG} = 1612:250:8$. The predicted $i_{thyristor}$, $i_{faulted}$ and $i_{unfaulted}$ using (7.4)-(7.8) were found to coincide with the simulation results very well, and the predicted $i_{thyristor}$ is also plotted in Figure 7.11(a) for comparison. The thyristor conducted for about 150°, which approximately equaled the firing angle. Apparent differences existed between the waveforms of $i_{faulted}$ and $i_{unfaulted}$. Analysis using (7.4)-(7.8) showed that $i_{faulted}$ contained a large fundamental component and a damped oscillating component; $i_{faulted}$ was therefore a positive pulse. However, $i_{unfaulted}$ had almost no fundamental component and had an oscillating component of $14\omega_1$ (see Figure 7.11(b)). The voltage distortion caused by controlled short-circuits was presented in Figure 7.11(c). The peak disturbance in phase A-to-neutral voltage was 0.12kV (or 1.5% of the rated phase-to-neutral peak voltage). The impact of such a small disturbance to the load operation is negligible.

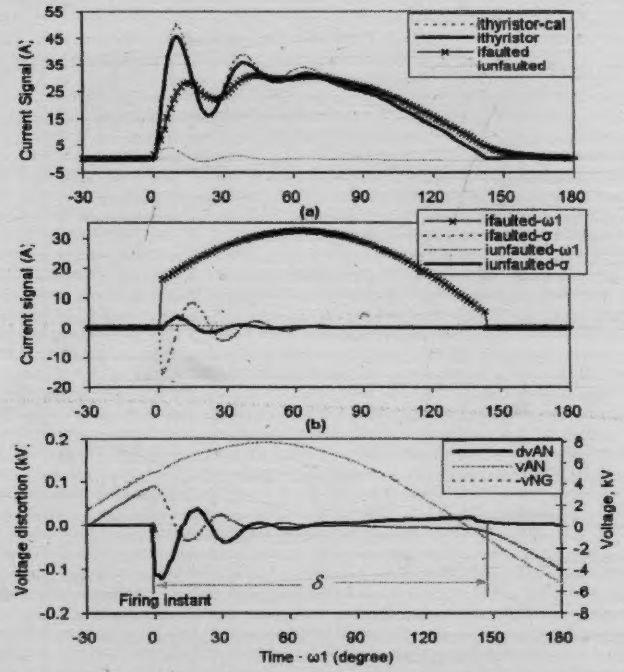

Figure 7.11 The responses of the ungrounded system with R_f=250ohm and δ=150°.

Simulation was also performed by moving the fault in the above example case to the line end. The results are close to those in Figure 7.11 except that the transient current magnitudes are lightly lower. Actually when the studied fault resistance is much larger than the line impedance, the impact of different fault locations is insignificant. In the rest of this chapter, only faults at line sending ends are studied.

7.4.3 Signal Variations with respect to δ, R_f and Grounding

An important feature of the proposed scheme is that the strength of the transient current signals is adjustable by changing the thyristor firing angle δ, so that the faulted line can be identified at different R_f values. Therefore, how the transient current signals vary with respect to R_f and δ need to be studied. Sensitivity studies were performed in the system in Section 7.4.2. Figure 7.12 plots the transient signals in the ungrounded system as δ remains 150° and R_f increases; Figure 7.13 shows the signals in the ungrounded system with a fixed R_f and increasing δ values. The signals in Figure 7.13 were aligned at the thyristor firing instants. All the results shown in Figure 7.12 and Figure 7.13 were checked with (7.4)-(7.10), and good agreements were found during the first thyristor conduction. The following observations were made:

- In Figure 7.12, as R_f increases, the positive pulse of $i_{faulted}$ becomes lower since the fundamental component in $i_{faulted}$ which is proportional to R_f^{-1}/Y_Σ reduces. The oscillatory components become more important due to the weakened damping represented by a smaller time constant τ . Therefore, a high R_f diminishes the difference between $i_{faulted}$ and $i_{unfaulted}$ and increases the difficulty of identifying the faulted line. The second thyristor conductions occur when R_f =500 and 2000 ohm. The reason is that as R_f increases, strong oscillations exist in the thyristor current and make it go to zero early when $-v_{NG}(t)$ is still negative and high. Since the thyristor firing pulse exists until $-v_{NG}(t)$ crosses zero, the thyristor conducts again. The second conduction increases the difference between $i_{faulted}$ and $i_{unfaulted}$, and helps the identification.

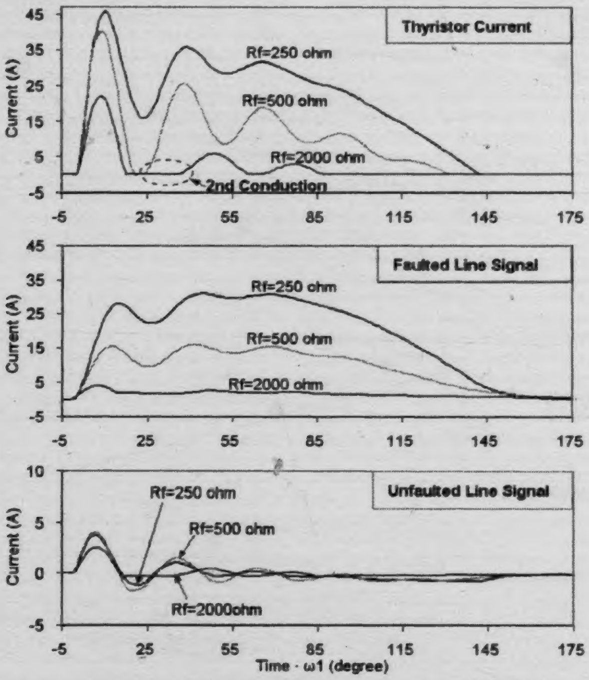

Figure 7.12 Responses of the ungrounded system with R_f=1000ohm and δ varies.

- In Figure 7.13, as δ increases, the positive pulses of $i_{faulted}$ last longer, while the oscillating components of $i_{unfaulted}$ still die out in a short time. Therefore, a higher δ makes the difference between $i_{faulted}$ and $i_{unfaulted}$ more apparent, and helps to identify the faulted line. The strongest oscillations occur around δ=90°, when the thyristor is fired at its voltage peak.

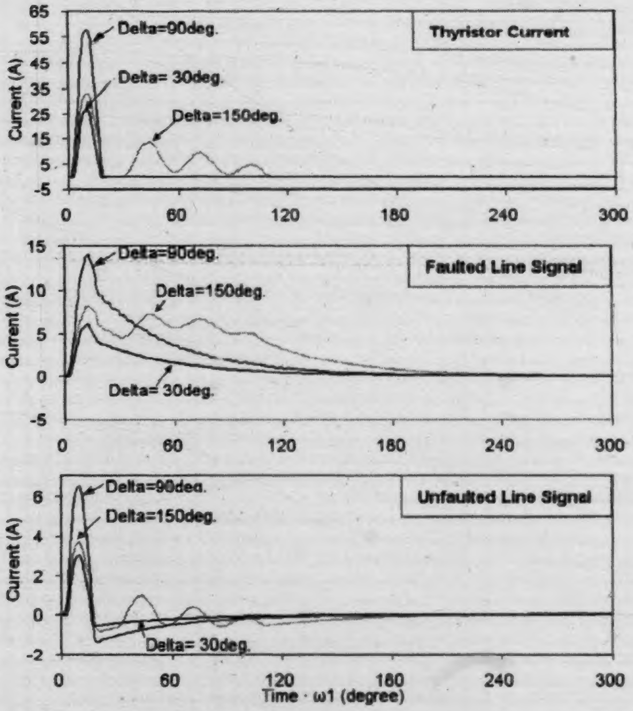

Figure 7.13 Responses of the ungrounded system with R_f=1000ohm and δ varies.

Simulations were also performed for other types of grounding schemes. The results with the high-resistance grounded system are close to those with the ungrounded system, except that when the system is high-resistance grounded, the faulted line transient current pulses have lower magnitudes. Figure 7.14 displays the transient current signals when the system is resonant grounded. Since the grounding inductor tends to maintain the current flowing through it, it affects the transient signals in two ways. Firstly, it makes the thyristor conduct longer than it does in an ungrounded system, especially when R_f is high. Secondly, due to the current still flowing through the inductor after the thyristor turns off, the $i_{faulted}$ waveforms are no longer positive pulses. They turn negative after the thyristor extinction and then die out. However, the $i_{faulted}$ waveforms in Figure 7.14 can still be distinguished from those of $i_{unfaulted}$ according to the bigger magnitudes of $i_{faulted}$.

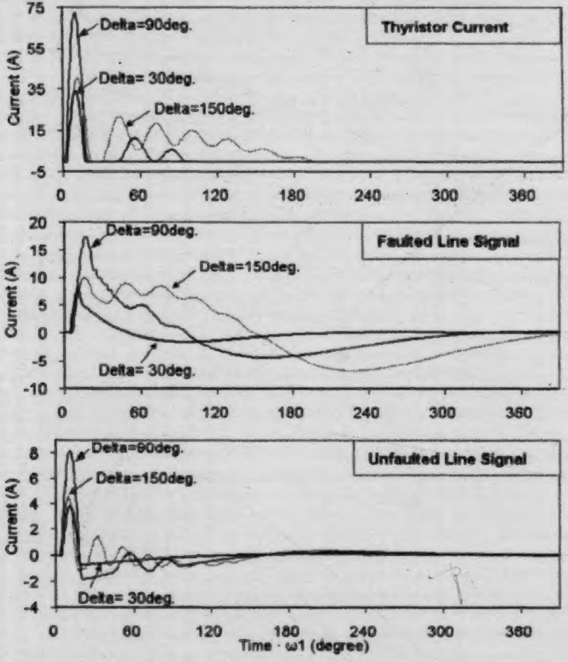

Figure 7.14 Responses of the resonant grounded system with R_f=1000ohm.

7.5 Criterion for Identifying the Faulted Line

Based on the features of transient current signals, this section establishes a criterion for identifying the faulted line.

7.5.1 Construction of the Detection Criterion

After the transient current signals are extracted using the method in Figure 7.7, Discrete Fourier Transform (DFT) is performed for the transient signals to further investigate the differences between $i_{faulted}$ and $i_{unfaulted}$. A DFT window of 2 fundamental cycles is used unless otherwise specified. The spectra of the transient signals in Figure 7.12 and Figure 7.14 are plotted in Figure 7.15(a) and (b), respectively. Since these signals are non-periodical, their spectra spread out in a wide frequency range. Figure 7.15 reveals that

- For the ungrounded system, the energy of $i_{faulted}$ concentrates in the DC to 2nd harmonics. The energy of $i_{unfaulted}$ is very low compared to $i_{faulted}$.
- For the resonant grounded system, the energy of $i_{faulted}$ signals concentrate around the 1st harmonic. The energy of $i_{unfaulted}$ is low compared to

$i_{faulted}$.

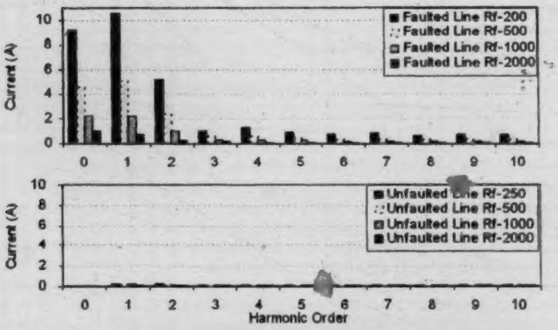

(a) $\delta = 150°$ and R_f varies (DFT Window of 1 cycle);

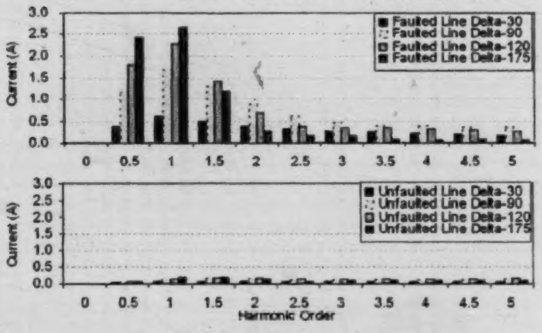

(b) R_f =1000 ohm and δ varies;

Figure 7.15 The spectra of the transient current signals.

Therefore, for both the underground and resonant grounded system, the most distinct differences between $i_{faulted}$ and $i_{unfaulted}$ exist in the low order (DC~2nd) harmonics. A general criterion is proposed for noneffectively grounded systems

$$I_{criterion} = \sqrt{I_{DC}^2 + I_{h0.5}^2 + I_{h1}^2} \tag{7.16}$$

where I_{DC}, $I_{h0.5}$ and I_{h1} are the DC, 0.5th interharmonic and fundamental components in the transient current signal on each line. The faulted line is identified as the one corresponding to the highest $I_{criterion}$ among all the distribution lines.

The criterion (7.16) is supported by frequency-domain theoretical analysis of the circuit in Figure 7.9(c). For ungrounded systems, the thyristor current, which is a positive pulse, flows through two components R_f and C_Σ. Since C_Σ is a high-pass filter, the DC component of $i_{thyristor}$ flows only through R_f. Therefore, $i_{faulted}$ contains a high DC component, which can be used to differentiate the faulted and an unfaulted line. In high-resistance grounded systems, the DC thyristor current flows through the faulted line and the grounding resistor. Similarly, the criterion (7.16) should also work. In resonance grounded systems, due to the existence of the arc-suppression inductor, which is a low-pass filter, the DC component in the thyristor current no longer flows through R_f. However, as long as the studied $R_f << X_C$, the fundamental current flows through R_f is much larger than that flows through $3C_0$. This fundamental component can be utilized to differentiate $i_{faulted}$ and $i_{unfaulted}$. Therefore, the criterion in (7.16) is suitable for all three types of noneffectively grounded systems.

7.5.2 Sensitivity Study of the Current Criterion

Sensitivity studies were performed to test the effectiveness of the identification criterion (7.16) using the simulation system in Section 7.4.2. Figure 7.16(a) studies the impact of the firing angle on the magnitudes of $I_{criterion}$. In the ungrounded system, when R_f = 250 and 500 ohm, the faulted line $I_{criterion}$ increases as the firing angle δ rises from 0° to 175°, while the unfaulted line $I_{criterion}$ is almost zero. However, when the fault resistance is as high as 2000 ohm, the highest faulted line $I_{criterion}$ is achieved at $\delta = 90°$ instead of at $\delta = 175°$. The reason is when R_f gets high and becomes comparable to $X_{C\Sigma}$ (=1612 ohm), the σ-component in $i_{faulted}$ starts to play a more important role than the ω_1-component. When $\delta = 90°$, the σ-component in $i_{faulted}$ is the strongest and therefore produces the highest faulted line criterion.

According to Figure 7.16(a), in the resonant grounded system the faulted line $I_{criterion}$ follows similar increasing tendency as the firing angle goes higher. The faulted line $I_{criterion}$ in the resonant grounded system is slightly higher than that in the ungrounded system with the same R_f since the resonant grounded system has higher neutral voltage V_{NG} than the ungrounded system does when $R_f \geq 250$ ohm. When R_f=2000 ohm, the thyristor conducts for multiple cycles with a firing angle above 150°. This long thyristor conduction may degrade the signal extraction process in Figure 7.7. To avoid this situation, the thyristor firing angle can be limited to below 90° for resonant grounded systems.

Figure 7.16(b) investigates the impact of an increasing fault resistance in the ungrounded, high-resistance grounded and resonant grounded system with δ =90°. In all these three systems, the faulted line $I_{criterion}$ drops as R_f increases. The unfaulted line $I_{criterion}$ remains almost zero in the ungrounded and high-resistance grounded system. In these two systems, the faulted line can be accurately identified until the faulted line $I_{criterion}$ drops below a minimum discriminable level. Since this level is determined by the current acquisition and calculation precision, theoretically the highest fault resistance that can be identified is also limited by the current precision. In the resonant grounded system, the unfaulted line $I_{criterion}$ slightly rises as R_f increases. The faulted line can be correctly identified until the fault resistance increases to a level close to that of the line shunt impedance X_C.

Figure 7.16(c) shows the influence of distribution line number on the current criterion. A firing angle of 90° is used in the study. For the ungrounded system, the faulted line $I_{criterion}$ maintains a relatively constant level. For the resonant grounded system, the grounding inductance reduces as the line number increases, and its current sustaining effect becomes stronger. Therefore the faulted line $I_{criterion}$ slightly rises as the line number increases. To summarize, increase in the line number will not deteriorate the performance of the identification criterion.

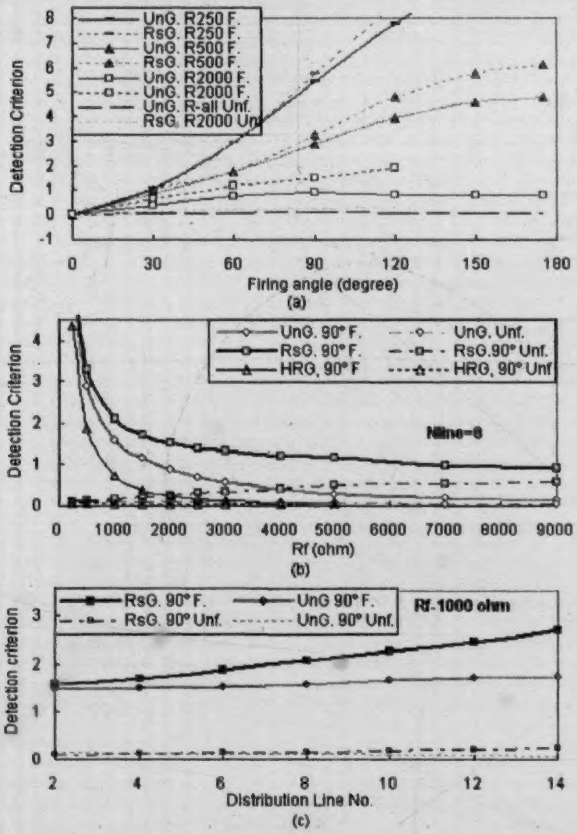

Figure 7.16 Sensitivity study with respect to δ, R_f and line number.

7.6 Lab Test Results

Laboratory tests were performed to verify the effectiveness of the proposed scheme. The test system was designed by scaling down the voltage level of a distribution system from 10kV to 220V and maintaining the impedance values. The system was supplied by a 380/220V Y_g/Y connected transformer and was ungrounded at the secondary side. Two 3-phase distribution lines were connected, both of 20km, π modeled, with R_1=R_0=12ohm, L_1=L_0=0.025H, and C_1=C_0=0.2uF. The load fed by each line was Y connected, with each phase composed of a R_{load}=77ohm in series with L_{load}=0.15H. A Controllable Grounding Device was installed between the neutral and the ground, with the signal transformer modeled by an impedance of 34+j70 ohm. A single-phase-to-ground fault occurred at the end of one line.

The transient current signals created in the tests coincided with the analysis in (7.4)-(7.10). Figure 7.17 and Figure 7.18 present some example signals and their spectra, respectively, when $R_f = 1000$ ohm and $\delta = 35°$, 91° and 146° respectively. The tests verified the positive impact of increasing the firing angle to the identification. $I_{criterion}$ vs. firing angle curves similar to those in Figure 7.16(a) were obtained.

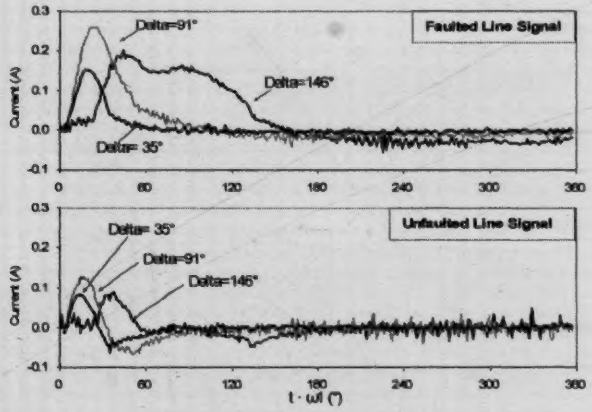

Figure 7.17 The transient current signals for the lab test system.

(Current values in the 220V system are plotted.)

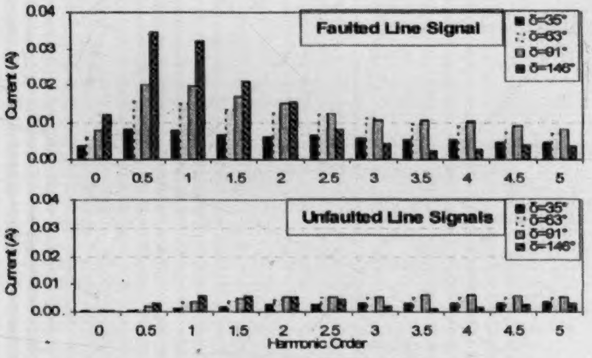

Figure 7.18 The spectra of transient current signals in the lab test.
(Current values in the 220V system are plotted.)

7.7 Design of the Controllable Grounding Device

There are two key steps to design the Controllable Grounding Device. The first step is to size the signal transformer, and the second step is to set the thyristor current and voltage ratings. The following two aspects are considered in sizing the signal transformer. A large signal transformer can generate strong transient current signals for identifying the faulted line; however, it also causes large voltage disturbances to the load and implies high costs. In the following, the transformer is sized according to the constraint on voltage disturbance. It may be further adjusted according to costs.

The disturbance to the faulted phase-to-neutral voltage is calculated by adding up voltage drops on the positive-, negative- and zero-sequence system inductances L_{s1}, L_{s2} and L_{s0} in the circuit in Figure 7.9(b). When $R_f = 0$ and the fault is at the sending-end, the maximum voltage disturbance occurs and equals (see Figure 7.19)

$$\begin{aligned} dv_{AN\max}(t) &= \frac{-e_{virtual}(L_{s1}+L_{s1}+L_{s0})}{L_{s1}+L_{s1}+L_{s0}+3L_{SG}}, \\ &= \frac{X_{self}}{X_{self}+X_{SG}}\sqrt{2}E_{AN}\sin(\omega_1 t-\delta) \end{aligned} \tag{7.17}$$

where X_{self} is the self-impedance of the distribution system.

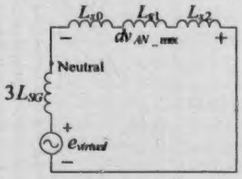

Figure 7.19 The circuit for calculating the voltage disturbance.

As the firing angle is adjusted, a peak voltage disturbance equaling $\sqrt{2}E_{AN}dv_{peak\%}$ is created, where

$$dv_{peak\%} = \frac{X_{self}}{X_{SG} + X_{self}} \times 100\% = \frac{1}{1 + x_{SG}S_{PG} / S_{SG}}. \tag{7.18}$$

S_{PG} is the single-phase-to-ground fault level of the supply system, and S_{SG} is the capacity of the single-phase signaling transformer.

An acceptable $dv_{peak\%}$ ranges from 5% to 10%. The signal transformer can be sized according to this constraint. For example, for the simulation system in Section 7.4.2, given x_{SG}=3.5%, $S_{PG} = 66.7$ MVA. Assume $dv_{max\%}$=6%, the calculated S_{SG}=150kVA. The expense of such a transformer is acceptable. Therefore 150kVA is chosen as the final size.

Simulations are performed to see as the firing angle is adjusted within 0° ~180°, whether strong enough current signals can be generated at the same time that the created voltage disturbance is in an acceptable range. Figure 7.20 plots the faulted line $I_{criterion}$ vs. the peak voltage disturbance, as the firing angle increases from 0° to 30°, 60°, 90°, 120°, 150° and 175°. Six curves with 3 different R_f values were plotted for the ungrounded system and the resonant grounded system respectively. Assume the smallest identifiable current criterion at 10kV level is 1A. When the curve is in a region with the current criterion above 1A and the voltage disturbance below 5%, which is denoted as *Operable Region*, both requirements on signal strength and voltage disturbance are satisfied. Figure 7.20 shows a wide operable region.

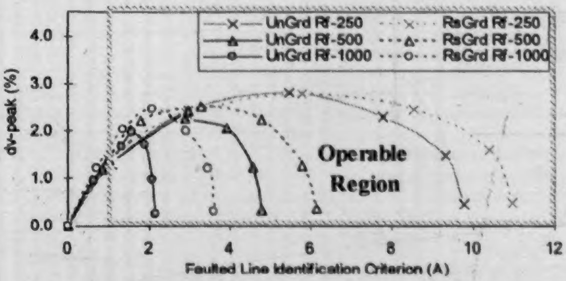

Figure 7.20 The current criterion vs. the voltage disturbances.

The thyristor current ratings are set based on the most serious case of $R_f = 0$ and the fault at the line sending-end. According to Figure 7.19, the thyristor current waveform is

$$i_{thyristor}(t) = \frac{\sqrt{2}E_{AN}}{X_{self} + X_{SG}}[\cos(\omega t - \delta) - \cos\delta]. \tag{7.19}$$

The RMS value of thyristor current is

$$i_{RMS.\delta} = \frac{1}{E_{AN}(S_{PG}^{-1} + x_{SG}S_{SG}^{-1})}\sqrt{\frac{\delta(2 + \cos 2\delta) - 1.5\sin 2\delta}{\pi M}} \tag{7.20}$$

M represents the interval between two firing events in the unit of number of cycles. For the studied case, a firing angle of $\delta = \pi/2$ would be far enough for the identification. The thyristor current RMS rating is set according to $\delta = \pi/2$. For the simulation system in Section 7.4.2, the calculated thyristor RMS current rating is 247A.

7.8 Conclusion

This chapter proposes a novel concept and associated scheme for identifying the faulted line in ungrounded, high-resistance grounded and resonant grounded distribution systems. The proposed scheme turns the original system into a temporarily effectively grounded system through a controlled short-circuit. A strong transient current pulse flows through the faulted line and is used for identification. A thyristor-based device is used to create the temporary short-circuit. The firing angle of the device can be adjusted so that strong enough signals can be generated for identification when the fault resistance varying in a wide range. The device is also sized so that the created voltage disturbance is negligible to the load.

Characteristics of the transient current signal flowing through the faulted line were studied in comparison with those of a signal flowing through an unfaulted line. A criterion was then developed for identifying the faulted line. The key system parameters influencing the identification were examined, including the fault resistance, and the number of feeders. Simulations and experimental tests verified the effectiveness of the criterion. The proposed scheme is shown to be a promising solution to the problem of faulted-line identification in noneffectively grounded distribution systems.

Chapter 8. CONCLUSIONS AND RECOMMENDATIONS

In recent years, power electronics circuits have been sporadically applied to power systems to create small yet discernible signals online for communication, monitoring, fault diagnosis, and other signal-oriented applications. As well, power systems are faced with many challenges which are suitable for solutions requiring injection of special disturbances into the power systems. This research work was conducted to deal with the above challenges, aiming at applying the power-electronics-based signaling technique to design effective and economical solutions to several challenging problems in power systems.

The islanding detection of synchronous DGs is a significant technical barrier in the fast-growing DG industry. This thesis has presented a new and powerful islanding detection concept and associated scheme for DG applications. With this concept, a signal is sent through the power line from a substation to the DG sites. A DG is considered as "islanded" if the signal cannot be detected at the DG site. The scheme is applicable to any distribution systems regardless of the availability of telecommunication methods. More importantly, since the signal passes through any switches, breakers and other openable components connected between the substation and DG sites, the scheme is able to 'detect' automatically the opening of any components. In addition, the scheme is also economically attractive for DG owners and utilities, especially for those systems with multiple DG installations. This thesis investigated one implementation of the signal generator by using thyristors-controlled short circuits. The design considerations of the signal generator were presented. The thesis also investigated the characteristics of the signals. The key factors that can affect the signal strength, attenuation and frequency were identified. Based on the signal characteristics, three signal detection algorithms were proposed. Field tests were carried out to verify the effectiveness of the proposed islanding detection scheme. The main findings were:

- The proposed scheme performed successfully during the field test. The four false islanding events encountered during the test can be eliminated by using the improved signal detection algorithms.
- The improved algorithms, either spectrum-based or template-based, are more reliable than the previous algorithm for signal detection. They are recommended for uses in the signal detector of the proposed scheme. The

degree of implementation (programming) difficulties will decide which one of them will be eventually selected.

- Investigation of the interference between the AMR and the islanding detection scheme showed that the AMR system is unlikely to cause problems to the anti-islanding scheme. Although field experience found that the anti-islanding scheme did not interfere with the AMR system, more field tests are needed to clarify this issue.
- The field test experience suggests that a signal level of 4% is probably the best compromise between reliable signal detection and the cost of the signal generator. Power quality is not a concern at this signal level.

The thesis further studied an improved version of the above power-line-signaling-based islanding detection scheme: the scalable scheme. The new scheme is designed to increase the implementation flexibility for various DG interconnection scenarios. In the scalable scheme, the signal generator can be located at any place between the substation and the DG sites. Installation of the signal generator no longer requires access to the substation, so that installation is convenient for the distribution utility. In a typical arrangement, the signal generator can be installed at the upstream of an area with DG installations. In this way, the costs of the signal generator can be reduced and shared among the DG owners. A problem arises with the scalable scheme, for the signal generator must be able to detect its connection status to the main supply. This procedure is done by examining the transient current signal created during the signaling process at the upstream of the signal generator. A high DC level in this transient signal implies the signal generator is connected to the main supply, while a low DC current indicates the signal generator is isolated from the main supply. Experimental tests showed that the DC criterion can work reliably in various system conditions.

In future research about power-line-signaling-based islanding detection, a signaling technique that can take advantage of the simple requirement for islanding detection signals to reduce the cost of signal generator should be developed. For the proposed implementation using the zero-crossing-distortion technique, the interference between the islanding detection scheme and a TWACS AMR system (if one exists) needs to be further investigated. A possible solution to the interference is to incorporate the function of islanding detection into AMR systems. This solution requires cooperation from the AMR systems.

Online power system harmonic impedance data are desirable in many applications. However, inexpensive devices are lacking for measuring harmonic impedance online at constant time intervals with negligible impacts on power quality. This thesis proposed an effective new method for measuring supply system harmonic impedances, and this method can be easily implemented in a low-cost and portable device. The method utilizes a thyristor to create a controlled short-circuit at the driving point. Transient current and voltage signals are generated and used for harmonic impedance measurement. The strength of the transient signals is adjusted through the thyristor firing angle so that accurate measurements are supported, and the disturbances to the load operation are negligible. The proposed method uses multiple transient signals created with different firing angles for measurements, so that enough current energy and thus good precision can be achieved over a wide spectrum. Also, the method uses combinations of multiple channels to generate signals for measuring multi-phase systems. A criterion was established for predicting the range of reliable measurements. Simulations and lab tests verified the effectiveness of the proposed method. The proposed device can be applied to DG islanding detection by monitoring the system impedances at the DG terminals.

Identifying the line experiencing a single-phase-to-ground fault is another challenge faced by ungrounded, high-resistance grounded or resonant grounded systems. This thesis proposed a thyristor-based scheme to solve this difficulty. The scheme temporarily turns the faulted system into an effectively grounded system through a controlled grounding of the system neutral. A strong current pulse flows through the faulted line and can be used for identification. The current pulse is controlled through the thyristor firing angle so that enough strength is achieved for the identification, while the disturbance to the load operation is negligible. The current pulse flowing through the faulted line was studied in comparison with those current signals flowing through unfaulted lines. As the faulted line current pulse contains abundant low-frequency components, these components were used to compose a criterion for identifying the faulted line. The system parameters influencing the performance of the criterion were examined, including the fault resistance, the total shunt capacitance of all the feeders, or the number of feeders. Simulations and experimental tests verified the effectiveness of the proposed scheme.

BIBLIOGRAPHY

[1] Muhammad H. Rashid, *Power Electronics Handbook: Devices, Circuits and Applications*. Burlington: Academic Press, 2007, Chapter 26-33.

[2] Jeffrey D. Merwin, John G. Konopka, "Power-line communication system using pulse transmission on the AC line", U.S. Patent 5691691, Nov. 25, 1997.

[3] Reed H. Johnston, Dennis C. Jeffreys, Lawrence J. Stratton, "Method and apparatus for transmitting interlligence over a carrier wave", US Patent No. 4106007, Aug. 1978.

[4] Sioe T. Mak, Thomas G. Moore, "TWACS, A New Viable Two-Way Automatic Communication System for Distribution Networks. Part II: Inbound Communication", *IEEE Transactions on Power Apparatus and Systems*, v103, n8, pp.2141-2147, Aug. 1984

[5] Sioe T. Mak, "A new method of generating TWACS type outbound signals for communication on power distribution networks", *IEEE Trans. Power Apparatus and Systems*, v103, no. 8, pp.2134-40, Aug. 1984.

[6] Sioe T. Mak, Richard L. Maginnis, "Power frequency communication on long feeders and high levels of harmonic distortion", *IEEE Trans. Power Delivery*, v10, n4, pp.1731-1736, Oct. 1995.

[7] Peter M. Foord, "Bi-directional muti-frequency ripple control system", US Patent No. 4868539, Sep. 1989.

[8] Paul C. Hunt, "Low frequency bilateral communication over distribution power lines", US Patent No. 6154488, Nov. 2000

[9] Sumner, M., Palethorpe, B., Thomas, D. W. P.: 'Impedance measurement for improved power quality-Part 1: the measurement technique', IEEE Trans. Power Delivery, 2004, 19, (3), pp.1442-1448

[10] Photovoltaic Semiconductor Converters Part 1: Utility Interactive Fail Safe Protective Interface for PV-Line Commutated Converters—Design Qualification and Type Approval, European Standard EN 50330-1, 1999.

[11] Lucian Asiminoaei, Remus Teodorescu, Frede Blaabjerg, and Uffe Borup, "Implementation and Test of an Online Embedded Grid Impedance Estimation

Technique for PV Inverters", *IEEE Trans. Industrial Electronics*, v52, n4, pp. 1136-1144, Aug. 2005

[12] Guillermo Hernández-González, Reza Iravani, "Current injection for active islanding detection of electronically-interfaced distributed resources", *IEEE. Trans. Power Delivery,* v21, n3, pp.1698-1705, Jul. 2006

[13] H. Karimi, A. Yazdani, R. Iravani, "Negative-Sequence Current Injection for Fast Islanding Detection of a Distributed Resource Unit", *IEEE Trans. on Power Electronics*, v23, n1, pp.298 - 307, Jan. 2008

[14] Cooper, C. B., "Standby generation –problems and prospective gains from parallel running", Power System Protection '89, Singapore, 1989.

[15] S. Lee and T. Habetler, "An online stator winding resistance estimation for temperature monitoring of line-connected induction machines", *IEEE Trans. Ind. Appl*, v39, pp. 685-694, May/Jun, 2003.

[16] Zhang, Pinjia; Lu, Bin; Habetler, Thomas G.; "A Nonintrusive Induction Motor Stator Resistance Estimation Method using a Soft-Starter", Proceeding of *IEEE International Symposium on Diagnostics for Electric Machines, Power Electronics and Drives, 2007. SDEMPED*, pp.197 - 202, Sep. 2007

[17] Herimilo Guzman, "Ground fault detector and locator", US Patent 4,884,034, Nov. 1989

[18] BBC BROWN BOVERI & CIE, "Method and Apparatus for detecting ground shorts in electrical systems", Worldwide Patent No. GB1601235, Oct. 1981

[19] C. J. Mozina, "Advances in generator field ground protection using digital technology" Proceedings of IEEE Industrial and Commerical Power Systems Technical Conference, May 2002, pp.126 – 130

[20] Kato, Y.; Watanabe, A.; Konishi, H.; Kawai, T.; Inoue, Y.; Irokawa, H.; "Neutral Line Protection System for HVDC Transmission" Power Delivery, IEEE Transactions on, v1, n3, Jul. 1986, pp. 326-331

[21] Standard for interconnecting distributed resources with electric power systems, IEEE Std. 1547-2003, 2003.

[22] ANSI/IEEE, IEEE Guide for Interfacing Dispersed Storage and Generation Facilities with Electric Utility Systems, IEEE/ANSI Std., 1988.

[23] Electricity Association, G59/1 Recommendations for the Connection of Embedded Generating Plant to the Regional Electricity Companies Distribution Systems, Electricity Association Std., 1991.

[24] W. Bower and M. Ropp. (2002). Evaluation Of Islanding Detection Methods For Photovoltaic Utility. *International Energy Agency, Report IEA PVPS T5-09.* [online]. Available: http://www.oja-services.nl/iea-pvps /products/download/rep5_09.pdf

[25] W. Xu, K. Mauch, and S. Martel. (August 2004). An Assessment of the Islanding Detection Methods and Distributed Generation Islanding Issues for Canada, A report for CANMET Energy Technology Centre - Varennes, Nature Resources Canada, 65 pages. [Online]. Available: http://cetc-varennes.nrcan.gc.ca/fichier.php /39002/2004-074_e.pdf.

[26] N. Jenkins, R. Allan, P. Crossley, D. Kirschen, and G. Strbac, Embedded Generation, 1st ed. Institute of Electrical Engineers, 2000.

[27] M. Guillot, C. Collombet, P. Bertrand, B. Gotzig. "Protection of Embedded Generetation connected to a Distribution network and loss of mains detection", Schneider Electric, France, CIRED 2001, 18-21 June 2001, Conference Publication No.482 IEE 2001, pp 82 -85.

[28] G. Heggie, H Yip, " A Multi-function relay for loss of mains protection", IEE Colloquium on System Implications of Embedded Generation and its protection and control No. 1998 / 277, Feb 1998, p.5/1-4.

[29] Cooper Power Systems Product Manual, "UM30SV Vector Jump/Islanding Relay", Electric Apparatus Literature150-23, 1999.

[30] W. Freitas and W. Xu, "False Operation of Vector Surge Relays" IEEE Trans. on Power Delivery,Volume: 19 , Issue: 1 , Jan. 2004, Pages:436 - 438.

[31] W. Freitas, Z. Huang, W. Xu, "A practical method for assessing the effectiveness of vector surge relays for distributed generation applications", *IEEE Trans. Power Delivery*, v 20, n 1, pp. 57-63, Jan. 2005.

[32] M. A. Redfern , J. I. Barret , O. Usta. "A new microprocessor based islanding protection algorithm for dispersed storage and generation units", IEEE Transactions on Power Delivery, v10, n3, July 1995. pp 1249 – 1254.

[33] S. K. Salman, D. J. King and G. Weller. "New Loss of Mains detection algorithm for Embedded generation using Rate of change of voltage and Changes in power factors", Developments in Power Systems Protection, Conference Publication N 479 IEE 2001.

[34] F. Pai, S. Huang, " A detection algorithm for Islanding-Prevention of Dispersed Consumer owned storage and generating units", IEEE Transactions on Energy Conversion, v16, n4, pp 346 - 351, December 2001.

[35] M. E. Ropp, M. Begovic, A. Rohatgi, “Prevention of islanding in grid-connected photovoltaic systems”, in *Progress in Photovoltaics: Research and Applications*, v7, n1, pp. 39-59, 1999.

[36] P. O. Kane, B. Fox, “Loss of mains detection for embedded generation by system impedance monitoring”, *Development in Power System Protection, IEEE Conference Publication*, n434, pp. 95-98, Mar. 1997.

[37] J. E. Kim and J. S. Hwang “Islanding detection method of distributed generation units connected to Power Distribution System”, Proceedings of IEEE PowerCon 2000 International Conference, v2 , 4-7 Dec. 2000, Pages:643 - 647

[38] J. Motohashi, Y. Imai, T. Ishikawa, T. Kai, H. Kaneda, T. Fujimoto, T. Ishizuka. “Development of Detecting System of islanding operation for dispersed Synchronous Machine Generator Interconnected to Distribution line”, pp 1019 - 1022, Meiden Review Magazine, Series 110, 2000, n1

[39] M. A. Referrn, O. Usta, G. Fielding. “Protection Against lost of Utility Grid Supply for a Dispersed Storage and Generation Unit”, IEEE Transactions on Power Delivery , v 8, n 3, July 1993. pp 948 - 954.

[40] Charles J. Mozina. “Interconnection Protection of IPP Generators at Commercial / Industrial Facilities”, IEEE Transactions on Industry Applications, v 37, n 3, May / June 2001. pp 681 -689.

[41] R. M. Rifaat. “Critical considerations for Utility/Cogeneration Inter-Tie protection scheme configuration”, *IEEE Transactions on Industry Applications*, v 31, n5, September/October 1995. pp 973 – 977.

[42] R. Benato, R. Caldon, “Distribution line carrier: analysis procedure and applications to DG”, *IEEE Transactions on Power Delivery*, v22, n1, pp. 575-83, Jan. 2007

[43] R. Benato, R. Caldon, F. Cesena, “Application of distribution line carrier-based protection to prevent DG islanding: an investigating procedure”, *IEEE Bologna PowerTech*, 2003, pt. 3, p7, v3

[44] M. Ropp, K. Aaker, J. Haigh, N. Sabbah, "Using power line carrier communications to prevent islanding [of PV power systems]", Photovoltaic Specialists Conference, 2000. Conference Record of the 28th IEEE, pp. 1675-1678, Sep. 2000

[45] M. Ropp, D. Larson, S. Meendering, D. Mcmahon, J. Ginn, J. Stevens, W. Bower, S. Gonzalez, K. Fennell, L. Brusseau, “Discussion of a Power Line Carrier Communications-Based Anti-Islanding Scheme using a Commercial

Automatic Meter Reading System", IEEE 4th World Conference on Photovoltaic Energy Conversion, May 2006, v2, pp. 2351 – 2354.

[46] Robert, A., Deflandre, T., et al: 'Guide for assessing the network harmonic impedance', Proc. 14th Int. Conf. Electricity Distribution, Brussels, Belgium, June 1997, Part 1. Contributions, 1, pp. 3/1- 310.

[47] Oliveira, A., Oliveira, J. C., Resende, J. W., Miskulin, M.S.: 'Practical approaches for AC system harmonic impedance measurements', IEEE Trans. Power Delivery, 1991, 6, (4), pp. 1721-1726.

[48] Morched, A. S., Kundur, P.: 'Identification and modelling of load characteristics at high frequencies', IEEE Trans. Power Systems, 1987, 2, (1), pp. 153-160.

[49] Girgis, A. A., McManis, R. B: 'Frequency domain techniques for modeling distribution or transmission networks using capacitor switching induced transients', IEEE Trans. Power Delivery, 1989, 4, (3), pp.1882-1890.

[50] Xie, C.; Tennakoon, S.B.; Langella, R.; Gallo, D.; Testa, A.; Wixon, A., "Harmonic impedance measurement of 25 kV single phase AC supply systems", Proceedings of 9th International Conference on Harmonics and Quality of Power, vol.1, pp. 214 – 219, Oct. 2000

[51] Jason P. Rhode, Arthur W. Kelley, Mesut E. Baran, " Complete Characterization of Utilization-Voltage Power System Impedance Using Wideband Measurement", IEEE Trans. Industry Applications, vol. 33, no. 6, pp. 1472-1479, 1997

[52] "Introduction to Power Line Communications", [Online]. Available: http://plugtek.com/powerline-communication-intro.shtml

[53] Sumner, M., Abusorrah, A., Thomas D. and Zanchetta P.: 'Improved power quality control and intelligent protection for grid connected power electronic converters, using real time parameter estimation', Proc. IEEE/IAS Annual Meeting, Florida, USA, October 2006, 4, pp. 1709-1715.

[54] Bendel, C., Nestle, D., Viotto, M.: 'Safety aspects of decentralized net-coupled electrical generators', [Online]. Available: http://www.iset.uni-kassel.de/abt/FB-A/publication/2004/Safety%20Aspects%20of%20Net-Coupled%20DER%20Bendel%20Nestle%20Viotto%20Press.pdf, accessed October 2006.

[55] Ngpal, M., Xu, W., Sawada, J.: 'Harmonic Impedance measurement using three phase transients', IEEE Trans. Power Delivery, 1998, 13, (1), pp. 272-277.

[56] IEEE Guide for the Application of Neutral Grounding in Electrical Utility Systems, Part IV -Distribution, IEEE Std. C62.92.4-1991, 1992.

[57] Y. Hao, Y. Yang, Y. Ren, L. Qi, W. An, "Faulted line identification through magnitude and phase angle comparison", Information on electric power (Chinese), n2, pp. 15-19, 1994.

[58] T. Baldwin, F. Renovich, Jr., L. F. Saunders, D. Lubkeman, "Fault locating in ungrounded and high-resistance grounded systems", *IEEE Trans. on Industry Applications*, v37, n4, pp. 1152-59, Jul. 2001.

[59] Guobiao Tan, Dongming Tu, and Dapeng Chen, "Microcomputerized Faulty Line Discriminator Based on Theory of Maximizing $I\sin\varphi$ or $\Delta(I\sin\varphi)$", *Electric Power* (Chinese), no. 7, 1995, pp.16-20.

[60] Zhangliang Zhang, "Mechanism analysis for single-phase-to-ground faults in noneffectively grounded systems", *Guangdong Electric Power* (Chinese), v11, n3, Jun. 1998, pp. 20-22.

[61] J. Yuan, T. Zhang, "Theory and application of capacitive current automatic tracing compensation and grounded line selection", *Electric Power* (Chinese), v31, n1, 1998, pp. 67-68.

[62] L. Mu, Q. Meng, "Ground-fault protection based on active component of zero-sequence current in resistance neutral grounded distribution systems", Proceedings of IEEE TENCON'02, v3, pp. 1897-1900, Oct. 2002.

[63] Geise F. Erdschluβ and Erdschluβ Relais. Siemens Zeitschrift, 1952(26) (Germany)

[64] Y. Xue, Z. Feng, B. Xu, Y. Chen, J. Li, "Ground fault protection in non-solidly grounded networks based on transient zero sequence current comparison" Automation of Electric Power Systems (Chinese), v27, n9, pp. 48-53, 2003.

[65] P. Mao, Y. Sun, Z. Zhang, H. Du, "Wavelets packet based detection of phase-to-ground fault in distribution automation system", *Power System Technology*, v24, n6, Jun. 2000 (Chinese)

[66] Youzhong Miao, Yaming Sun, Hua Yang, "A new principle of single-phase ground fault protection for feeders in ungrounded distribution systems", Proceedings of the Chinese Society of Electrical Engineering, v24, n2, Feb 2004 (Chinese)

[67] Daniel R. Seese, Alfred A. Regotti, "High resistance ground fault detector and locator for polyphase electrical systems" US Patent 4,151,460, Apr. 1979

[68] Hao Zhou, Junjie Zhang, Hai Yuan, Zhida Zhao, Xuemei Tao, "Research the detection of grounded lines in 10kV distribution system by parallel resistor", *Electro Technical Journal* (Chinese), n11, 2003, pp. 56-58

[69] Zaizhong Sang, Huifen Zhang, Zhengcui Pan, "Current injection based single-phase ground fault localization in noneffectively grounded systems", Power System Automation, v20, n2, 1996. (Chinese)

[70] T. Baldwin, F. Renovich, and L. F. Saunders, "Directional Ground-Fault Indicator for High-Resistance Grounded Systems", *IEEE Trans. Industrial Applications*, v39, n2, 2003, pp. 325-332.

[71] Wilsun Xu, Guibin Zhang, Chun Li, Wencong Wang, Jacek Kliber, "A Power Line Signaling Based Technique for Anti-islanding Protection of Distributed Generators: Part I: Scheme and Analysis", IEEE Transaction on Power Delivery, v22, n3, July 2007, Page(s):1758 – 1766

[72] Wencong Wang, Jacek Kliber, Guibin Zhang, Wilsun Xu, Blair Howell and Tony Palladino, "A Power Line Signaling Based Technique for Anti-islanding Protection of Distributed Generators: Part II: Field Test Results", IEEE Transactions on Power Delivery, v22, n3, July 2007, Page(s): 1767 – 1772.

[73] Wencong Wang, Jacek Kliber, Wilsun Xu, "A scalable power-line-signaling-based technique for islanding detection of distributed generators", *IEEE Transactions on Power Delivery* (accepted)

[74] Wencong Wang, Edwin E. Nino, and Wilsun Xu, "Harmonic Impedance Measurement Using A Thyristor-Controlled Short-Circuit", IET Generation, Transmission and Distribution, v1, n5, Sept. 2007, pp.707 - 713

[75] Wencong Wang, Ke Zhu, Peng Zhang and Wilsun Xu, "Identification of the Faulted Distribution Line Using Thyristor-Controlled-Grounding", IEEE Transactions on Power Delivery (accepted)

APPENDIX A. EQUATIONS ABOUT THE ANTI-ISLANDING SIGNAL

According to (3.9), the frequency-domain equation of an anti-islanding signal is

$$v_{signal}(s) = -v_{TAB}(s) K_{SD} \frac{1}{1+(s/\sigma)^2},$$

where $K_{SD} = \frac{L_u}{L_u + L_t} \cdot \frac{L_{DG}}{L_2 + L_1 + L_t // L_u}$; $-v_{AB}(s)$ is the Laplace transform of $-v_{AB}(t) = \sqrt{2} V_N [\sin(\omega t - \delta) u(t) - \sin(\omega t - \delta) u(t - \alpha/\omega)]$; α is the total thyristor conduction angle and $\alpha \approx 2\delta$; $\sigma = 1/\sqrt{L_{eq} C}$, $L_{eq} = L_2 // (L_1 + L_u // L_t)$.

The time-domain equation of an anti-islanding signal is derived below.

Step 1:

The Laplace transform of $\sin(\omega t - \delta) u(t)$ is as

$$L[\sin(\omega t - \delta) u(t)] = L[(\sin \omega t) u(t) \cos \delta - (\cos \omega t) u(t) \sin \delta]$$
$$= \cos\delta \frac{\omega}{s^2 + \omega^2} - \sin\delta \frac{s}{s^2 + \omega^2} = \frac{\omega \cos\delta - s \sin\delta}{s^2 + \omega^2}$$

Therefore,

$$L[\sin(\omega t - \delta) u(t - \alpha/\omega)]$$
$$= L[\sin[(\omega t - a) - \delta + a] u(t - \alpha/\omega)]$$
$$= e^{-s\alpha/\omega} F[\sin(\omega t' - \delta + a) u(t')] \qquad (t' = t - \alpha/\omega)$$
$$= e^{-s\alpha/\omega} \frac{\omega \cos(\delta - \alpha) - s \sin(\delta - \alpha)}{s^2 + \omega^2} = e^{-s\alpha/\omega} \frac{\omega \cos\beta + s \sin\beta}{s^2 + \omega^2} \qquad (\beta = \alpha - \delta)$$

Step 2: Assume

$$v_{signal}(s) / (\sqrt{2} V_N) = \frac{K_{SD}}{1 + s^2/\sigma^2} * L[\sin(\omega t - \delta) u(t) - \sin(\omega t - \delta) u(t - \alpha/\omega)]$$
$$= \frac{K_{SD}}{1 + s^2/\sigma^2} \frac{\omega \cos\delta - s \sin\delta}{s^2 + \omega^2} - e^{-s\alpha/\omega} \frac{K_{SD}}{1 + s^2/\sigma^2} \frac{\omega \cos\beta + s \sin\beta}{s^2 + \omega^2} = v_1(s) + v_2(s) e^{-s\alpha/\omega}$$
$$= \frac{k_1}{s + j\omega} + \frac{k_2}{s - j\omega} + \frac{k_3}{s + j\sigma} + \frac{k_4}{s - j\sigma} - e^{-s\alpha/\omega} \left[\frac{k_5}{s + j\omega} + \frac{k_6}{s - j\omega} + \frac{k_7}{s + j\sigma} + \frac{k_8}{s - j\sigma} \right]$$

$$k_1 = v_1(s)(s+j\omega)\big|_{s=-j\omega}$$

$$= \frac{K_{SD}}{1+s^2/\sigma^2}\frac{\omega\cos\delta - s\sin\delta}{s-j\omega}\bigg|_{s=-j\omega} = \frac{K_{SD}}{1-\omega^2/\sigma^2}\left[\frac{\cos\delta + j\sin\delta}{-2j}\right] = \frac{K_{SD}}{1-\omega^2/\sigma^2}\left[\frac{e^{j(\delta+\pi/2)}}{2}\right]$$

$$k_2 = V_{dg}(s)(s-j\omega)\big|_{s=j\omega}$$

$$= \frac{K_{SD}}{1+s^2/\sigma^2}\frac{\omega\cos\delta - s\sin\delta}{s+j\omega}\bigg|_{s=j\omega} = \frac{K_{SD}}{1-\omega^2/\sigma^2}\left[\frac{\cos\delta - j\sin\delta}{2j}\right] = \frac{K_{SD}}{1-\omega^2/\sigma^2}\left[\frac{e^{-j(\delta+\pi/2)}}{2}\right] = k_1^*$$

$$k_3 = V_{dg}(s)(s+j\sigma)\big|_{s=-j\sigma}$$

$$= \frac{K_{SD}\sigma^2}{s-j\sigma}\frac{\omega\cos\delta - s\sin\delta}{s^2+\omega^2}\bigg|_{s=-j\sigma} = \frac{K_{SD}\sigma}{-2j}\left[\frac{\omega\cos\delta + j\sigma\sin\delta}{-\sigma^2+\omega^2}\right] = \frac{K_{SD}\sigma}{2}\left[\frac{j\omega\cos\delta - \sigma\sin\delta}{-\sigma^2+\omega^2}\right]$$

$$k_4 = V_{dg}(s)(s-j\sigma)\big|_{s=j\sigma}$$

$$= \frac{K_{SD}\sigma^2}{s+j\sigma}\frac{\omega\cos\delta - s\sin\delta}{s^2+\omega^2}\bigg|_{s=j\sigma} = \frac{K_{SD}\sigma}{2}\left[\frac{-j\omega\cos\delta - \sigma\sin\delta}{-\sigma^2+\omega^2}\right] = k_3^*$$

$$k_5 = k_1\big|_{\delta\to-\beta} = \frac{K_{SD}}{1-\omega^2/\sigma^2}\frac{e^{j(-\beta+\pi/2)}}{2}, \quad k_6 = k_5^*$$

$$k_7 = k_3\big|_{\delta\to-\beta} = \frac{K_{SD}\sigma}{(-\sigma^2+\omega^2)}\left[\frac{j\omega\cos\beta + \sigma\sin\beta}{2}\right] ,$$

$$k_8 = \frac{K_{SD}\sigma}{-\sigma^2+\omega^2}\frac{-j\omega\cos\beta + \sigma\sin\beta}{2} = k_7^*.$$

Step 3:

$$v_1(t) = \left[k_1 e^{-j\omega t} + k_1^* e^{j\omega t} + k_3 e^{-j\sigma t} + k_3^* e^{j\sigma t}\right]u(t)$$

$$= \left[2\operatorname{Re}(k_1)\cos\omega t + 2\operatorname{Im}(k_1)\sin\omega t + 2\operatorname{Re}(k_3)\cos\sigma t + 2\operatorname{Im}(k_3)\sin\sigma t\right]u(t)$$

$$= \left\{\frac{K_{SD}}{1-\omega^2/\sigma^2}\left[-\sin\delta\cos\omega t + \cos\delta\sin\omega t\right] + \frac{K_{SD}\sigma}{\sigma^2-\omega^2}\left[\sigma\sin\delta\cos\sigma t - \omega\cos\delta\sin\sigma t\right]\right\}u(t)$$

$$= \left\{\frac{K_{SD}}{1-\omega^2/\sigma^2}\sin(\omega t-\delta) + \frac{K_{SD}}{1-\omega^2/\sigma^2}\sqrt{\sin^2\delta + \frac{\omega^2}{\sigma^2}\cos^2\delta}\,\cos\left[\sigma t + \tan^{-1}(\omega/(\sigma\tan\delta)\right]\right\}u(t)$$

$$L^{-1}\left[e^{-s\alpha/\omega}v_2(s)\right] = -v_1(t-\alpha/\omega)\big|_{\delta\to-\beta}$$

$$= \frac{K_{SD}}{1-\omega^2/\sigma^2}\left[-\sin(\omega(t-\alpha/\omega)+\beta) - [-\sin\beta\cos(\sigma(t-\alpha/\omega)) - \frac{\omega}{\sigma}\cos\beta\sin(\sigma(t-\alpha/\omega))]\right]u(t-\alpha/\omega)$$

$$= \frac{K_{SD}}{1-\omega^2/\sigma^2}\left\{-\sin(\omega t-\delta) + \sqrt{\sin^2\beta + \frac{\omega^2}{\sigma^2}\cos^2\beta}\,\cos[\sigma(t-\alpha/\omega) - \tan^{-1}(\omega/(\sigma\tan\beta)]\right\}u(t-\alpha/\omega)$$

$$
\begin{aligned}
v_{signal}(t)/(\sqrt{2}V_N) &= v_1(t) + L^{-1}(e^{-s\alpha/\omega}v_2(s)) \\
&= \frac{K_{SD}}{1-\omega^2/\sigma^2}\sin(\omega t-\delta)[u(t)-u(t-\alpha/\omega)] \\
&+ \frac{K_{SD}}{1-\omega^2/\sigma^2}\sqrt{\sin^2\delta+\frac{\omega^2}{\sigma^2}\cos^2\delta}\cos[\sigma t+\tan^{-1}(\omega/(\sigma\tan\delta)]u(t) \\
&+ \frac{K_{SD}}{1-\omega^2/\sigma^2}\sqrt{\sin^2\beta+\frac{\omega^2}{\sigma^2}\cos^2\beta}\cos[\sigma(t-\alpha/\omega)-\tan^{-1}(\omega/(\sigma\tan\beta)]u(t-\alpha/\omega)
\end{aligned}
$$

With resistive components existing in real circuits, the σ-frequency oscillating components are damped.

APPENDIX B. NUISANCE TRIPPING EVENTS IN ATCO FIELD TESTS

Events	Signal Plots
Nuisance Trip SG on -I Sep25 23:32:26	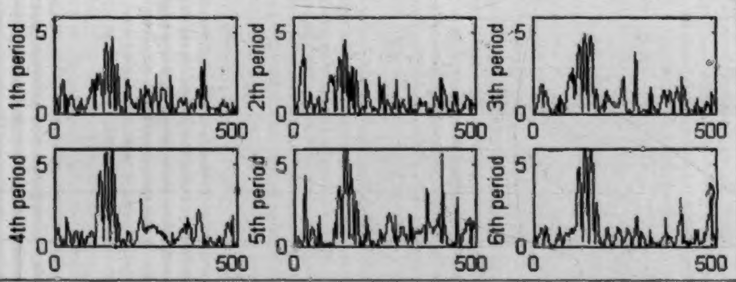
Nuisance Trip SG on -I Sep. 26 00:01:22	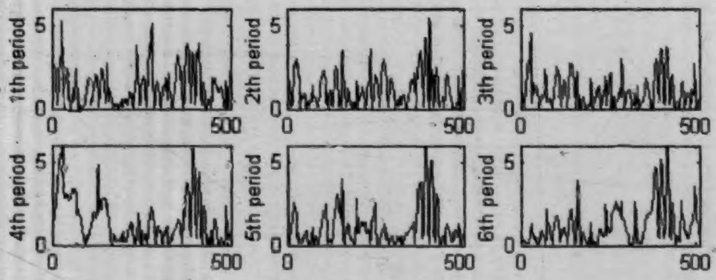
Nuisance Trip SG on -I Sep. 26 00:08:57	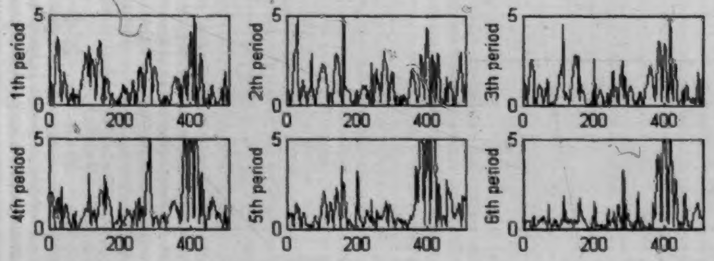
Nuisance Trip SG on- IV Oct. 13 17:00:38	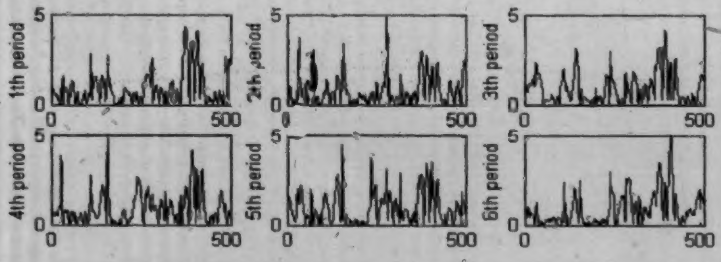

APPENDIX C. EQUATIONS FOR CALCULATING HARMONIC IMPEDANCES

Consider the following three-phase balanced system

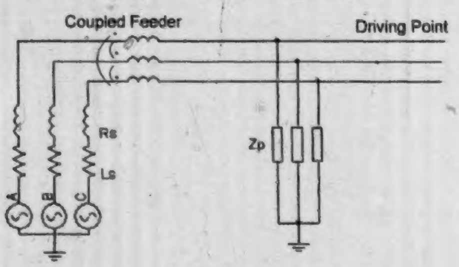

Figure B.1 The 3-phase simulation system.

The system impedances at the driving point are

$$Z_{self} = \frac{Z_p[(Z_s + Z_{Ls})(Z_s + Z_{Ls} + Z_p + Z_{Lm}) - 2Z_{Lm}^2]}{(Z_p + Z_s + Z_{Ls})^2 + Z_{Lm}(Z_p + Z_s + Z_{Ls}) - 2Z_{Lm}^2}$$

$$Z_{mutual} = \frac{Z_p^2 Z_{Lm}}{(Z_p + Z_s + Z_{Ls})^2 + Z_{Lm}(Z_p + Z_s + Z_{Ls}) - 2Z_{Lm}^2}$$

where $Z_s = R_s + j\omega L_s$ is the source impedance, Z_p is the shunt load harmonic impedance, Z_{Ls} is the feeder self impedance, and Z_{Lm} is the feeder mutual impedance.

The harmonic impedances of both the 25kV three-phase simulation system and the lab test system can be calculated using the above equations.